Conception of antenna systems for monitoring and localization applications in the industrial Internet of things

Amina Benouakta

UNIVERSITÉ CÔTE D'AZUR

ÉCOLE DOCTORALE
SCIENCES ET TECHNOLOGIES DE L'INFORMATION ET DE LA COMMUNICATION

THÈSE DE DOCTORAT

Conception de Systèmes Antennaires pour Applications de Supervision et de Localisation dans l'Internet des Objets Industriel

Amina BENOUAKTA

Laboratoire d'Électronique, Antennes et Télécommunications (LEAT)

Présentée en vue de l'obtention du grade de docteur en Électronique **d'**Université Côte d'Azur

Dirigée par : Robert Staraj
Co-dirigée par : Fabien Ferrero
Co-encadrée par : Leonardo Lizzi
Soutenue le : 17 Avril 2024

Devant le jury, composé de :
Thierry Monédière, Professeur des Universités, Laboratoire XLIM, Université de Limoges.
Laurent Cirio, Professeur des Universités, Laboratoire ESYCOM, Université Gustave Eiffel.
Philippe Pannier, Professeur des Universités, Laboratoire IM2NP, Polytech Marseille.
Robert Staraj, Professeur des Universités, Laboratoire LEAT, Université Côte d'Azur.
Fabien Ferrero, Professeur des Universités, Laboratoire LEAT, Université Côte d'Azur.
Leonardo Lizzi, Maître de Conférences, Laboratoire LEAT, Université Côte d'Azur.

cnrs

Conception de Systèmes Antennaires pour Applications de Supervision et de Localisation dans l'Internet des Objets Industriel

Jury :

- Président :

Philippe PANNIER, Professeur des Universités, Laboratoire IM2NP, Polytech Marseille.

- Rapporteurs :

Thierry MONÉDIÈRE, Professeur des Universités, Laboratoire XLIM, Université de Limoges.
Laurent CIRIO, Professeur des Universités, Laboratoire ESYCOM, Université Gustave Eiffel.

- Examinateurs :

Robert STARAJ, Professeur des Universités, Laboratoire LEAT, Université Côte d'Azur.
Fabien FERRERO, Professeur des Universités, Laboratoire LEAT, Université Côte d'Azur.
Leonardo LIZZI, Maître de Conférences, Laboratoire LEAT, Université Côte d'Azur.

"Move from reason that observes to reason that acts."

Haruki Murakami

UNIVERSITÉ CÔTE D'AZUR

Résumé

Conception de Systèmes Antennaires pour Applications de Supervision et de Localisation dans l'Internet des Objets Industriel

Cette thèse s'inscrit dans le contexte de l'Internet des Objets (Internet of Things, IoT), de l'identification et de la traçabilité d'objets dans des environnements dits complexes, réalisées au moyen de la technologie ULB (Ultra-Large Bande) dite de haute précision temporelle. L'ambition est de contribuer à l'évolution des systèmes ULB de localisation en temps réel par la conception et l'optimisation d'antennes ULB qui soient reconfigurables, multistandards et multifonctionnelles. Ainsi, tout système de localisation intégrant des antennes optimisées sera doté d'une qualité de localisation meilleure et de fonctions nouvelles.
Les contributions principales développées dans cette thèse ont consisté en l'apport d'améliorations aux systèmes de localisation en temps réel (RTLS) basé sur la technologie ULB : conception et fabrication d'antennes ULB reconfigurables en fréquence ; conception et fabrication d'une carte électronique de localisation multistandards (ULB et Long Range - LoRa) ; étude expérimentale des systèmes RTLS intégrant les antennes conçues et validation de l'évolution de la localisation en termes de portées supérieures, de détectabilité d'objets sans connaissance préalable de leurs orientations, et en précision améliorée par l'atténuation de signaux multi-trajets.

Mots clés : Antennes, localisation, systèmes de localisation en temps-réel (RTLS), ultra-large bande (ULB), lecteur, tag, long range (LoRa), internet des objets.

UNIVERSITÉ CÔTE D'AZUR

Abstract

Conception of Antenna Systems for Monitoring and Localization Applications in the Industrial Internet of Things

This thesis is part of the concept of the Internet of Things (IoT), object identification, and traceability in so-called complex environments through Ultra-Wide Band (UWB) technology known for its high temporal precision. The objective is to contribute to the advancement of real-time UWB-based localization systems through the design and optimization of UWB antennas that are reconfigurable, multi-standards, and multi-functions. Therefore, any localization system integrating the optimized antennas will have improved localization quality and new functionalities.
The main contributions developed in this thesis involve enhancements to real-time localization systems (RTLS) based on UWB technology: design and fabrication of frequency reconfigurable UWB antennas; design and fabrication of a multi-standard localization electronic board (UWB and Long Range - LoRa); experimental study of RTLS systems incorporating the designed antennas and validation of the evolution of the localization in terms of extended reading ranges, detectability of objects without prior knowledge of their orientations, and improved location accuracy through the attenuation of multi-path signals.

Key words : Antennas, localization, real-time locating system (RTLS), ultra-wide bandwidth (UWB), reader, tag, long range (LoRa), internet of things.

Acknowledgements

First and foremost, I would like to express my sincere gratitude to my supervisors, Prof. Robert Staraj, Prof. Fabien Ferrero and Prof. Leonardo Lizzi for their support, valuable guidance and significant contributions to the progression of my scientific journey during all these past three years. I have learnt not only scientific but also life lessons, because of their continuous help and patience with me, I will also become a person who can help others. For this reason, I can never thank them enough.

I would like to express my genuine gratitude to the jury members, Prof. Thierry Monediere, Prof. Laurent Cirio and Prof. Philippe Pannier, for accepting to review and evaluate my work and who will be the first people to read these pages. Thank you.

I would like to thank the LEAT laboratory members and colleagues for all the meaningful time, and valuable experiences. I wish you all the best in your future endeavors.

Finally, I want to extend my heartfelt appreciation and gratitude to my family, my parents and my sister, for their unwavering support during this academic journey, and without whom I wouldn't be where I am today. All my achievements including these words wouldn't have become reality without them.

Contents

List of Figures

List of Tables

Introduction

Often, in the telecommunications domain, we find that the word Internet-of-Things is employed everywhere in literature and applied research, this is because this word designates any wireless communication between two or several objects or "things". This wireless communication consists in the ability of each object to identify another one, which can either be near or far from it in space. Mostly, and depending on the type of devices, not only objects can identify each other, but they can also localize one another. The localization concept is also known as tracking or positioning. In this context, this thesis addresses mostly the indoor type of localization.
Although outdoor localization is widely known and accessible to the public and any individual due to the popularity of the Global Positioning System (GPS), indoor localization however, is more of an in-domain subject. Indoor tracking of things seems to also be more present in applied industrial settings than in research areas, especially nowadays, as it has a huge impact in many practices (such as: logistics, intelligent resource management, supply and stock tracking). Moreover, in research areas, localization and positioning are more pervasive for fundamental localization techniques (such as: time-of-flight, time-difference-of-arrival and angle-of-arrival) or optimization of algorithms relying on probabilistic estimations of object positions. Even though, less popular, localization in research also concerns the investigation of the front-end electronics, notably the choices and optimizations of the antennas employed for radio frequency transmission and reception of the positioning signals.
This thesis exploits and combines both, the research, and industry's available localization means and solutions to advance towards the improvement of the quality of localization, more precisely, towards a higher accuracy, a longer reading range, and detectability without prior knowledge of the target's orientation.

In the first chapter, an overview of the indoor localization techniques and techonologies is presented, followed by a more specific view of the Ultra-Wide Band (UWB) technology which allows for high-precision localization of objects. Then, a state of the art of the conventional UWB antennas is presented.

In the second chapter, a time-domain analysis of the ranging with UWB signals and antennas is performed through simulations. First, a UWB signal complying with the most recent specifications of the UWB standard is generated. Then this signal is applied to an UWB antenna, and the far-electric field at receiver probes is studied. The time of arrival of the signals at each probe is then extracted and compared between the receivers. This time is is the time used to determine the distance in localization.

In the third chapter, a technical review of the existing industrial solutions for localization is realized. These solutions are real-time locating systems (RTLSs) based on UWB technology. Then, the characteristics of the antennas integrated in these systems are highlighted. After that, a discussion about the performance results of these industrial RTLSs is realized. Notably, the discussion is focused on the influence of the antennas on these results in terms of range and accuracy.

In the fourth chapter, the design and conception of a UWB antenna is presented. This antenna is frequency reconfigurable and circularly polarized over two UWB channels. The design specifications of the antenna are derived from the observations made in the previous chapter (third chapter). These specifications are set to

make the antenna suitable for recent UWB requirements on the bandwidth and allow a better reading range and accuracy than conventional UWB antennas.

In the fifth chapter, the previously designed UWB antenna is employed in an industrial RTLS to perform ranging between a reader and a tag. The objective is to highlight the advantages of this antenna and its role in enhancing the quality of the localization results compared to the commercial antenna of the RTLS. The influence of the characteristics of the antenna employed on the results is discussed in detail and is in terms of reading range, accuracy and multipath mitigation, and detection of the tag without prior knowledge of its orientation.

In the sixth chapter, a multi-standard localization RTLS transceiver is designed employing the previously designed antenna. This RTLS works with UWB technology and Long-Range (LoRa) techonology to perform both high-accuracy and long range localization of a sensor. The objective is to overcome the low datarate of LoRa techonology which is not suited for real-time localization by employing a UWB technology reader as an intermediate node between a LoRa gateway and a sensor. Ranging is then performed and the system is assessed.

Finally, a general conclusion on the presented work is realized on the main contributions of this thesis, and the foreseen perspectives of the work are highlighted.

Chapter 1

Towards high-precision localization of objects

1.1 Introduction

This chapter will present an introduction to indoor localization, its techniques, the error sources that can be encountered in different scenarios (line-of-sight and non-line-of-sight), and its technologies such as : Bluetooth, Wi-Fi, and Ultra-Wide Bandwidth (UWB). Although some of these technologies were not specifically made for localization purposes, they have already been exploited to locate objects. Furthermore, the characteristics of the UWB technology, its advantages, applications, standards and consortiums are presented. Moreover, a state-of-the-art of UWB antennas is realized. Then, the chapter addresses the old and recent expectations of UWB antennas which need to be considered specifically in the field of localization to evolve towards more optimized and efficient locating systems. Finally, the technological axes explored in this thesis are briefly highlighted.

1.2 Indoor localization

Localization of objects starts with inferring the distance between two nodes, this measure is called "ranging" [1, 2]. After that, obtaining the space coordinates of one of these nodes is possible through methods like triangulation or with combining the distance measured with an angle-of-arrival measurement.

1.2.1 Localization techniques

First, to perform ranging, there are many techniques relying on the characteristics of the signals exchanged between a reader and a tag. The most pervasive techniques are received signal strength-based ranging (RSS-based), or time-based ranging technique (figure 1.1).

1.2.2 Received signal strength-based ranging (RSS)

This technique analyses the strength of the signal received at the reader side [3–8]. The strength of the signal is inversely proportional to the distance, that is, the stronger the signal, the farther it means the object is. The distance estimate is retrieved from the signal power strength measure by using an a priori existing propagation model [9], the simplest being the model of propagation of signals in free space. Another typical one is the two-path model which considers the direct path and the reflection from the ground path [10]. Indeed, the more paths the model contains, the more accurate the distance estimate will be. However, for the model to

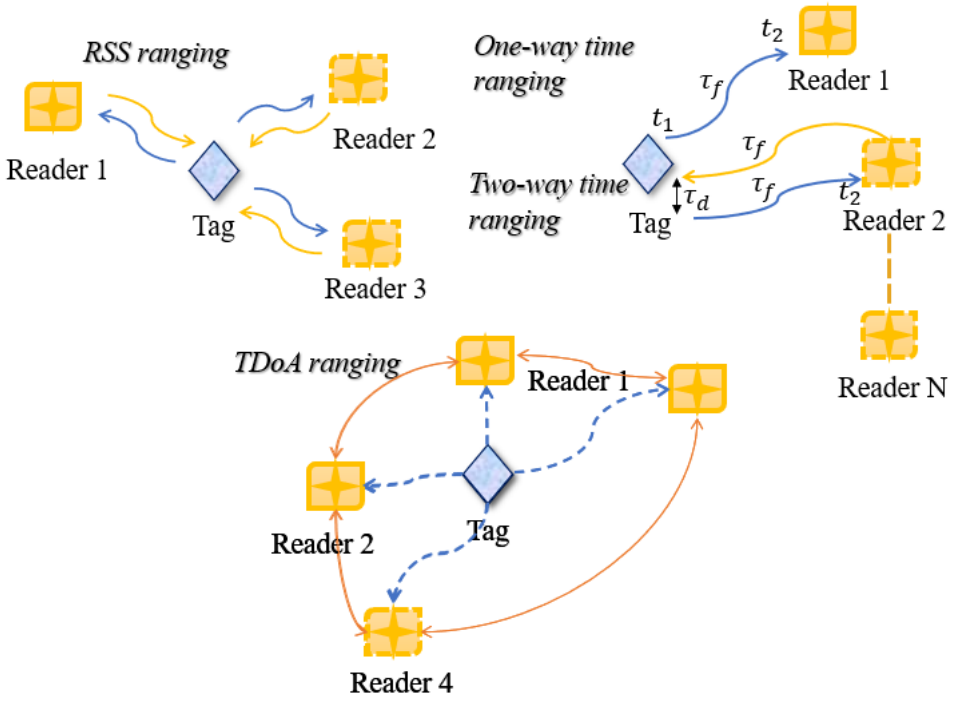

FIGURE 1.1: Indoor localization techniques: RSS-based ranging and time-based ranging (one way, two way and TDoA).

contain the most paths possible, knowledge of the specific environment where localization needs to be performed, is necessary. Thus, this ranging technique is more complicated to implement if high accuracy of the distance estimates is needed [2]. Furthermore, the strength of the propagating signal is very sensitive to environmental factors, such as obstacles (partial or complete blockage of the reader and tag's line-of-sight (LoS)), multipath reflections and interferences with other existing signals, as a low received signal power could indicate that the tag is far away from the reader but it could also indicate that the direct propagation path is blocked by an obstacle [11]. While these factors make RSS-based ranging less reliable for applications requiring highly accurate position information, this technique is easier to implement as it typically doesn't require additional electronics in the chain of the usual radio propagation systems, moreover, it can operate with different technologies (Wi-Fi [5], RFID [6], Bluetooth [7]) as long as a wireless connection is implemented.

1.2.3 Time-based ranging

This technique exploits time measurements to infer the distance information between a reader and a tag [1, 12, 13], this time is referred to as the "time-of-flight" (ToF) or "time-of-arrival" (ToA) $\tau = d/c$ where d is the unknown distance and c is the speed of light $(3.10^8 m/s)$. Time-based ranging exists in many forms [14, 15]: one-way ranging, two-way ranging, time-difference-of-arrival (TDoA), and angle-of-arrival (AoA), each of which is described below.

One-way ranging

This method requires the internal clocks of the reader and the tag to be perfectly synchronized [1,2,9]. The tag sends a packet to the reader containing the information

on time instant t_1, which is the instant at which the tag sent this message. The reader receives this information at instant t_2, and is thus, able to compute the ToF $\tau = t_2 - t_1$. This method may seem quicker; however, clock differences exist even in identical electronics modules, which can induce errors in the time measurements and thus degrade the estimation accuracy.

Two-way ranging

In this method, the constraint of clock synchronization between the reader and tag is omitted as the time measurement will be mainly performed by the reader. Here the time measured is the round-trip time (RTT) [1, 2, 9]. For this, the reader transmits a request (or interrogation) packet to the tag, to which, this latter replies by an acknowledgment packet after a response delay time τ_d. The RTT is then computed as $RTT = 2\tau_f + \tau_d$, with RTT known as it is the time duration it took from the time instant the first signal was sent to the time the reply signal arrives to the reader, and τ_d known as it mostly is specified by the manufacturer.

Time difference of arrival ranging (TDoA)

This method requires multiple readers which are usually synchronized through a wired network connection. A tag broadcasts a signal which is received by the readers at different time instants depending on their position [16–18]. The readers share with each other these times of arrival and compute the differences between them (TDoA). To compute the position of the tag with space coordinates, at least three readers and two TDoA measurements are required. Each TDoA measurement is interpreted geometrically as a hyperbola formed by a set of points to determine the tag position coordinates.

Angle of arrival localization (AoA)

This method involves angle measurements and allows for not only ranging (distance estimation with ToA), but also localization (coordinates estimation) of a target. Conversely to the triangulation method which requires at least three readers it is possible to combine a ToA measurement method with AoA measurements to estimate the coordinates. The arrival angle can be determined from the TDoA between signals received by two or more antenna elements of a single reader. For a two radiating element antenna array spaced by s, the TDoA depends on the AoA as described by the equation below [19]:

$$\tau_{diff} = \frac{s}{c}\, sin(\phi) \tag{1.1}$$

where ϕ is the AoA, τ_{diff} the TDoA and c the speed of light.

1.2.4 Error sources in distance estimation with time-based technique

The accuracy of the distance or position information is the most important characteristic and metric of locating systems, and more so in indoor localization. This accuracy depends on the quality of the time measurements realized. Many factors can degrade this quality and lead to unreliable measurements and thus to their unreliable interpretation while computing the distance estimates. Furthermore, the principal measurement in time-based ranging is the measure of the arrival time of the direct path (first path) signal between the reader and tag. While the direct path in

most cases exists, there can be cases where it does exist, but it is in a non-line-of-sight scenario, that is for example: if the view between the reader and tag is obstructed (or blocked) by any obstacle (object, walls...). There is also the case where the direct path signal may not arrive at all, and the first arriving signal will be a reflection from one of the objects present in the environment. Indeed, the measurement is considered ideal and most accurate if the first arriving path is a line-of-sight signal, that is, the signal travels in a straight line through a medium with constant known relative permittivity such as in air.

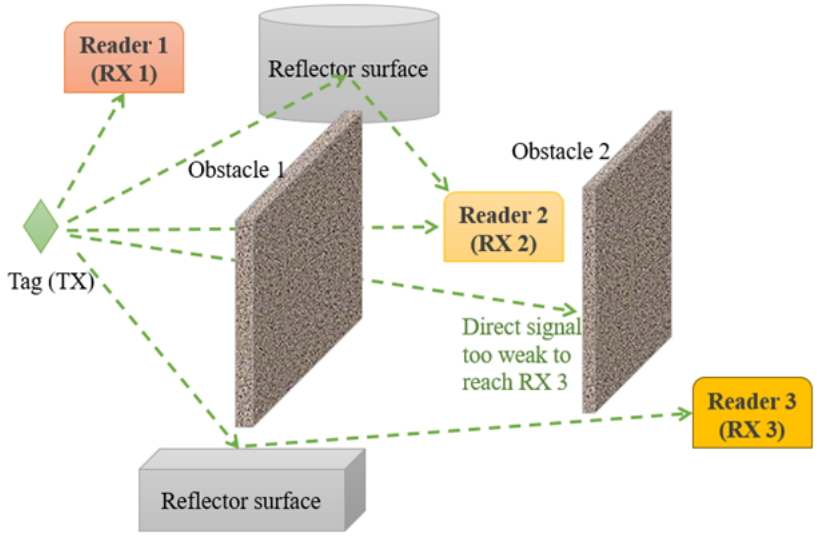

FIGURE 1.2: Various LOS and NLOS ranging conditions from a transmitting tag (TX) to different readers (RXn). RX1 in LOS-scenario, RX2 in NLOS-scenario with existing direct path and RX3 in NLOS-scenario and complete blockage of the direct path.

The possible error sources in time measurements can be divided to three categories: error sources present in LOS-scenario, error sources present in NLOS scenarios and error sources present in both LOS and NLOS scenarios, as described in the following

Line-of-sight scenario (LOS) specific error sources

In this case, no blockage is present in the direct path between the reader and tag. The first and fastest arriving signal will be the direct path signal and reflections from walls and objects arrive later (as they travel longer paths). This is the case where the measurement will be the most accurate.

Non-line-of-sight scenario (NLOS) specific error sources

In the case where there is blockage between the reader and tag, the first arriving path may be either the direct path signal after traveling through different mediums (non-constant relative permittivity) or a reflection signal from an object, the faster signal is the one that will arrive first and this depends on the permittivities encountered by the signal while traveling, and how far the reflecting object is. In both cases, the error will be "excess delay", which is an added positive bias in the time measured (and thus in the distance estimate). In the case, of the signal being a reflection signal, the distance traveled is naturally longer and thus produces a higher time of arrival

value. While, in the case of the signal being the direct path signal obstructed in its way by an obstacle, it's the speed that is reduced. Indeed, the speed of electromagnetic waves traveling in a homogenous material is reduced by $\sqrt{\epsilon_r}$ compared to the speed of light c. The delay $\Delta\tau$ introduced by a material of thickness d_w and permittivity ϵ_r is given by [9]:

$$\Delta\tau = (\sqrt{\epsilon_r - 1})\,\frac{d_w}{c} \tag{1.2}$$

Recent measurement campaigns in indoor environments, resulted in demonstrations that the mean of the ranging error (distance bias) caused by material blockage is in the order of the thickness of the obstacle.

Error sources in both LOS and NLOS

In all the scenarios, LOS or NLOS, if ranging is performed in cluttered complex environments, signal reflections will be present, that is: "multipath effect". If ranging is performed with narrowband technologies (Bluetooth, Wi-Fi, RFID...), multipath components (signals arriving via different propagation paths) combine at the reader side. These signals can usually not be resolved. Their combination results in constructive or destructive interference which makes the detection of the direct path signal difficult. Furthermore, in complete blockage, multipath signals are the only signals detected, the problem itself is not one reflection (as this only introduces a positive bias like explained previously) but is that the combination of the signals changes its original form which makes its recognition at the reader side impossible [20]. For this reason, UWB technology is privileged in indoor locations because of its fine time resolution compared to narrowband technologies, which helps resolve signals from each other to recognize the correct ranging signal. The advantages of UWB for ranging are further described in detail in the next section.
Other sources of errors include cochannel interference, which is caused by coexisting wireless systems sharing the same radio band.

1.3 Indoor localization technologies

The indoor environments are very challenging; thus, multiple technologies have been proposed to cope with their constraints. Indeed, throughout the years, indoor localization has been studied and performed using several technologies (figure 1.3), each conforming to different standards and radio frequencies. These technologies are heterogenous and include notably : Wi-Fi, Bluetooth, RFID, Near Field Communications (NFC), and UWB.
At the earliest stages of RTLSs, technologies started from exploiting ultra-sound, sonar (in radar domains), laser from optics (such as telemeters) and vision technologies (such as in the robotics domain) [1, 14]. However, recently the current trend to approach tracking and localization problems is to use standard, low cost and already deployed technologies. Consequently, in the following, we focus only on technologies based on radio signal exchange.
Just until recently, most wireless communication standards have been designed for other purposes and are not intended for localization and ranging purposes, however, this did not prevent their exploitation for positioning at the cost of some localization performance limitations such as shorter range, low or average accuracy and, small detectability coverage. Table 1.1 presents a summary of the existing technologies along with their characteristics allowing a qualitative comparison, the numbers are

only indicative as such systems are highly sensitive to the environment changes and also due to the random nature of the propagation of radio signals.

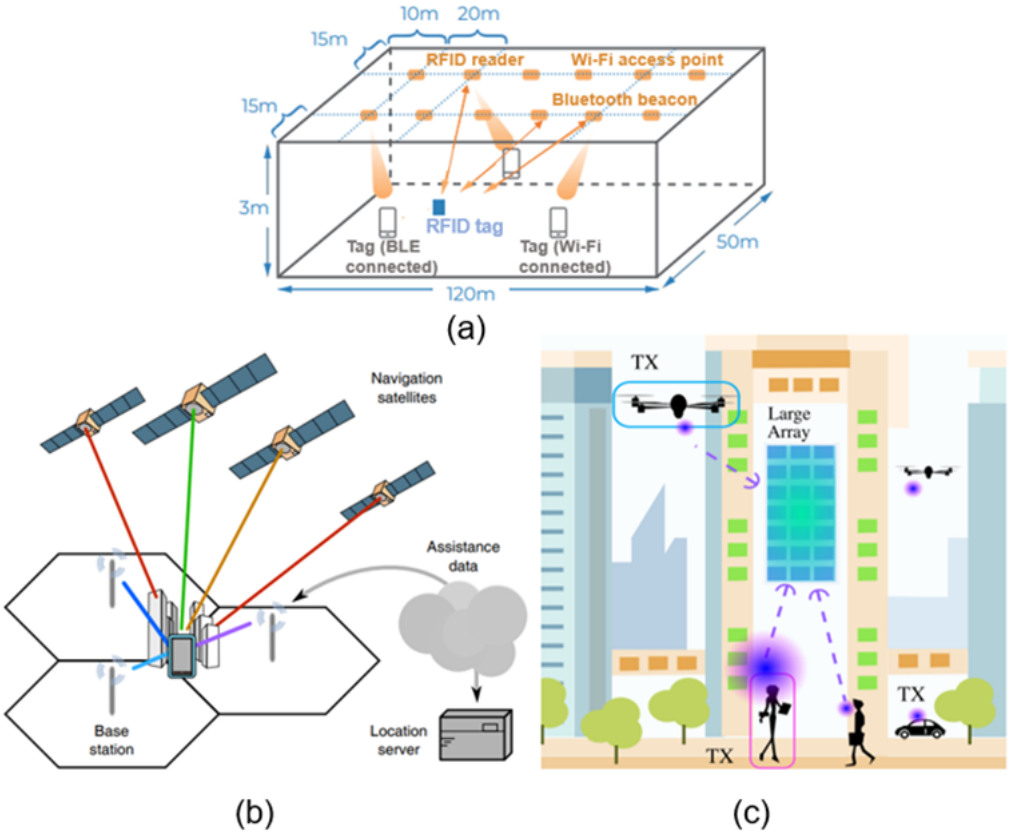

FIGURE 1.3: Architecture of the locating systems of different technologies: (a) Short-range technologies (Wi-Fi, Bluetooth, RFID) [26], (b) Mobile and network based cellular localization [15], (c) Near field technology positioning system [29].

Technology	Measurement technique	Accuracy	Advantages	Disadvantages
GPS [1,22]	TDoA	10 – 20 m	Worldwide	No indoor coverage Expensive
Galileo [1,22]	TDoA	1 – 5 m	Continent	No indoor coverage, Expensive
A-GNSS [1,22]	TDoA	< 5 m	Global or regional	Low indoor accuracy
Cellular (2G/3G) [1, 15], [23]–[26]	TDoA / RSSI	50 – 500 m	Country	Requires synchronized base stations, Low accuracy
Cellular (LTE) [1, 15], [23]– [26]	TDoA / RSSI	20 m	Country	Requires synchronized base stations, low accuracy
Wi-Fi [1, 23, 24,27]	RSS-fingerprinting	1 – 5 m	Indoor usage low cost, already deployed in most infrastructures	Low accuracy, requires a fingerprinting data base
WSN (ZigBee) [1]	RSS / PDoA	1 – 10 m	Indoor usage, low cost, low power consumption	Low accuracy, short range
UWB [1]–[14], [23], [28]	ToF / TDoA / AoA	0.1 – 1 m	Indoor usage, high accuracy	Problems in NLOS scenarios, infrastructure cost
RFID / Bluetooth [1, 14, 23]	RSS / Proximity / PDoA	Connectivity range (< 10 m)	Indoor usage Low cost, low power consumption, small size	Low accuracy, short range
Near Field Technology [29]	Electromagnetic Near Field characteristics	1 – 5 m	Indoor usage, low cost	Low frequency, large antennas, short distances
LoRaWAN [30]	TDoA, RSSI	RSSI: 1000 – 2000 m TDoA: 20 – 200 m	Low power consumption, large coverage	Outdoor usage

TABLE 1.1: A qualitative comparison of the available positioning technologies.

1.3.1 Short range technologies

Standards for technologies that offer short-range connections between objects are the most widespread, each of them aiming at a different application. Wi-Fi is the standard for wireless local area network applications (WLAN) [23, 27], Bluetooth for wireless personal area network applications (WPAN) [14, 23], RFID for radio frequency identifications [14, 23], and IEEE 802.15.4 / Zigbee for wireless sensor networks (WSN) [1]. Since these standards were developed for these specific applications and not for localization purposes, their exploitation for positioning relies mostly on extracting parameters of the radio signal received [1, 23, 24, 27], such as signal strength (RSS) or signal phase for example and then on the correlation of these parameters with the distance between the tag and reader. Consequently, even though systems employing such standards are capable of tracking tags, high accuracy of the position information is not trivial. Indeed, because of their narrow frequency bandwidth, multipath effects on the measurements can be very significant. The advantage of these technologies is their wide availability and accessibility almost anywhere indoor, which removes the necessity of implementing new infrastructure specifically for the sake of localization. Smartphones are now often utilized as receivers for both Bluetooth and Wi-Fi signals, following recent advancements. While, Beacons are small devices for BLE that are mounted on the walls and represent small base stations.

1.3.2 Cellular mobile radio localization

As cellular systems evolved from a dedicated mobile communication system to an almost omnipresent system with unlimited coverage anywhere and anytime for any device, it is no surprise that it additionally finds applications in other domains such as positioning and localization. All mobile phone tracking methods have in common that they use the locations of nearby antennas mounted at radio towers to infer the mobile's position. The positioning methods with cellular communications is classified into two categories: Mobile-based and Network-based. In mobile-based positioning, the target mobile itself computes its location by exploiting signal measurements from terrestrial transmitters and/or satellites. In network-based positioning, the network calculates the position of the mobile through relative measurements between the network and target, these measurements can either be performed by the network or by the target and transmitter to the network. Potentially, 2G/3G cellular physical (PHY) layer can provide ranging information through signal TOA estimation (more precisely, observed TDOA), although the relatively narrow bandwidth and time signal structure limit the achievable time resolution (1 μs for Global System for Mobile Communication (GSM), about 200 ns for 3G systems). LTE technology mostly employs TDoA and offers a tight synchronization between BSs and the possibility to use wideband signals with low interference, which showed great improvement compared to previous cellular generations. The deployment of 5G and the forthcoming 6G communications are expected to enable high precision positioning due to the adoption of small cells and massive antenna arrays at millimeter waves. Indeed, 5G operation frequencies are 700 MHz, 3.5 GHz, and millimeter waves at 26 and 28 GHz. High frequencies allow high accuracy ranging in direct (more so in LOS scenarios) but will highly suffer from attenuation, multipath and reflections (especially in NLOS scenarios) [24]. Conversely, lower frequencies are more robust to attenuation, hence reaching longer coverage, however, multipath effects can still deteriorate the accuracy of the ranging.

1.3.3 Near Field Technology (NFT)

Near field technology is a low frequency approach for localization, it is recently gaining interest in parallel with the use of arrays of a high number of antennas such as in applications for 6G. With large arrays, the system operates in the near-field propagation region (Fresnel region) where the wavefront of the electromagnetic field is spherical. In this context, the curvature of arrival (CoA) is a measure of the spherical wavefront and can be used to infer the position of a transmitter target [29]. The CoA depends on the transmitter position and the array geometry. The drawbacks of NFT for localization is that the state-of-the-art studies usually refer to only very short distances and that the used antenna array must be large enough to capture the spherical characteristic of the received wave, which makes the infrastructure not so practical.

1.4 UWB technology for indoor localization

Over the years, ultrawide bandwidth signals have existed under many different appellations notably: impulse radio signal, time domain radio signal, baseband radio signal, non-sinusoidal radio signal; until the US Department of Defense (DoD) first set the term ultrawide band to this technology in 1989 [31]. An ultrawide band signal is defined as constituted of a series of short narrow impulses following each other with very low duty cycles [28, 32].

1.4.1 History of UWB

Although UWB technology officially acquired its name in 1989, the idea of emitting very short-duration pulses was not new. In fact, we can say radio was born with UWB; Indeed, its initiation phase began when James Clark Maxwell proposed the laws of electromagnetism in 1860 by unifying electrodynamics and magnetism into a single theory. A few years later in 1888, Heinrich Rudolph Hertz, while trying to verify Maxwell's equations, demonstrated the existence of electromagnetic waves and finally, in 1893, he was able to generate short duration pulses using electrostatic discharges. These were the dominant wave generators for about 20 years after the first Hertz experiments [28]. Following that, despite of this UWB glimpse, wireless communications abandoned impulse transmissions and shifted their focus to the use of sine waves by employing modulated signals on sinusoidal carriers to allow multi-user coexistence on the shared radio spectrum and, for almost 50 years, pulse radio was abandoned.
By the beginning of the Cold War, the second phase had in fact begun. Impulse transmission was rediscovered and contributions to the development of UWB signals and their applications began in the 1960s with the innovation of Harmuth [33–37], Ross and Robbins [38–40], and Etten [41]; In 1970, implemented systems for radar applications appeared with the introduction of short-pulse generators using tunnel diodes. But until the early 1990s, this work remained confidential because it was aimed at military applications.
Finally, the third phase which consisted in the standardization and commercialization of UWB, started with the publication of several studies and pioneering works of Scholtz and Win [42–50] that demonstrated the potential of UWB for broadband telecommunications. These works design the transmission of information by associating several pulses to the same bit according to position and amplitude spreading codes to allow the sharing of the spectrum between several users. Research

on UWB evolved further with its experimental characterization for communications and indoor positioning, in [51]. In February 2002, the US FCC (Federal Communication Commission) adopted the first report and order [52] which authorized the use and marketing of certain UWB products in the United States subject to precise but license-free regulations. This step was a real boost to UWB, as a few years later, Europe and other continents and countries adopted similar regulations, and since then, a great deal of work has been done in the industrial, academic, and military worlds.

1.4.2 Definitions

A UWB system is defined as a device using a fractional bandwidth of 25 % or more [53, 54]. The US regulatory authority FCC extends this definition to a broader category of signals, including signals with a fractional bandwidth (FBW) at -10 dB of more than 20 % (or with a frequency bandwidth of more than 500 MHz), as illustrated in the figure 1.4. The FBW is represented by the equation below [52] :

$$FBW = \frac{BW}{f_c} = 2\,\frac{f_H - f_L}{f_H + f_L} \tag{1.3}$$

Where f_H and f_L are, respectively, the upper and lower frequencies of the signal frequency band at – 10 dB of the maximal power spectral density (DSP) and BW is the signal bandwidth at this level, f_c is the central frequency and Q is classically defined as the quality factor.

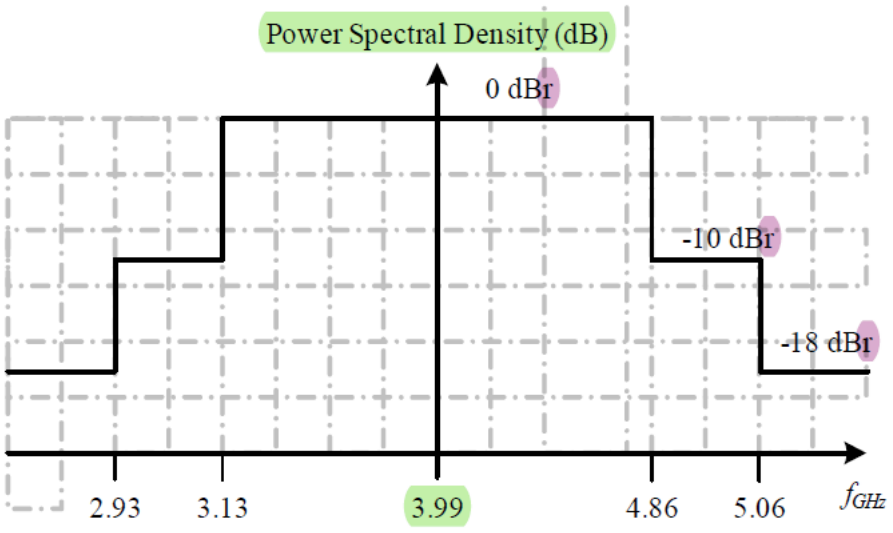

FIGURE 1.4: IEEE standard-compliant power spectral density of a UWB transmitted signal, illustrated here at the center frequency of UWB channel 2 [55].

1.4.3 Operating frequency bands of UWB

The RF requirements for the physical layer of UWB technology impose its operation on specific defined frequency channels, these channels are listed in table 1.2 and are categorized in three different band groups numbered from 0 to 2 (respectively: the channel below 1 GHz, the low band channel group and the high band channel group), each group contains a mandatory channel for UWB systems operating in one of its frequency channels and the other channels remain optional if multiband

operation is desired. The mandatory channels are channel number 0 below 1 GHz, the channel number 3 for low band operation and channel number 9 for high band operation [55].

Band group 1,2	Channel number	Center frequency (MHz)	Bandwidth (MHz)	Mandatory / Optional
0	0	499.2	499.2	Mandatory below 1 GHz
1	1	3494.4	499.2	Optional
1	2	3993.6	499.2	Optional
1	3	4492.8	499.2	Mandatory in low band
1	4	3993.6	1331.2	Optional
2	5	6489.6	499.2	Optional
2	6	6988.8	499.2	Optional
2	7	6489.6	1081.6	Optional
2	8	7488.0	499.2	Optional
2	9	7987.2	499.2	Mandatory in high band
2	10	8486.4	499.2	Optional
2	11	7987.2	1331.2	Optional
2	12	8985.6	499.2	Optional
2	13	9484.8	499.2	Optional
2	14	9984.0	499.2	Optional
2	15	9484.8	1354.97	Optional

TABLE 1.2: IEEE standard's UWB PHY frequency band allocations.

Furthermore, figure 5.5 represents the graphical representation of the previous table, highlighting the channel indexes with respect to frequency, where each channel is shown as a heavy black line centered on the channel's center frequency. The length of the lines depicts the channel bandwidth.

1.4.4 Principal characteristics of UWB

With the need to increase the data rate of wireless systems, UWB technology seems to be an ideal candidate for future radio communication systems for different types of networks, thanks to its following characteristics:

Bandwidth

The main characteristic of UWB signals is the width of the frequency band they occupy, and information theory suggests that with the use of an appropriate code, it is possible to transmit data at a BER (Bit Error Rate) below an arbitrarily low threshold, provided that the data rate at which it is desired to transmit data, is below the maximum capacity of the transmission channel.

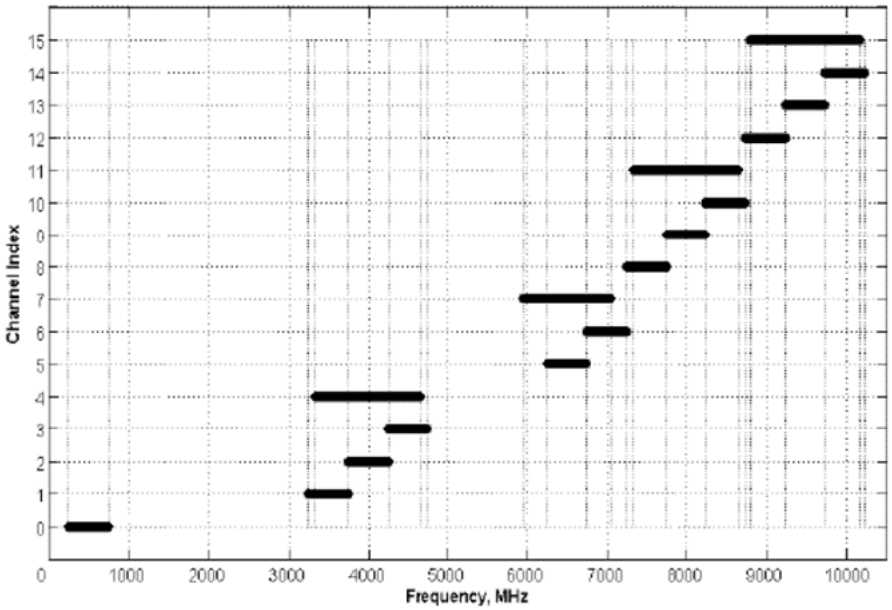

FIGURE 1.5: Graphical representation of UWB PHY frequency band allocation [55].

The Shannon theorem and UWB

The advantages and possibilities of UWB can be summarized by examining the famous Shannon capacity equation. Capacity is important when demanding applications require higher and higher data rates [28, 56] such as audio and visual applications. The Shannon equation is expressed as [57] :

$$C = BW\ log_2(1 + \frac{S}{N}) \tag{1.4}$$

Where C is the maximum channel capacity [bit/s], BW is the channel bandwidth [Hz], S is the signal power [W] and N is the noise power [W].
The maximum channel capacity increases linearly with the signal bandwidth BW, and only logarithmically with the signal to noise ratio $\frac{S}{N}$. From this, it can be deduced that UWB systems have great potential for high-capacity wireless communications.

Power spectral density

The energy used to transmit a wireless signal is non-infinite and, in general, needs to be as low as possible, especially for today's consumer electronics. For a fixed sum of energy one can either transmit a high energy density over a narrow band or a very small sum of energy densities over a wide band (figure 1.6). For UWB systems, the energy propagates over a very wide band and, in general, they have very low power spectral density (0.5 to 1 mW) [28, 53]. UWB radar systems are the major exception to this general rule. This characteristic is not intrinsic to UWB signals but is imposed by radio spectrum regulation organizations.

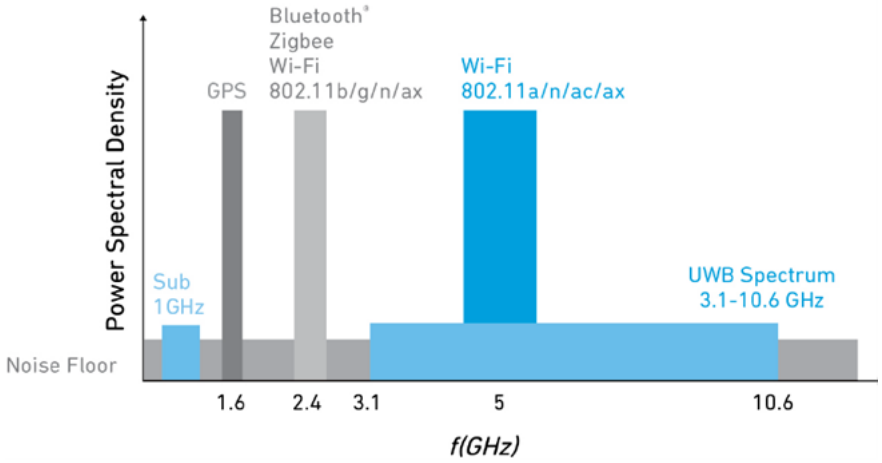

FIGURE 1.6: Power spectral density of the transmit power for different wireless technologies.

High temporal resolution

Due to their wide bandwidth, UWB signals have a high temporal resolution, usually of around one nanosecond. A first implication of this property is related to localization: knowing the delay of a signal with an accuracy of about 0.1 to 1 ns [56], it is possible to obtain information on the position of the transmitter with an accuracy of 3 to 30 cm.

Robustness against fading cause by multipath propagation

In conventional propagation channels, narrowband systems suffer from fading caused by multipath propagations as these signals often interfere destructively with the desired signal. In the case of pulsed signals, the transmitted waveforms can have a large bandwidth, so that multipaths having sub-nanosecond delays can be resolved and added constructively [56].

Secure and protected communication

UWB signals are inherently difficult to detect. This is because they are spread over a wide band and transmitted at power spectral density levels close to the noise floor of conventional radio receivers [56]. These characteristics allow the establishment of secure transmissions with a low probability of detection and interception.

Obstacle penetration properties

UWB signals offer good penetration capabilities through walls and obstacles, especially at lower frequencies of the spectrum [53]. This allows for good accuracy in terms of localization and tracking, thus enabling the development of through-the-wall vision of radar systems [58].

1.4.5 Applications of UWB

As a result of the imposed standard regulations, UWB systems are grouped according to their applications into three principal categories [52] :

Imaging systems

This first category includes imaging with Ground Penetrating Radar Systems (GPRs), Through-Wall Imaging, In-Wall Imaging, Surveillance Systems and Medical Systems. The UWB signal can penetrate the ground or a wall and even go through it to detect what is hidden behind it. It can also be used to measure distances accurately. The same principle applies to the human body. Therefore, the main users of systems in this category would be specialists in law enforcement, search and rescue, construction and mining, and geology.

Vehicle radar systems

In this category, UWB devices can detect the location and movement of objects in the vicinity of a vehicle, enabling features such as anti-collision, improved airbag activation and suspension systems to better comply with road conditions. With this technique, many lives can be saved.

Communications systems

An important application in this class is wireless personal area networks (WPANs), where data is transmitted over distances of 10 m or less. Two types can be distinguished in this application, High-Data-Rate (HDR) communications, which are mainly applied in computer networks (wireless USB) and consumer electronic devices (digital TV). The particularity of this class is that it allows for a very high data transfer rate (ranging from 100 Mbps to 1 Gbps) and a low-cost installation.
The second type is Low-Data-Rate (LDR) communications, which refers to all practical applications of sensor networks. These sensor networks are used for intelligent control of lighting and energy in buildings, automation of industrial processes and storage processes. These applications require the transfer of small amounts of data between transmitters (1 Mbps). The UWB's characteristic of low power transmission allows LDR communications to use network equipment with very small batteries, minimizing the infrastructure footprint and cost.
Regardless of these data rate considerations, the environments considered are mainly office buildings, meeting and conference rooms and public places (e.g., airports or shopping centers).

Ranging, localization and positioning.

Localization is the subject application, which is detailed in this thesis.

1.4.6 UWB Regulations, standards, and consortiums

Regulations

In the same manner for all technologies which are allocated a place in the radio spectrum, the regulations imposed depend on the geographical regions and countries in the world (US, Europe, Canada, Asia...) and on applications. These regulations specify notably the frequencies and the power spectral masks allowed for transmission for a certain technology. Thus, when a new radio communication technology is introduced, spectrum regulation authorities issue strict rules for the emission of signals, the aim being to protect existing systems from interference.

Although the transmission power of its signals is very low, UWB must also be regulated because it will occupy frequency bands already allocated to other technologies. One of the main particularities of UWB is the absence for the need of a license to access the UWB frequencies, allowing content to be produced and accessed freely. However, the decisions taken around the emission of UWB signals can vary from one regulation to another.

- Regulations in the United States (US) : In February 2002, the FCC issued a first order on UWB technology that allows signals to be transmitted mainly in the 3.1 - 10.6 GHz band [52]. This part of the spectrum allows the use of a bandwidth of up to 7.5 GHz. The power spectral density allowed is of - 41.3 dBm/MHz. Although this power level is low, it is compensated by the band width used, allowing a total power of 0.5 mW to be transmitted.

- Regulations in Europe (EU) : In March 2006, the standards' authority ETSI (European Telecommunications Standards Institute) published a decision that specifies the technical conditions under which UWB devices can operate in Europe. The decision covers the use of UWB devices in consumer electronics applications [59]. UWB devices can use the 6 to 8.5 GHz band with a maximum power spectral density of -4 1.3 dBm/MHz, which is the same level used in US UWB signals.

- Regulations in Asia : In Japan, the MIC (Ministry of International Affairs and Communications) proposed the issuance of unlicensed UWB signals in 2006. Similar to the FCC, regulations allow emissions at - 41.3 dBm/MHz for UWB devices. Japan has adopted the European model for the 3.4 - 4.8 GHz band.

In conclusion, spectrum masks depend on applications and regions: in Europe and Asian countries the regulations tend to be stricter, while in the USA and Canada they tend to be more extensive. Finally, it should be noted that the regulations imposed by Europe, the United States and Asia have a common band, the 7.25 GHz - 8.5 GHz band, without any mitigation techniques and which will eventually make systems completely nomadic from one continent to another.

Standards

To respond to a real demand and to avoid having incompatible UWB systems which do not use the same transmitted signal waveform, it is important to establish norms or standards for communication systems using UWB. The IEEE organization handles the development of standards around the UWB technology. Standards mostly specify frequencies, signal power masks, data rates and application ranges.
UWB was first briefly introduced in the standard IEEE 802.15.03a (standard for high-rate communications), however it was first associated with high-accuracy localization applications relying on impulse radio in the IEEE 802.15.4a standard (standard for low-rate communications), for ranges of maximum one meter.
In this thesis, we focus on the most recent IEEE standards, notably the two HRP UWB IEEE 802.15.4a and IEEE 802.15.4z standards, where HRP stands for High-Rate Pulse (pulse with high repetition frequency). A summary of the evolution of the IEEE standards introducing UWB technology is presented in table 1.3, and these standards are discussed in the following.

IEEE 802.15.4a (2007)	• Starting point for UWB standardization. • UWB PHY changed from an Orthogonal Frequency Division Multiplexing (OFDM)-based data communication to an impulse radio technology (IR-UWB). • Focus on low data rate wireless communication and precision ranging.
IEEE 802.15.4 (2011)	• First amendment to IEEE 802.15.4a (2007) [20]. • Specifies the High-Rate Pulse (HRP) mode of UWB PHY, that is transmission of pulses at high rate.
IEEE 802.15.4f (2012)	• Second amendment to IEEE 802.15.4a (2007). • Specifies the Low-Rate Pulse (LRP) mode of UWB PHY, that is transmission of pulses at low rate. • As the maximum transmitted energy remains the same, LRP mode transmits stronger pulses, but their number is fewer than the number of pulses transmitted with HRP mode.
IEEE 802.15.4 (2015)	• Specification of two PHY UWB modes: HRP and LRP modes, corresponding to the 2011 and 2012 amendments.
802.15.4z (2020)	• UWB PHY enhancement with two principal contributions: increased integrity and increased accuracy of the ranging measurements. • Additional coding and preamble options. • Improvements to existing modulations. • Addition of the secure fine ranging feature.

TABLE 1.3: Summary of the evolution of the IEEE standards introducing UWB technology specifications for precise ranging.

First, the IEEE 802.15.4 standard specifies the PHY and MAC layers of Low-Rate Wireless Personal Area Networks (LR-WPANs). The IEEE 802.15.4 PHY and MAC layers are used by higher-layer standards, such as ZigBee® and WirelessHart®. Multiple PHY schemes are specified in different amendments of the IEEE 802.15.4 standard :

- IEEE 802.15.4a introduced a high-rate pulse repetition frequency (HRP) UWB PHY used for ranging (i.e., localization).
- IEEE 802.15.4f introduced a low-rate pulse repetition frequency (LRP) UWB PHY used for RFID, ranging, and reduced energy consumption.

- IEEE 802.15.4z introduced new enhanced modes for both the HRP and LRP UWB IEEE 802.15.4a/f PHYs.

The HRP UWB PHY specifies a channel bandwidth of 0.5 - 1.3 GHz which correspond to pulse durations from 2 ns to as little as 0.78 ns. Since the calculations used for ranging techniques rely on the time duration of packet transmission, the extra short pulse duration makes UWB PHYs suitable for ranging applications. A finer granularity in the time domain translates to smaller errors in distance estimation. UWB specifications which are mostly described in IEEE 802.15.4a standard and its amendment IEEE 802.15.4z, specify that UWB waveform generation needs to be standard-compliant with HRP UWB 802.15.4a/z waveforms for three pulse repetition frequency (PRF) transmission modes (802.15.4a, and 802.15.4z BPRF and HPRF). For IEEE 802.15.4a, the valid mean PRF values are 3.9, 15.6 or 62.4 MHz. The IEEE 802.15.4z amendment defines these two PRF modes:

- Base pulse repetition frequency (BPRF), where the mean PRF is 62.4 MHz and the payload data rate is 6.81 Mbps
- Higher pulse repetition frequency (HPRF), where the mean PRF is either 124.8 or 249.6 MHz.

The scrambled timestamp sequence (STS) field is another key feature introduced by 802.15.4z to enhance data integrity. Transmission of the STS field is optional for the BRPF and HPRF modes.

- Notes, particularities, points in the amendments :

- In the base pulse repetition frequency (BPRF) mode of IEEE 802.15.4a/z, mean PRF is 62.4 MHz and data rate is 6.81 Mbps.
- The key difference between the BPRF and the HPRF mode is that in BPRF the PHR and the payload are modulated with the burst position modulation (BPM) BPSK technique.
- Similarly to the BPRF mode in IEEE 802.15.4z, IEEE 802.15.4a uses the BPM-BPSK modulation scheme.
- IEEE 802.15.4a has no STS field.
- The IEEE 802.15.4a/z HRP standard specifies a mandatory compliance check for HRP pulses. Specifically, the cross-correlation between the used pulse and a root raised cosine pulse with a roll-off factor of 0.5, must be higher than 0.8 for 0.5 ns in the main (central) lobe, and all other side lobes must have cross-correlation lower than 0.3.
- The IEEE 802.15.4z amendment specifies that transmitted pulses conform a specific time-domain mask.
- The IEEE 802.15.4 standard specifies a mask for the transmit power spectral density PSD.

UWB Consortiums

The official IEEE standardization has opened doors for other standards and consortiums aiming to reunite the different specifications for UWB RTLSs from different manufacturers and make them as interoperable as possible. The emerging consortiums were mostly aimed at precise ranging, but others are aimed at different applications. Below, some of these consortiums (figure 1.7) are described:

FIGURE 1.7: Available UWB consortiums names and logos.

- Fine Ranging Consortium (FiRa): This consortium is an industry consortium which's main aim is to enable precise location awareness for people and devices. FiRa describes UWB as a technology that is now demonstrating its potential and quickly becoming a vital mainstream wireless technology like Wi-Fi and Bluetooth, showed by its adoption in mass market consumer products (figure 1.8) including devices such as smartphones (iPhones, Samsung, Xiaomi, ...) and smart watches (Apple) since 2019. In addition to the IEEE specified protocol layers for UWB, FiRa has announced that it is preparing a Common Service Management Layer (CSML) specification layer that will drive the interoperability of FiRa certified devices.

FIGURE 1.8: Envisaged application use-cases for UWB technology by the FiRa Consortium.

- Car Connectivity Consortium (CCC)®: Conversely to the FiRa consortium that focuses on leveraging UWB for precise location, the CCC consortium leverages UWB in the automotive domain and advances technologies for smartphone-to-car connectivity solutions. The Digital Key 3.0 standard of the CCC, allows consumers to use their mobile devices, regardless of manufacturer or operating system type, to access their vehicles easily and securely (handsfree, location-aware, keyless access). Indeed, it provides location aware features for cars by enabling them to localize the device related to the specific car and thus, allowing its user the access to it. Its member companies include smartphone and vehicle manufacturers, automotive tier-1 suppliers, silicon/chip vendors and many more. CCC and FiRa consortiums collaborate complementarily with the same goal of UWB interoperability to develop an ecosystem of UWB devices.

- Apple's Nearby Interactions: Nearby Interaction is an accessory protocol and industry standard developed by Apple, it can be used through an application

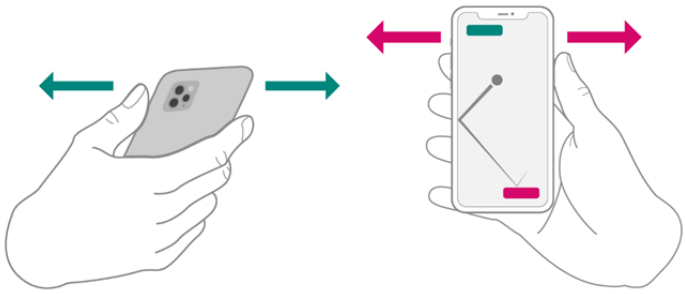

FIGURE 1.9: Illustration of the Nearby Interaction ranging session with UWB-enabled Apple devices [60].

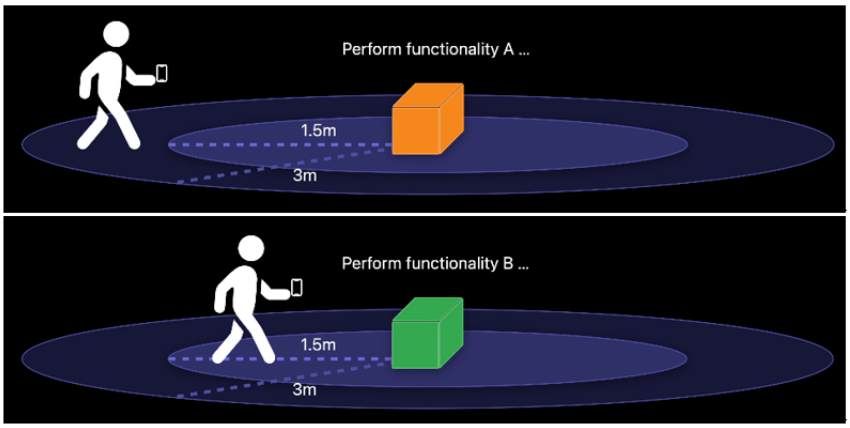

FIGURE 1.10: Illustration of UWB's use case: conditionally performing functionalities depending on the presence of a user within the limits of specific ranging areas [60].

to acquire the position of devices with a U1 (Apple's UWB chip) or another UWB chip, such as iPhone 11 or later, Apple Watch, and UWB enabled third-party accessories. Apple defines it as lightweight application-level protocol which specifies the configurations needed to start an interaction session, in which devices that are in physical proximity can participate (figures 1.9 and 1.10), and share their position and device identity, the application notifies of the peers of their positions by reporting their direction and distance in meters.

- Omlox Consortium: Omlox name was derived from Latin terms "omni-present" and "locus" (location), is the first emerging open locating standard dedicated to RTLSs, it aims to enable each manufacturer to implement its own location-based services based on the standardized architecture, this architecture introduces the omlox core-zone that ensures interoperability across RTLS and devices from different vendors. Its members include Huawei, Tencent, Haier, Inspur, and Hikvision.

1.4.7 Conventional UWB antennas

According to the FCC regulation authority and standards defined by the IEEE organization, a UWB antenna is defined as an antenna having a bandwidth equal or greater than 500 MHz, i.e., a fractional bandwidth equal or greater than 20 %.
In the first part of this section, an overview of UWB antennas, how they emerged, and their evolutions are described as generally known; In the second part, details,

and expectations of UWB antennas are described in the context of localization and ranging.

1.4.8 An overview of conventional UWB antennas

Similarly with standard narrowband front ends, UWB antennas are designed to operate within the bandwidth of the system where they are planned to be integrated. Hence, in the past years, UWB antennas were majorly designed to work with UWB systems which transmit signals over a power mask covering all the 7.5 GHz spectrum bandwidth allocated for UWB applications (3.1 to 10.6 GHz). Furthermore, UWB antennas are no exception to other antennas and need to adhere to the same design specifications and constraints such as: impedance bandwidth, radiation pattern, directivity and gain, polarization, efficiency, size constraint, cost, etc. However, the fact that these parameters are frequency dependent make the design procedure of UWB antennas more difficult and challenging compared to its narrowband counterparts. First, UWB systems transmit signals with either one of these transmission techniques [61]: pulsed transmission, known as impulse radio UWB (IR-UWB) and covers all the UWB bandwidth, or multiple broad sub-bands transmission, known as multiple orthogonal frequency-division multiplexing (OFDM). Catering to each method, the same constraints apply either in all the ultra-wide frequency bandwidth or in multiple wide frequency bands, and the principal objectives of UWB antenna design stand as: steady directional or omni-directional radiation pattern, stable directivity and gain at the radiation directions of interest, constant polarization type with respect to frequency, high radiation and total efficiencies, and for IR-UWB systems, constant group delay of the antenna (to avoid pulse distortions) is added.
Since the emerging pioneering works of Scholtz and Win (Scholtz et al. 2005) on UWB transmissions, research leaned again towards the design of their antennas. In fact, UWB antennas belong to the category of the broadband antennas, more commonly called: frequency independent antennas.
To design frequency independent antennas, two theoretical principals exist: the Mushiake principle (1940) and the Rumsey principle (1950) [61].

Mushiake's principle

Mushiake's principle is related to the Babinet principle [62] and states that an antenna's performance will be frequency independent if the antenna is self complementary. A self-complementary antenna (SCA) has a geometry such that its complement (where air is replaced by metal and metal replaced by air) can exactly overlay the original structure through translation and/or rotation [61]. The principle states that such antennas have constant impedance independent of the frequency, and applies to any shape of the structure. Figure 1.11 illustrates rectangular and circular shape SCAs. In theory, the shapes extend infinitely, however, in practice they are truncated in size [61] as the shape extends from the feed point of the antenna.

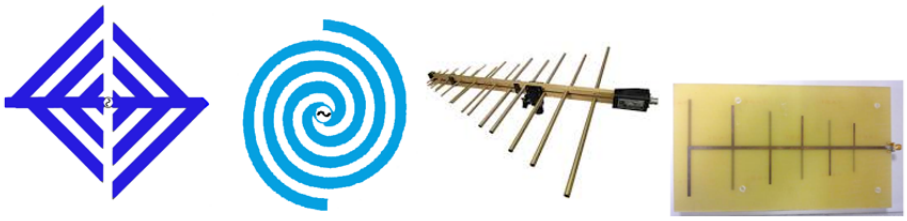

FIGURE 1.11: Two self-complementary antennas of different shapes (rectangular and spiral) and log-periodic antenna in 3D and planar forms.

This principle led directly to the invention of the class of antennas called log-periodic dipole antennas (figure 1.11), which is a modified folded up SCA, and has high gains and relatively constant omni-directional radiation patterns and impedances over bandwidths of 10:1 and more. The log-periodic antenna is a multi-resonant antenna, this type of antennas consists of an arrangement of multiple narrowband radiating elements, this creates a large array resonating at multiple frequencies. Despite their UWB characteristic, these antennas are not suitable for IR-UWB systems because their phase centers are not fixed in frequency which leads to dispersion [61].

Rumsey's principle

Rumsey's principle [63] states that for an antenna to be frequency independent, its shape needs to be specified only in terms of angles (figures 1.12, and 1.13). Examples of such antennas are the balanced spiral antenna, the logarithmic spiral antenna and conical spiral antenna [63, 64].

FIGURE 1.12: Antennas defined by angles: Spiral antenna, logarithmic spiral antenna and conical spiral antenna.

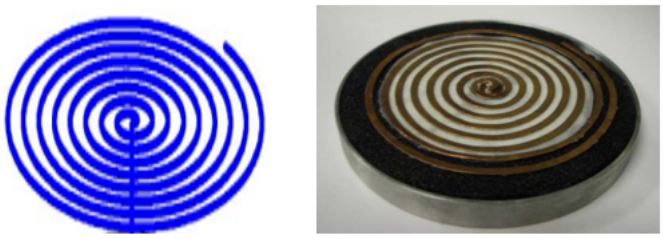

FIGURE 1.13: Spiral antenna with unbalanced excitation and ground plane.

These classic frequency independent antennas may exhibit broadband frequency performance however they still have drawbacks such as their physical dimensions

which tend to be significant as both Mushiake and Rumsey's principles describe shapes which theoretically extend infinitely to obtain the desired bandwidth.
Other classic broadband antennas include horn antennas and tapered slot antennas (TSA) (figure 1.14) [61], they belong to the traveling-wave antennas type and provide directional radiation. Their principal characteristic is having a gradual transition structure (flaring waveguide shape) which helps radiating the waves efficiently into space, they were introduced in [65, 66].

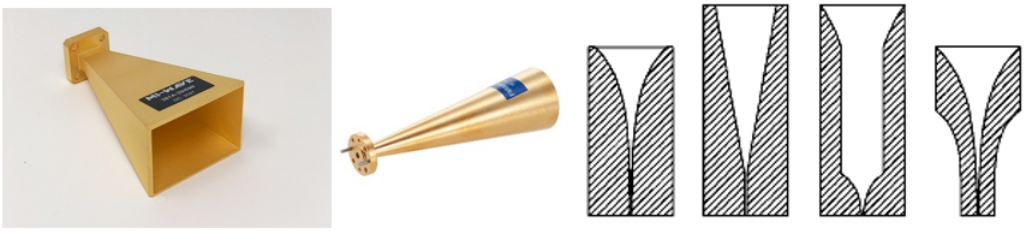

FIGURE 1.14: Horn antennas (rectangular and circular cross-sections), TSA antennas of different shapes.

Horn antennas' shape can be a pyramid with rectangular cross-section to be used with rectangular waveguides, or a cone shape with circular cross-section to be used with cylindrical waveguides. TSA antennas consist of a tapered slot carved into the metallization on top of a dielectric substrate, depending on the etched slot shape, TSA antennas are categorized in: linear taped slot antenna (LTSA), constant width tapered slot antenna (CWTSA), broken linearly tapered slot antenna (BLTSA) and finally the well-known Vivaldi antenna or the exponentially or elliptically tapered slot antenna. TSAs radiate unidirectionally in the plane of the substrate; their directivity increases with frequency and some antennas can achieve up to 10 dBi of gain [61].

In addition to frequency independent antennas and TSAs, broadband antennas have also been derived as an evolution of popular monopole and basic dipole antennas [61]. Examples of these antennas are the biconical dipole antenna (Lodge's) and its planar evolution the bowtie dipole antenna, represented in figure 1.15.

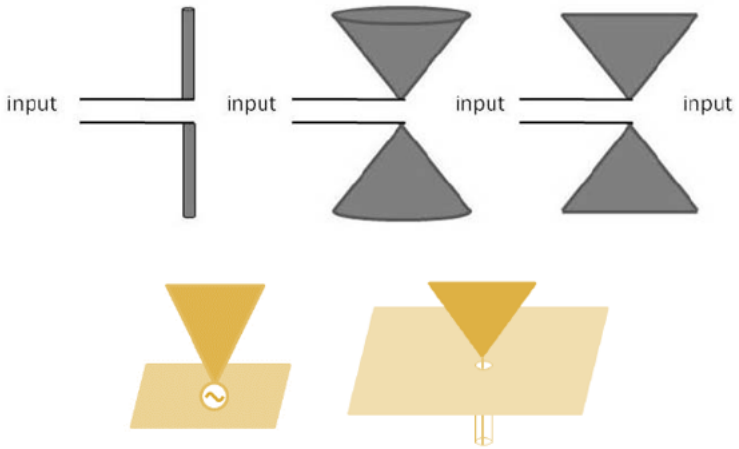

FIGURE 1.15: Evolution from classic dipole antenna to biconical dipole and bowtie antennas, wire monopole antenna with ground plane orthogonal to the radiating pole [61].

These antennas represent a modified dipole which has thicker arms the more it is extended from the feeding point. The biconical antenna also evolved towards the discone antenna, which instead has a single cone, and is more limited in the bandwidth, however, presents a more stable antenna phase center compared to the biconical version [61].
Single cone antenna could also be seen as the evolution of monopole antenna by considering the second pole as a conducting ground plane, which will resemble the wire monopole configuration (figure 1.15). Until today, manufacturers lean towards the UWB monopole antenna more than any other structure, and widely integrate these in most UWB RTLSs, due to the numerous advantages they present such as: their simple structure, low cost, broadband bandwidth, omni-directional radiation pattern and simple matching capabilities. However, since they are not planar structures due to their ground plane being perpendicular to the radiating element, this makes their integrability occupy a large area [61]. Hence, research has moved towards printed monopole antennas and different shapes microstrip designs printed on a dielectric substrate were proposed, such as the disc [67], elliptic [68] and two-step-rectangular monopole antenna [69] and other shape modified antenna and ground notched designs to enhance the bandwidth (figure 1.16). These antennas are fed by microstrip lines or coplanar waveguide transmission lines.

FIGURE 1.16: Planar monopole UWB antennas: two-step band-notch monopole antenna, circular monopole antenna, hexagonal monopole antenna, elliptical monopole antenna with truncated ground plane.

1.4.9 Requirements for UWB antennas in localization systems

Although the interest in developing and designing Ultra-wideband (UWB) antennas has been growing since the FCC of the United States has allocated the 3.1 - 10.6 GHz frequency range to UWB technology and its applications, the performance requirements are no longer the same for these antennas since the IEEE.802.15.4a has declared the use of UWB channels of either 500 MHz or 1333 MHz instead of all of the 7.5 GHz bandwidth. The requirements also enhanced since the apparition of the first UWB real time locating system from Decawave in 2014 [70]; Naturally the change in the design specifications and analysis metrics for these antennas has followed. In this section, we describe how these requirements have changed and what they have become.

The old requirements

In previous literature work, UWB antenna researchers demonstrated that pulse distortion and undesired phase response variations (non-linear response) are hindrances that affect the performance of the IR-UWB RTLS. Thus, classic figures-of-merits depending on frequency, such as: reflection coefficient of the antenna, radiation pattern, and gain, not only are required to be analyzed for all the ultra-wide bandwidth

frequencies, but they are also no longer sufficient to evaluate UWB antennas' response and performance. Consequently, new metrics were introduced to reliably characterize and predict the behavior of UWB antennas, such as: the system fidelity factor (SFF) which indicates the amount of distortion occurred in the transmitted UWB pulse was caused by the antenna [71], by comparing its shape between the transmit and receive sides of the RTLS. Another metric that was introduced, is the distance estimation error (DEE) which indicates the amount of bias (error) is affecting the ranging estimates.

The recent requirements

Initially, as the IR-UWB systems considered the transmission of baseband ultra-short electromagnetic pulses over a bandwidth up to 7.5 GHz, antenna designers focused their research on developing techniques that allow the bandwidth enhancement of antennas such that they can transmit sub-nanosecond pulses, with the minimum level of pulse distortion possible. However, UWB developments have followed at system and standardization levels, where the specifications replaced the extremely short time pulses (sub-nanoseconds) by modulated pulses of bandwidths of 500 MHz or 1 GHz (mostly 500 MHz), that is: pulse widths of 2 ns or more. Although the bandwidth of these channels is smaller, the benefits of UWB such as the ability to resolve individual multipath signals and to perform precise ranging remain unchanged. Consequently, UWB antennas are now required to cover only a relative bandwidth less than 10 %.
Furthermore, with recent advances in UWB RTLS development aiming for mass production of these radio chips in the industry, other physical and electrical constraints are being paid attention to, such as: small size of the antenna and the study of their integration environment to guarantee their behavior in their integration platform. For this reason, standard antenna simulations and design in free-space and standalone conditions are no longer sufficient to adhere to all performance expectations of the designed IR UWB RTLS.

1.5 Objectives and developed axes of the thesis

The general objective is to propose improvement and evolution perspectives to UWB real-time locating systems, specifically through the optimization of UWB antenna designs. Among the objectives initially foreseen, the developed leads and works carried out in the context of this thesis has focused on the following aspects :

- Adaptability to new UWB standard specifications.
- Enhancement of current RTLS ranging quality through the conception of optimized UWB antennas.
- Introduction of a new feature: multi-standard UWB-LoRa joint localization.

Bibliography

[1] D. Dardari, P. Closas, et P. M. Djuric, « Indoor Tracking: Theory, Methods, and Technologies », IEEE Trans. Veh. Technol., vol. 64, no 4, p. 1263-1278, avr. 2015, doi: 10.1109/TVT.2015.2403868.

[2] D. Dardari et al., « Chapter 5 - Innovative Signal Processing Techniques for Wireless Positioning », in Satellite and Terrestrial Radio Positioning Techniques, D. Dardari, E. Falletti, et M. Luise, Éd., Oxford: Academic Press, 2012, p. 207-315. doi: 10.1016/B978-0-12-382084-6.00005-2.

[3] S. Salem Al-Bawri, M. Tariqul Islam, M. Jit Singh, M. Faizal Jamlos, A. Narbudowicz et al., "Rss-based indoor localization system with single base station," Computers, Materials and Continua, vol. 70, no.3, pp. 5437–5452, 2022.

[4] C. Esposito, M. Ficco, Deployment of RSS-Based Indoor Positioning Systems. Int J Wireless Inf Networks 18, 224–242, 2011, https://doi.org/10.1007/s10776-011-0131-7.

[5] W. K. Zegeye, S.B. Amsalu, Y. Astake and F. Moazzami, "WiFi RSS fingerprinting indoor localization for mobile devices," in Proceedings of the 2016 IEEE 7th Annual Ubiquitous Computing, Electronics and Mobile Communication Conference (UEMCON), New York, NY, USA, 20–22 October 2016.

[6] S. Phimmasean, T. Chuenurajit, and P. Cherntonomwong, "Indoor localization system based on fingerprint technique using RFID passive tag," in Proceedings of the 2013 10th International Conference on Electrical Engineering/Electronics, Computer, Telecommunications and Information Technology, Krabi, Thailand, 15–17 May 2013; pp. 1–6.

[7] F. Subhan, H. Hasbullah, A. Rozyyev, and S. T. Bakhsh, "Indoor positioning in Bluetooth networks using fingerprinting and lateration approach," in Proceedings of the International Conference on Information Science and Applications, Jeju Island, Korea, 26–29 April 2011.

[8] C. Zhang, N. Qin, Y. Xue, and L. Yang, "Received Signal Strength-Based Indoor Localization Using Hierarchical Classification," in Sensors 2020, 20, 1067, https://doi.org/10.3390/s20041067

[9] D. Dardari, A. Conti, U. Ferner, A. Giorgetti, et M. Z. Win, « Ranging With Ultrawide Bandwidth Signals in Multipath Environments », Proc. IEEE, vol. 97, no 2, p. 404-426, févr. 2009, doi: 10.1109/JPROC.2008.2008846.

[10] K. Haneda, R. Rudd, E. Vitucci, D. He, P. Kyösti, F. Tufvesson, S. Salous, Y. Miao, W. Joseph, E. Tanghe, "Chapter 2 - Radio propagation modeling methods and tools," in "Inclusive Radio Communications for 5G and Beyond," Academic Press, 2021, Pages 7-48, ISBN 9780128205815, https://doi.org/10.1016/B978-0-12-820581-5.00008-0.

[11] J. Dai, M. Wang, B. Wu, J. Shen, and X. Wang, "A Survey of Latest Wi-Fi Assisted Indoor Positioning on Different Principles," in Sensors 2023, 23, 7961. https://doi.org/10.3390/s23187961

[12] G. Shen, R. Zetik, H. Yan, O. Hirsch and R. S. Thomä, "Time of arrival estimation for range-based localization in UWB sensor networks," 2010 IEEE International Conference on Ultra-Wideband, Nanjing, China, 2010, pp. 1-4, doi: 10.1109/ICUWB.2010.5614041.

[13] R. M. Buehrer, and S. Venkatesh, "Fundamentals of Time-of-Arrival-Based Position Locations," In "Handbook of Position Location" (eds S.A. Zekavat and R.M. Buehrer), 2011, https://doi.org/10.1002/9781118104750.ch6.

[14] N. S. C. J, N. H. A. Wahab, N. Sunar, S. H. S. Ariffin, K. Y. Wong, et Y. Aun, « Indoor Positioning System: A Review », Int. J. Adv. Comput. Sci. Appl., vol. 13, no 6, 2022, doi: 10.14569/IJACSA.2022.0130659.

[15] J. A. del Peral-Rosado, R. Raulefs, J. A. Lopez-Salcedo, et G. Seco-Granados, « Survey of Cellular Mobile Radio Localization Methods: From 1G to 5G », IEEE Commun. Surv. Tutor., vol. 20, no 2, p. 1124-1148, 2018, doi: 10.1109/COMST.2017.2785181.

[16] J. Pospisil, R. Fujdiak, and K. Mikhaylov, "Investigation of the Performance of TDoA-Based Localization Over LoRaWAN in Theory and Practice," in Sensors 2020, 20, 5464.

[17] I. Daramouskas, D. Mitroulias, I. Perikos, D. Paraskevas, V. Kapoulas, "Localization in LoRa Networks Based on Time Difference of Arrival," Springer: Cham, Switzerland, 2022; pp. 130–143.

[18] J. J. Pérez-Solano, S. Ezpeleta, J. M. Claver, "Indoor localization using time difference of arrival with UWB signals and unsynchronized devices," Ad Hoc Networks, Volume 99, 2020, https://doi.org/10.1016/j.adhoc.2019.102067.

[19] V. Sipal, M. John, D. Neirynck, M. McLaughlin, et M. Ammann, « Advent of practical UWB localization: (R)Evolution in UWB antenna research », in The 8th European Conference on Antennas and Propagation (EuCAP 2014), The Hague, Netherlands: IEEE, avr. 2014, p. 1561-1565. doi: 10.1109/EuCAP.2014.6902082.

[20] C. Falsi, D. Dardari, L. Mucchi, et M. Z. Win, « Time of Arrival Estimation for UWB Localizers in Realistic Environments », EURASIP J. Adv. Signal Process., vol. 2006, no 1, p. 032082, déc. 2006, doi: 10.1155/ASP/2006/32082.

[21] Fira consortium. Accessed: Dec. 2023. [Online]. Available: https://www.firaconsortium.org/

[22] G. Bacci, E. Falletti, C. Fernández-Prades, M. Luise, D. Margaria, et F. Zanier, « Chapter 2 - Satellite-Based Navigation Systems », in Satellite and Terrestrial Radio Positioning Techniques, D. Dardari, E. Falletti, et M. Luise, Éd., Oxford: Academic Press, 2012, p. 25-74. doi: 10.1016/B978-0-12-382084-6.00002-7.

[23] R. Mautz, « Indoor positioning technologies », p. 1 Band, 2012, doi: 10.3929/ETHZ-A-007313554.

[24] C. S. Álvarez-Merino, H. Q. Luo-Chen, E. J. Khatib, et R. Barco, « WiFi FTM, UWB and Cellular-Based Radio Fusion for Indoor Positioning », Sensors, vol. 21, no 21, p. 7020, oct. 2021, doi: 10.3390/s21217020.

[25] L. Wang et M. Zawodniok, « RSSI-based localization in cellular networks », in 37th Annual IEEE Conference on Local Computer Networks – Workshops, Clearwater, FL, USA: IEEE, oct. 2012, p. 820-826. doi: 10.1109/LCNW.2012.6424069.

[26] Y. You et C. Wu, « Indoor Positioning System With Cellular Network Assistance Based on Received Signal Strength Indication of Beacon », IEEE Access, vol. 8, p. 6691-6703, 2020, doi: 10.1109/ACCESS.2019.2963099.

[27] M. A. C. Duran et al., « Chapter 3 - Terrestrial Network-Based Positioning and Navigation », in Satellite and Terrestrial Radio Positioning Techniques, D. Dardari, E. Falletti, et M. Luise, Éd., Oxford: Academic Press, 2012, p. 75-153. doi: 10.1016/B978-0-12-382084-6.00003-9.

[28] M. Ghavami, L. B. Michael, et R. Kohno, "Ultra Wideband Signals and Systems in Communication Engineering," 2nd ed. Wiley, 2007. doi: 10.1002/9780470060490.

[29] A. Guerra, F. Guidi, D. Dardari, et P. M. Djuric, « Near-field Tracking with Large Antenna Arrays: Fundamental Limits and Practical Algorithms », IEEE Trans. Signal Process., vol. 69, p. 5723-5738, 2021, doi: 10.1109/TSP.2021.3101696.

[30] LoRaWAN, « Why LoRaWAN is the logical choice for asset tracking connectivity », April 2020.

[31] T. W. Barrett, “History of Ultra WideBand (UWB) Radar and Communications: Pioneers and Innovators”, Progress In Electromagnetics Symposium 2000 (PIERS2000), Cambridge, MA, Jul. 2000.

[32] G. B. Giannakis, “Ultra-Wideband Communications, An Idea whose Time has Come”, Signal Processing Magazine, IEEE, Vol. 21 , pp 26 – 54, Nov. 2004.

[33] H. F. Harmuth, “Transmission of Information by Orthogonal Functions”, 1sr Edition, Springer, 1969.

[34] H.F. Harmuth, “Range-Doppler Resolution of Electromagnetic Walsh Waves in Radar”, IEEE Trans. Electromagn. Compat., EMC-17, 106-111, 1975.

[35] H.F. Harmuth, “Synthetic aperture radar based on nonsinusoidal functions pulse compression, contrast, resolution, and Doppler shift”, IEEE Transaction on Electromagnetic Compatibility, EMC-21, pp. 40-49, 1979.

[36] H.F. Harmuth, “Nonsinusoidal waves for radar and radio communication.” New York: academic, 1981.

[37] H.F. Harmuth, “Antennas and waveguide for nonsinusoidal waves”, New York: academic, 1984.

[38] G.F. Ross, K.W. Robbins, “Base-band radiation and reception system”. U.S. Patent 3,739,392, Jun. 1973.

[39] G.F. Ross, K.W. Robbins, “Narrow range-gate baseband receiver”. U.S. Patent 4,695,752, Sep. 1987.

[40] G.F. Ross, “Transmission and reception system for generating and receiving base-band duration pulse signals for short base-band pulse communication system”. U.S. Patent 3,728,632, Apr. 1973.

[41] P. Van Etten, “The present technology of impulse radars,” Int. Radar Conf. Proc. 535-539, Oct. 1977.

[42] R. A. Scholtz, “Impulse Radio: How it works,” IEEE Communications Letters, Vol. 2, NO. 1, Jan. 1998.

[43] R. A. Scholtz, “Wide Bandwidth Time-Hopping Spread-Spectrum Impulse Radio for Wireless Multiple-Access Communications”, Ultra IEEE Transactions On Communications, Vol. 48, No. 4, Apr. 2000.

[44] R. A. Scholtz, “Characterization of Ultra-Wide Bandwidth Wireless Indoor Channels”, a Communication Theoretic View, IEEE Journal On Selected Areas In Communications, Vol. 20, NO. 9, Dec. 2002.

[45] M. Z. Win, “On the Robustness of Ultra Wide Bandwidth Signals in Dense Multipath Environments,” IEEE communications letters, Vol. 2, NO. 2, Feb. 1998.

[46] M. Z. Win, “On the Energy Capture of Ultrawide Bandwidth Signals in Dense Multipath Environments”, IEEE Communications Letters, Vol. 2, No. 9, Sep. 1998.

[47] M. Z. Win, “Performance of Rake Reception in Dense Multipath Channels: Implications of Spreading Bandwidth and Selection Diversity Order”, IEEE Journal On Selected Areas In Communications, Vol. 18, NO. 8, Aug. 2000.

[48] M. Z. Win, “Spectral Density of Random UWB Signals”, IEEE Communications Letters, Vol. 6, NO. 12, Dec. 2002.

[49] M. Z. Win, “Spectral Density of Random Time-Hopping Spread Spectrum UWB Signals with Uniform Timing Jitter”, Military Communications Conference Proceedings. MILCOM. vol.2, pp 1196 – 1200, 1999.

[50] M. Z. Win, “A Unified Spectral Analysis of Generalized Time-Hopping Spread-Spectrum Signals in the Presence of Timing Jitter,” IEEE JOURNAL On Selected Areas In Communications, Vol. 20, NO. 9, Dec. 2002.

[51] J. Y Lee and R. A. Scholtz, "Ranging in a dense multipath environment using an UWB radio link," in IEEE Journal of Selected Areas Communication, 20(9), pp1677–1683, 2002.

[52] FCC, “Revision of part 15 of the commission’s rules regarding Ultra-Wideband transmission systems”, Federal Communications Commission, Washington, D.C., Tech. Ref. ET Docket 98-153, Apr. 2002.

[53] S. Frattasi, F.D. Rosa, and D. Dardari, "Ultra-wideband Positioning and Tracking," In "Mobile Positioning and Tracking (eds S. Frattasi and F.D. Rosa),". 2007, https://doi.org/10.1002/9781119068846.ch9

[54] D. J. Taylor, “Introduction to ultra wideband radar systems,” CRC Press, 1995.

[55] IEEE Standard for Low-Rate Wireless Networks, in IEEE Std 802.15.4-2015 (Revision of IEEE Std 802.15.4-2011) , vol., no., pp.1-709, 22 April 2016, doi: 10.1109/IEEESTD.2016.7460875.

[56] P. Pagani, F. T. Talom, P. Pajusco, B. Uguen, "Ultra-Wideband Radio Propagation Channels: A Practical Approach,” Wiley, 2008.

[57] C. E. Shannon, “Communication in the Presence of Noise,” Proceedings Of The Ire, vol. 37, no. 1, pp. 10–21, Jan. 1949.

[58] L.Fullerton, “UWB Waveforms and Coding for Communications and Radar,” Telesystems Conference, Proceedings. Vol.1., NTC, National, pp : 139 - 141, Mar. 1991.

[59] ECC, “L’utilisation dans des conditions harmonisées du spectre radioélectrique pour des équipements fonctionnant grâce à la technologie à bande ultra large," Journal Officiel de l’Union Européenne, Avr. 2009.

[60] Apple Nearby Interactions. Accessed: Apr. 2023. [Online]. Available: https://developer.apple.com/documentation/nearbyinteraction

[61] Y. Duroc and A. Imran, ‘UWB Antennas: Design and Modeling’, Ultra Wideband. Sciyo, Aug. 17, 2010. doi: 10.5772/10002.

[62] C. A Balanis, "Antenna Theory: Analysis and Design," 4th Edition | Wiley, (consulted July 18th, 2023).

[63] V. H. Rumsey, “Frequency independent antennas,” IRE International Convention Record Vol. 5, pp. 114-118, Mar. 1957.

[64] J. D Dyson, “The equiangular spiral antennas,” IRE on antennas and propagation, pp. 181-187, 1959.

[65] N. E. Lindenblad, “Wide band antenna,” in U.S Patent 2,239,724, 29, Apr. 1941.

[66] L. N. Brillouin, “Broad Band Antenna,” in U.S. ATENTE 2, p 454, 766, Nov. 1948.

[67] J. Liang, C. C. Chiau, X. Chen , C. G. Parini, “Printed circular disc monopole antenna for ultra-wideband applications,” Electronics Letters, Vol. 40, No. 20 3 (1246-1248), , Sep. 2004.

[68] C. Y. Huang, W. C. Hsia, “Planar Elliptical Antenna for Ultra wideband Communications,” Electronics Letters, Vol. 41, No. 6, 2 (296-297), Mar. 2005.

[69] S. H. Choi, J. K. Park, S. K. Kim, and J. Y. Park, "A new ultra-wideband antenna for UWB applications,” Microwave and Optical Technology Letters, Vol. 40, No.5, pp. 399-401, Mar. 2004.

[70] Qorvo DWM1000 UWB transceiver. Accessed: March. 2023. [Online]. Available: https://www.qorvo.com/products/p/DWM1000

[71] D. Coppens, A. Shahid, S. Lemey, B. V. H. C. Marshall, et E. De Poorter, « An Overview of Ultra-WideBand (UWB) Standards and Organizations (IEEE 802.15.4, FiRa, Apple): Interoperability Aspects and Future Research Directions », IEEE Access, vol. 10, p. 70219-70241, 2022, doi: 10.1109/ACCESS.2022.3187410.

Chapter 2

Time-domain analysis of time-based ranging with UWB antennas

2.1 Introduction

Starting from the IEEE amendment 802.15.4a, the transmitted UWB signals were changed from extremely wideband baseband pulses [1, 2] to modulated pulses with bandwidths of 500 MHz, that is, pulse durations equal or superior to 2 ns [3]. Consequently, from that point on, the efforts in the theoretical research in antenna design no longer needed to focus on finding solutions to the problems of extending antenna bandwidths to several GHz to cover the whole UWB frequency spectrum [4], nor on ensuring no pulse distortion occurs after the signal is transmitted in the propagation channel [5–8]. However, the fact that it is more easily feasible for antennas to accommodate 500 MHz bandwidths instead of 7 GHz bandwidths does not mean that research in the UWB antenna field has found a line end, instead, the focus of this research is turned to other interests, for example, studying the integration of the UWB antennas in real localization systems [9]. Indeed, just like in any other technology, designing UWB antennas as a stand-alone component is not sufficient to ensure that high accuracy localization will be achieved. To conduct these studies effectively, it is crucial to accurately simulate the UWB system as it operates in practical settings. This involves modeling the UWB signal as it is applied to the transmitting antenna, and subsequently examining its behavior after the antenna emits it into the propagation channel towards the receiver antenna. Therefore, this chapter presents a time and frequency domain study of the UWB signal and antennas with a focus on localization applications, by evaluating time-of-light performance for different metrics : reader-tag distance, and azimuth and elevation angles.

2.2 Time-domain analysis principle

Time domain analysis refers to the study of the changes in the UWB signal after it has been sent by the antenna through the propagation channel [10]. This definition applies to any signal and not just UWB signals. Specifically, here, for applications of localization, the study focuses on extracting the time-of-arrival of the signal as it is sent to reception probes [10–12], and then on analyzing the changes in this time depending on various factors. These factors are expected to influence the UWB signal [13]. Here we focus on the distortion of the signal, influence of azimuth and elevation angles, and the distances at which reception probes could be placed.

2.2.1 UWB signal processing chain

Figure 2.1 illustrates a UWB transceiver as specified by the IEEE organization. Although, the IEEE standards 802.15.4 and 802.15.4z only specify the transmitter operation [14], the receiver is also illustrated here, as it performs the inverse operations of the transmitter.

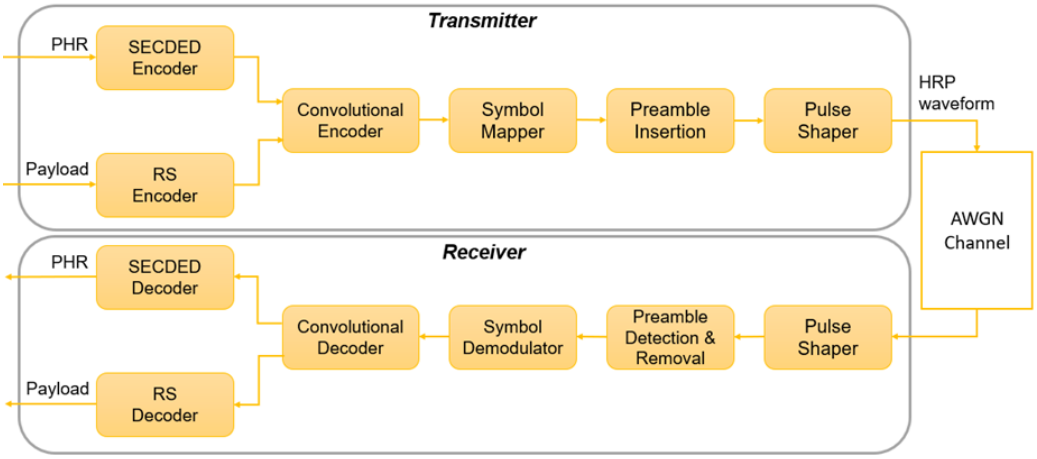

FIGURE 2.1: UWB Transceiver chain composition.

The transmitter consists of two inputs, the Physical Header (PHR) and a Payload. The PHR contains UWB specific information, such as datarate, preamble duration and frame lengths. The transmission chain operates by the following steps:

- First, the PHR is encoded with a Hamming code using "single-error correcting and double-error detecting" (SECDED) coding method.
- The payload is encoded / decoded with a (63, 55) Reed-Solomon code.
- The PHR and the payload are then encoded by a convolutional code.
- The bitstream is then converted to complex symbols by a symbol mapper.
- Next, the preamble insertion block selects a code sequence which is then spread and repeated, as the receiver expects the input waveform to begin with the preamble.
- The pulse shaper receives the output of symbol mapping and preamble insertion, which are ternary symbols (-1,0,1). The ternary symbol sequence is then applied as an input to a conformal filter (for example: butterworth filter or root-raised cosine filter) to create pulses.
- After pulse shaping, the ultra-wideband signal is transmitted over the air using UWB antennas.

In the following, the chapter focuses on the output UWB signal from the pulse shaper, its transmission from the UWB antenna and its propagation in the air until reception.

2.2.2 The IEEE 802.15.4a complying transmitted UWB signal

The amendment IEEE 802.15.4a specifies the conditions to which any time domain signal fed to UWB antennas must conform [3, 14], in terms of shape and also of power spectral density mask. This conformance is verified by the correlation of the used signal with a signal specified. For UWB signals, this specified signal is of type root-raised-cosine pulse (RRC) and recently, of duration 2 ns (that is, 500 MHz of bandwidth in the frequency domain), for most UWB defined channels. The amendment specifies that the correlation of the user-defined UWB pulse with the required RRC pulse must be at least of 0.8 (80 % correlation) or higher for the used baseband pulse to be considered complying with the UWB PHY Layer of the IEEE standard.
The standard states that the transmitted pulse shape p(t) shall be constrained by the shape of its cross-correlation function with a standard reference pulse, r(t). The normalized cross-correlation between two waveforms is defined as follows [14] :

$$\phi(\tau) = \frac{1}{\sqrt{E_r E_p}} Re \int_{-\infty}^{+\infty} r(t).p^*(t+\tau)dt \tag{2.1}$$

where E_r and E_p are the energies of $r(t)$ and $p(t)$, respectively, p^* denotes the complex conjugate of p, and, Re indicates that the real part is used. The reference $r(t)$ pulse used in the calculation of $|\phi(\tau)|$ is a RRC pulse with a roll-off factor of $\beta = 0.5$. Mathematically, the equation of a RRC pulse is as follows [14, 15] :

$$r(t) = \frac{4\beta}{\pi\sqrt{T_p}} \frac{cos[(1+\beta)\frac{\pi t}{T_p}] + \frac{sin[(1-\beta)\frac{\pi t}{T_p}]}{4\beta\frac{t}{T_p}}}{1-(\frac{(4\beta t}{T_p})^2} \tag{2.2}$$

where T_p is the required duration for a pulse operating in a UWB channel, for example the duration in channel 9 is 2 ns.
Furthermore, in order for a high-rate pulse (HRP) UWB PHY transmitter to be compliant with this standard, the transmitted pulse $p(t)$ shall have a magnitude of the cross-correlation function $|\phi(\tau)|$ whose main lobe magnitude is greater than or equal to 0.8 for a main lobe duration T_w of at least 0.5 ns for channel 9, and any sidelobe magnitude shall be no greater than 0.3.
To test a pulse for compliance, let $|\phi(\tau)|$ be the magnitude of the cross-correlation of $p(t)$ and $r(t)$, and let τ_i, for i = 1,2, . . . , be a set of critical points as follows [14] :

$$\frac{d}{d\tau}|\phi(\tau)|_{\tau=\tau_i} = 0 \tag{2.3}$$

The maximum happens at point τ_{max}, where the condition $|\phi(\tau_{max})| \geq |\phi(\tau)|$ is verified for all values of τ. In addition, the second constraint on the value of sidelobes may be stated mathematically as $|\phi(\tau_i)| \leq 0.3$ for all τ_i values.

Figure 2.2 illustrates an example of a HRP UWB-compliant pulse, $p(t)$ (left plot), along with the root raised cosine reference pulse $r(t)$ (middle plot) with $T_p = 2.0$ ns and the magnitude of the cross-correlation $|\phi(\tau)|$ (right plot). The pulse $p(t)$ is an 8 order butterworth pulse with a 3 dB bandwidth of 500 MHz. The figure is intended to show that this example pulse meets the requirements for compliance. Specifically, the main lobe is above 0.8 for nearly 1 ns, and no sidelobe is greater than 0.3 (in this case, the largest sidelobe peak is 0.2). The pulse $p(t)$ is a compliant pulse for UWB channels {0:3, 5:6, 8:10, 12:14}.

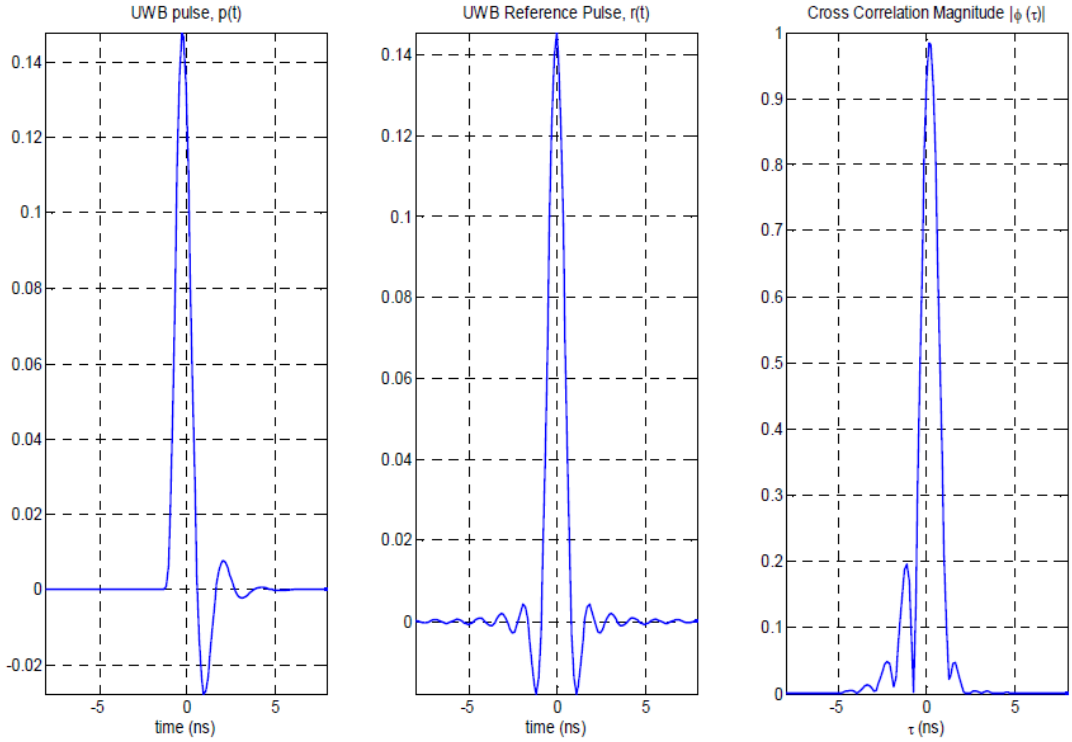

FIGURE 2.2: Example of a compliant pulse: butterworth pulse p(t) (left), root raised cosine reference pulse r(t) (middle), and magnitude of their cross-correlation $|\phi(\tau)|$ (right) [14].

2.2.3 UWB PHY Compliant signal generation

Although the conformance verification is based on the baseband pulse of bandwidth 500 MHz, the signal fed to the antenna consists in this pulse upconverted to the center frequency of a chosen UWB channel. The user-defined time-domain pulse signal can be of any type, for example, it can be a Butterworth pulse, or it can also be a RRC pulse (as long as its cross-correlation with the reference pulse is as specified by the standard).
In this work, MATLAB software is used to generate the signal which will be subsequently fed to the UWB antenna.

First, for the convenience of easier conformance a RRC pulse is chosen, described by equation 2.2. Then, this signal is upconverted to the frequency 7.9 GHz (center frequency of channel 9) by the principle of RF mixing with a continuous cosine wave oscillating at this frequency. That is, the RCC is used for amplitude modulation of the cosine signal. For this, the two signals are mixed by the multiplication of the time-domain RRC pulse with the 7.9 GHz cosine wave.
Besides, it is worth to note, that UWB channel 9 was chosen for its worldwide availability. The design of the antenna used in the following study was also focused on this channel.

The objective is to create a UWB signal ready to be applied at the antenna input to test its time-domain response through EM simulations. However, Matlab and most signal processing softwares, operate with samples to create signals, even continuous ones. In fact, this continuity can only be observed if the number of samples is high

enough to make the signal appear continuous. Consequently, requirements such as the Nyquist requirement [16] need to be considered in the construction of the signal with such softwares.

Nyquist requirement

Following on the number of samples used to create a time-domain signal, not only this number has to be high enough to be able to observe a correct signal, the sample rate (number of samples per second), must be at least equal or higher than the Nyquist frequency to avoid aliasing [17–19] as it causes the overlapping of frequency components of the signal.
Indeed, aliasing causes distortions to the signal that is being constructed from samples, making it differ from the original continuous signal. Consequently, to avoid aliasing and its negative impacts on the signal generated, the requirement suggests that the chosen sample rate, must be at least twice the frequency of the signal (here 7.9 GHz), to even approximately represent the signal. A better rule of thumb is that this rate should be at least 10 samples per period of the signal. Thus, for a signal at 7.9 GHz, a sampling rate of ideally 79 GHz to obtain a relatively clean representation of the signal. This would mean that, for example, for a 16 ns of time span, the number of samples required is:

$$N_{samples} = (time\ span).(sample\ rate) = (16.10^{-9})(79.10^{9}) = 1264 \qquad (2.4)$$

It is worth to note that in CST Microwave, the maximal number of samples that can be processed for the excitation signal is 40000 samples.

2.3 Analysis of an antenna operating at one UWB channel

Figure 2.3 illustrates the steps of the analysis. The IEEE compliant UWB pulse signal generated, is used as the excitation signal for the designed UWB patch antenna in CST Microwave. Field probes are placed at different distances from the antenna and play the role of receivers, that allows to assess the signal after it has left the antenna.

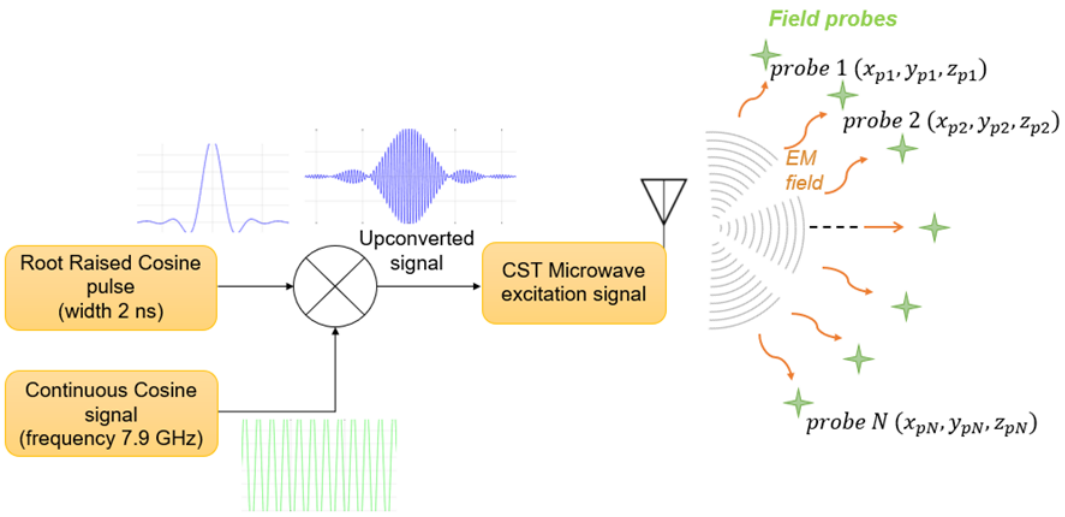

FIGURE 2.3: The steps of the time-domain analysis of UWB signals' propagation.

2.3.1 Excitation signal generation and processing using Matlab

The pulse chosen is a RRC pulse for the maximum correlation with the RRC specified by the standard. It was constructed using a time width of 2 ns, a roll off factor of 0.5 and with a time span of 16 ns. Then, this pulse is mixed with a continuous cosine wave oscillating at 7.9 GHz for modulation. The resulting signal is constructed with 8000 samples which corresponds to a higher number of samples necessary to avoid aliasing. Figure 2.4 below illustrates the subject signals.

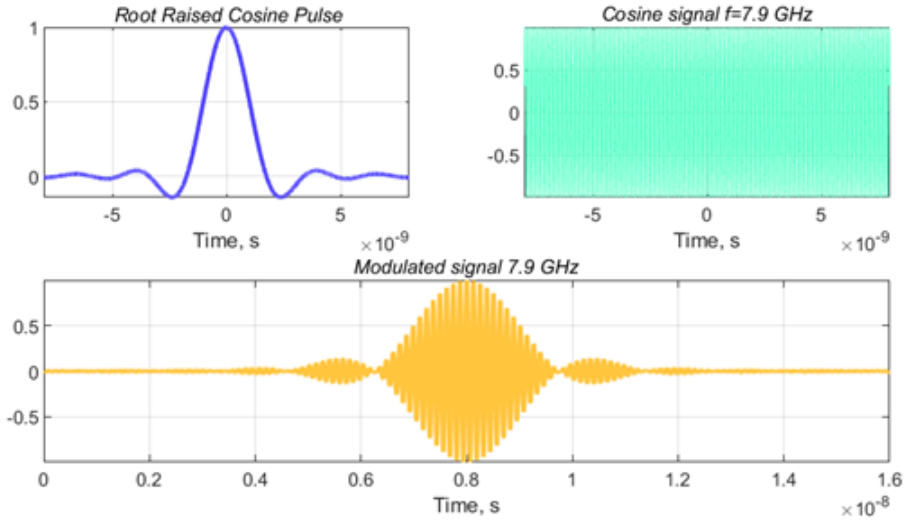

FIGURE 2.4: Construction of the IEEE compliant UWB pulse by RF mixing.

2.3.2 Antenna characteristics

Figure 2.5 presents the UWB antenna studied, and its characteristics described below:

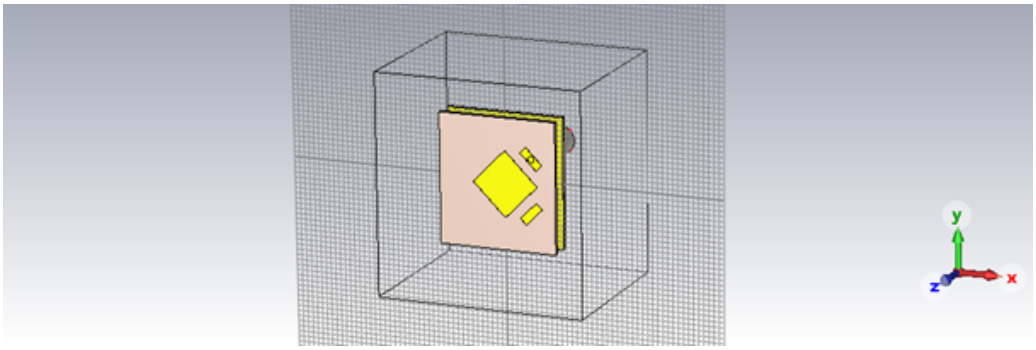

FIGURE 2.5: Studied UWB patch antenna structure.

- Bandwidth: 500 MHz (7.75 GHz – 8.25 GHz), operation on the worldwide available UWB channel 9.
- Antenna physical shape: probe-capacitively-fed UWB patch antenna.
- Antenna radiation type: 180° directional .

- Polarization types studied: first, linear polarization, then circular polarization added to the patch antenna by the means of a branchline coupler enabling two orthogonal capacitive feeds.
- Excitation signals studied: default CST excitation, then IEEE standard specified UWB excitation signal (RRC pulse of bandwidth 500 MHz).

Figures 2.6 and 2.7 show the reflection coefficient and radiation patterns of this antenna, respectively.

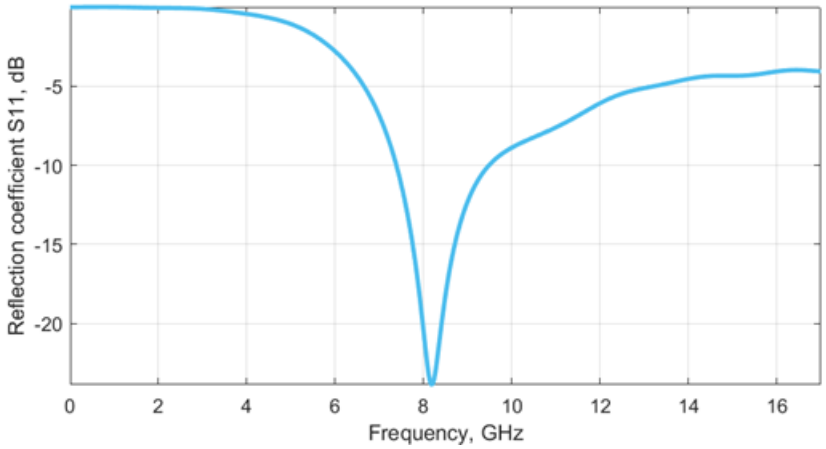

FIGURE 2.6: Reflection coefficient of the UWB antenna studied.

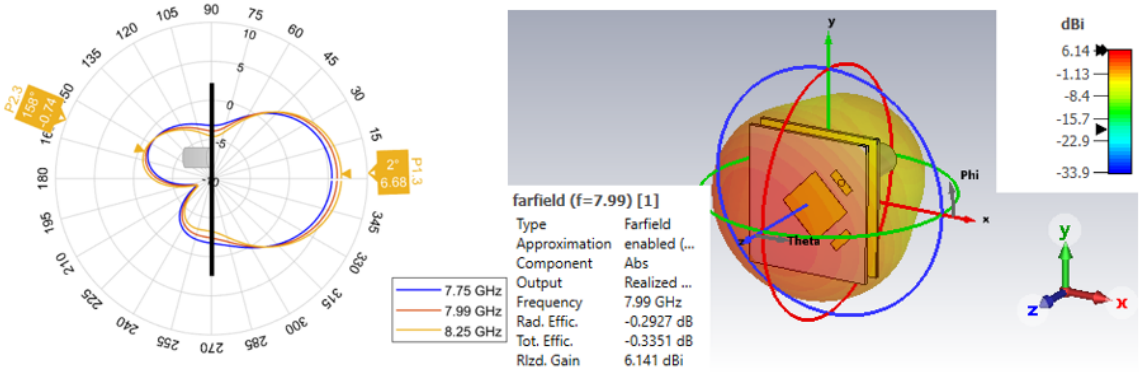

FIGURE 2.7: Radiation patterns of the UWB antenna, (left): 2-dimensional polar pattern, (right): 3-dimensional pattern.

2.3.3 EM simulation

The resulting signal is applied to the input port of the designed UWB probe-fed patch antenna by simulations in CST Microwave. The objective is to analyze its performance by extracting the time-of-arrival of the UWB signal to the field probes. First, since the farfield is the field of interest in this study, the near-field distance D limit is calculated. For a certain frequency, it can be obtained by [20] :

$$D = \frac{2\,d^2\,f}{c} \tag{2.5}$$

With d the largest length of the antenna, f is the center frequency of the channel, and c the light velocity. We have f = 7.9 GHz and d = 25 mm, thus:

$$D = \frac{2(0.025)^2\ 7.9\ 10^9}{3\ 10^8} = 0.0329\ m = 33\ mm \tag{2.6}$$

Starting from the distance 33 mm the near field area ends and the far field area begins. For the remaining study, probes are placed at a minimum distance of 68 mm, which represents more than twice the limit D calculated, to ensure being at the farfield region.

Received E-farfield assessment

The radiated Electric field (farfield) from the antenna is observed with probes placed at positions of coordinates (x_{pn}, y_{pn}, z_{pn}), with n an integer representing the probe number. The positions of these probes are varied and the following metrics are evaluated: the electric field waveform and magnitude in time and frequency domains, and the time of arrival at each probe.

- Observation probes along the z-propagation axis:

In this part, the aim is to observe the effect of distance increasing between a transmitting UWB antenna and receiver probes placed: along the propagation axis z (such as they are aligned with the center of the radiating element), thus the probes have coordinates $(0, 0, z_{pn})$ as shown in figure 2.8. The coordinate z_{pn} varies by probe and is chosen such that it is placed in the far field region of the antenna $(z_{pn} > 3.3\ cm)$.

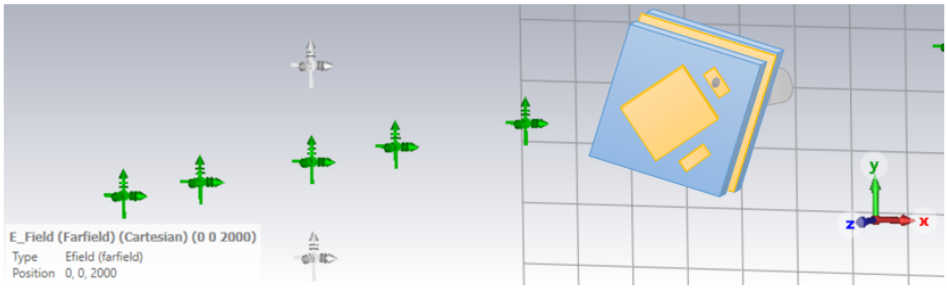

FIGURE 2.8: Receiver probes along the propagation axis of the antenna, for E-field observation.

The probes were placed at 10 cm, 25 cm, 50 cm, 1 m, and 2 m on the propagation axis. The resulting E-field magnitude in frequency domain for each receiving probe is illustrated in the figure 2.9. It shows that, for all distances, the magnitude is highest at the antenna's UWB channel frequencies (7.75 GHz – 8.25 GHz) and reaches its maximum at the channel's center frequency (7.9 GHz). Furthermore, the comparison between the E-fields at the different probes shows that the magnitude decreases with increasing the distance at all the frequencies.

Figure 2.10 presents the resulting E-field in the time domain, at the same observation probes. The time signals observed are the magnitude (absolute value) of the received E-field components time signals $E(E_x, E_y, E_z)$, which represents the absolute value of the RRC shape at each probe. It can be seen that the RCC waveforms do not present any distortions. Moreover, the important characteristic presented by these shapes is their time of arrival, as it shows that, the further the probe is from the

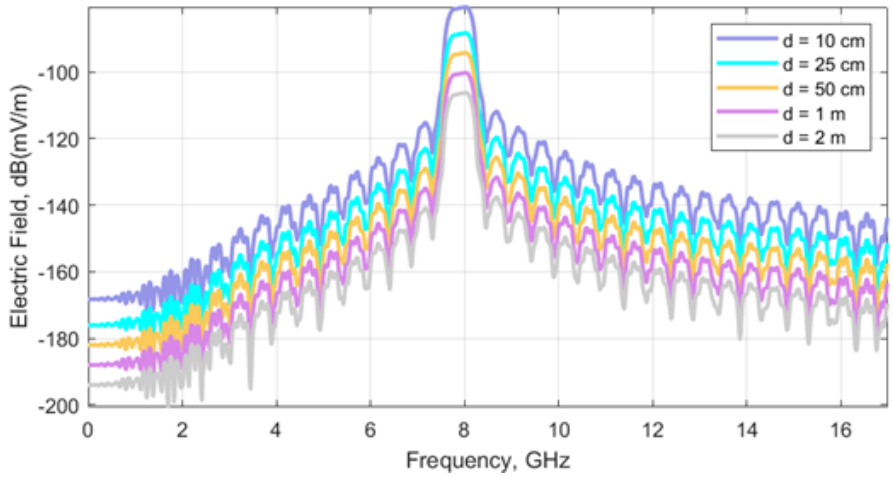

FIGURE 2.9: Received E-field waveform in frequency domain, and its variation with distance between the antenna and the probes.

antenna, the later in time the signal arrives. This time of arrival at the probe is the time used in ranging and localization to compute the distance between the reader and the target.

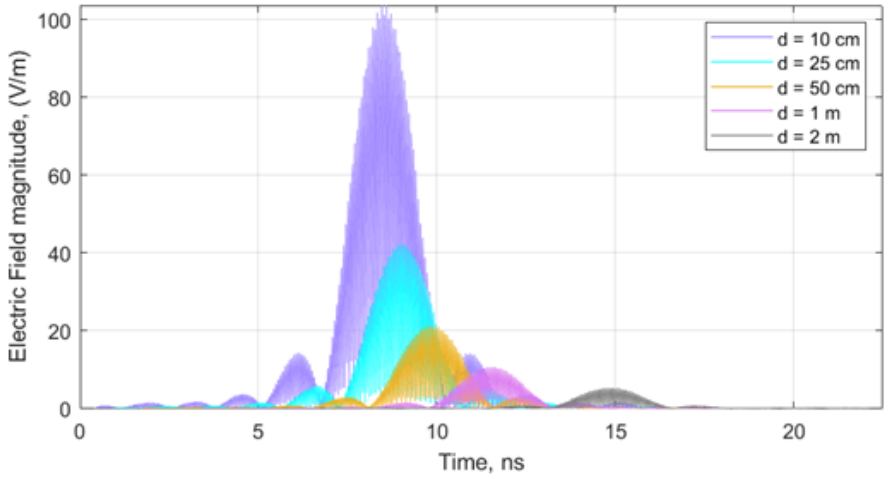

FIGURE 2.10: Received E-field waveform in time domain, and its variation with distance between the antenna and the probes.

- Observation probes along y-axis (in front of the antenna):

In this part, the purpose is to observe the effect of y-axis probes on the time of arrival, in front of the antenna, where the target's position can happen to be. Three probes were placed: along the y axis, at the same z_{pn} distance of 1 m, and the same $x_{pn=0}$ coordinate corresponding to the center of the antenna (figure 2.11). Thus, the probes have coordinates $(0, y_{pn}, 1)$ and the coordinate y_{pn} varies by probe.

First, for a clearer analysis, we analyze, the E-farfield components E_x, E_y, E_z, at one probe placed on the axis of propagation at a 1 m distance, that is, at coordinates (0,0,1). Figure 2.12 presents the resulting waveforms of the components of the field in the time domain.

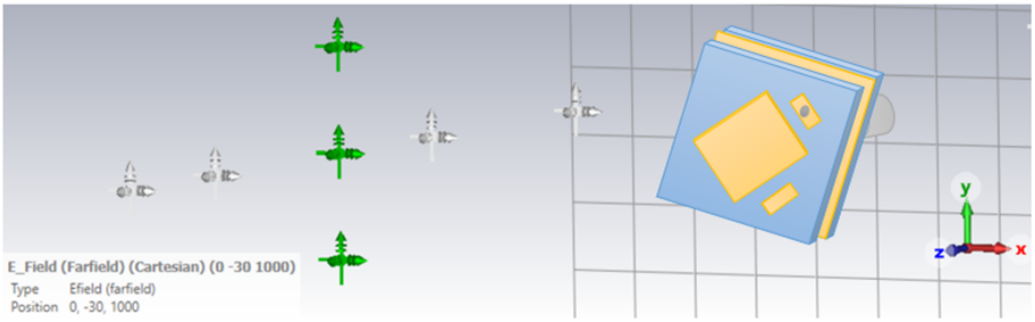

FIGURE 2.11: Receiver probes along y-axis of the antenna, for E-field observation.

The figure shows that the resulting time of arrival of all the waveforms $E_x(t)$, $E_y(t)$, $E_z(t)$ is the same as expected, with a $E_z(t)$ signal magnitude being null because the field has no component on the direction of propagation.
Furthermore, a difference in magnitude is observed between $E_x(t)$, $E_y(t)$ at all time instants, this difference is due to the excitation point of the antenna not being completely on the diagonal of the axes x and y, as it was not a necessity during the design process. A further observation is that the signal waveforms observed are identical to the input RRC waveform and present little to no distortion in shape. These observations remain the same for the waveforms of all E-farfield probes regardless of their coordinates. In the following, we compare between the resulting E-farfields at different probes' using only one field component for all, that is, either $E_x(t)$ or $E_y(t)$.

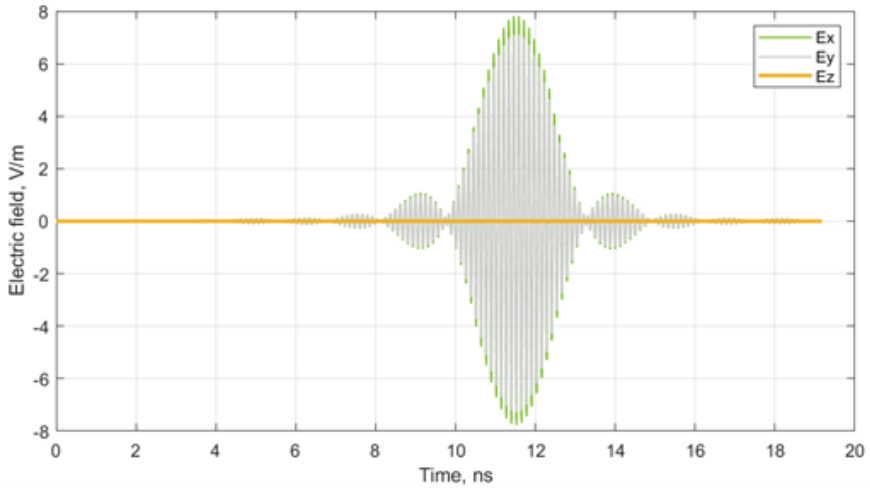

FIGURE 2.12: Waveforms of the components of the field (E_x, E_y, E_z) in the time domain, received at one probe.

We proceed with analyzing the farfield by its component $E_x(t)$ on the y axis at a distance of 1 m in front of the antenna, by placing the probes at coordinates $(0, y_{pn}, 1)$, as shown in figure 2.11. The values of y_{pn} simulated are 0 cm, - 6 cm, 6 cm , 10 cm, and -10 cm (with the reference 0 being the y coordinate of the center of the radiating element of the antenna). Figure 2.13 presents the result of the received $E_x(t)$, and figure 2.14 presents a zoomed-in version on the shapes of the RRCs at the center of the envelope.

The results show that the closer to the center of the antenna (y=0), the faster the

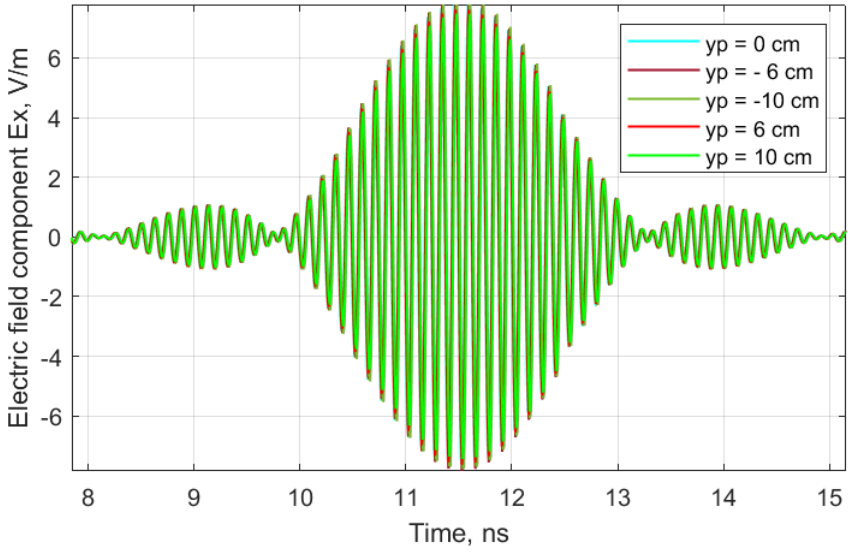

FIGURE 2.13: E-field component waveform $E_x(t)$ and its variation with y-axis coordinates.

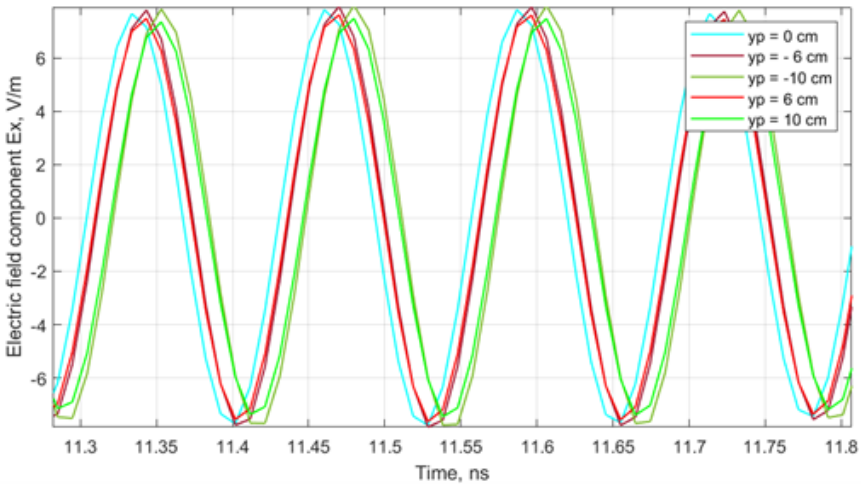

FIGURE 2.14: E-field component waveform $E_x(t)$ and its variation with y-axis coordinates, zoomed-in version.

field reaches the probe target (when analyzing for vertically placed probes on the y axis, at the same z distance from the antenna and the same x coordinate), hence the observed signal $E_x(t)$ has a smaller time of arrival for the probe of y=0 than all the other probes, and the signal that reaches last is the one corresponding to the probe of y=10 cm. Furthermore, a symmetry around the center of the radiating element is present, as the times of arrival are identical for probes placed symmetrically (y=6 cm and y=- 6 cm) and (y=10 cm and y= -10 cm).
The difference in the time of arrival is expected as the probes are in the farfield region, where the antenna can be modeled by a source point. Thus, the time of arrival measured corresponds to the time it takes the signal to travel from the center of the antenna to each probe, which makes the probes at y > 0 or y < 0 farther from the antenna compared to the probe at y = 0.

- Observation probes at the extremities (in front and at the sides of the antenna):

In the previous experiment with probes, it was found that the time of arrival is almost identical for probes at different height points, at the same distance in front of the antenna. The objective of the following experiment, is to evaluate if this time of arrival is also identical for probes at different points in around the antenna. For this, three probes are placed as follows: the first in front of the antenna, and the other two at both the left and right extremities (figure 2.15). The three probes are far away from the antenna by the same distance, first 10 cm and then 1 m distances are tested.

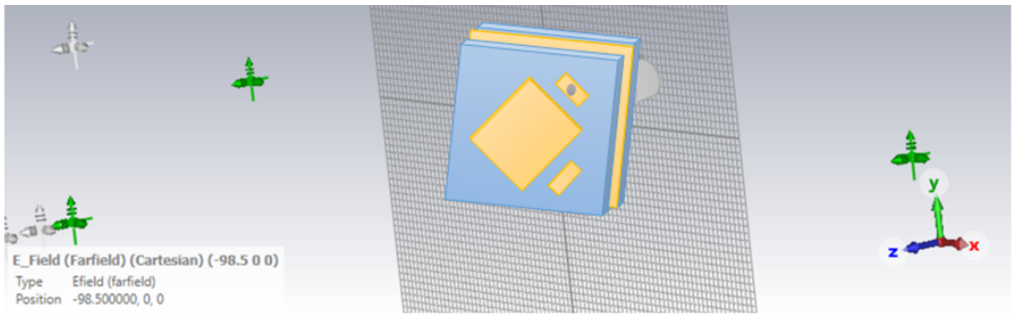

FIGURE 2.15: Receiver probes around the antenna, for E-field observation.

First, figure 2.16 illustrates the received magnitude of the E-field at each of the six probes. Results show that, for probes placed at the same distances from the antenna (10 cm or 1 m), the magnitude is higher in the case of the probe placed in front of the antenna compared to the extremities, in both distance cases 10 cm and 1 m. This is expected as the gain of the patch antenna is the highest in front of the antenna and weaker at the extremities.

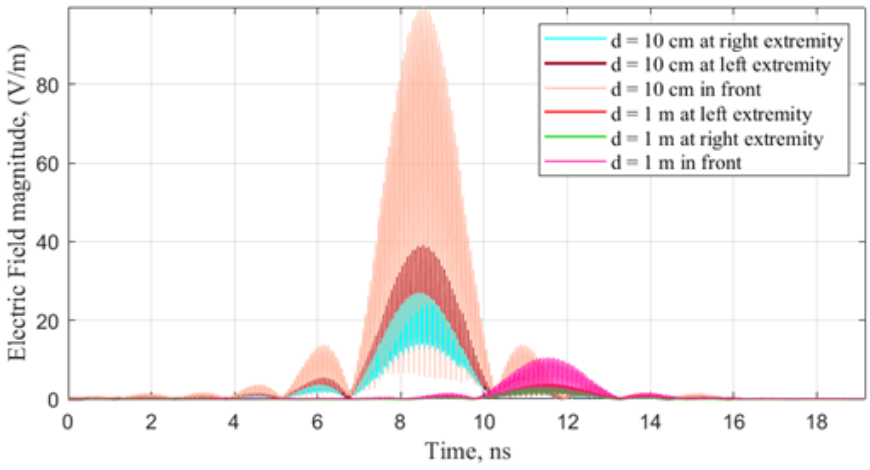

FIGURE 2.16: Received E-field magnitude waveform in time domain, and its variation with probes at center in front and at the extremities of the antenna.

2.3.4 Discussion

The analysis of the time of arrival of the E-field radiated by the UWB antenna has shown that:

- Probes (or any receiving tag) placed at a distance from the antenna will be characterized by the same time-of-arrival of the UWB signal as long as they belong to the circumference of the same sphere where the antenna is at the center (figure 2.17). This time will thus, yield identical distance estimates. This suggests that azimuth and elevation angles, at which a tag can be placed, do not influence the time-of-arrival of the signal if two tags are both placed at an azimuth (or elevation) circle of the same radius, around the antenna.
- The radiation pattern of an antenna does not have an influence on the accuracy of localization using time-based techniques, such as time-way ranging.

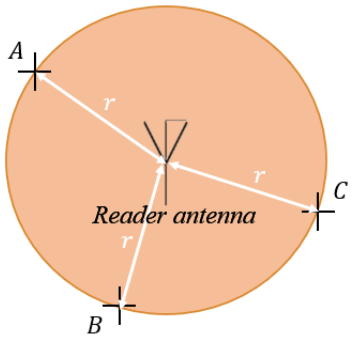

FIGURE 2.17: A, B, C tags yield the same times of arrival.

2.4 Conclusion

In this chapter, a time-domain analysis was performed to study UWB antennas and signals from transmission to reception.
An excitation signal UWB pulse conformal to the IEEE standard was generated and applied at the input of a UWB antenna of 500 MHz of bandwidth. In the context of localization with time-based technique, receive probes were placed at different distances and positions around the antenna to study the radiated electric field shape and the time of arrival of the signals. Results showed that the accuracy of localization with UWB antennas, is not influenced by different azimuth and elevation angles (same times of arrival) of the radiation pattern, however this latter influences the magnitude level of the signal as the antenna gain varies depending on the direction studied.

Bibliography

[1] K. Siwiak and D. McKeown, "Ultra Wideband Radio Technology", 2nd Edition, chapter "Generating and transmitting UWB signals". Chichester: John Wiley and Sons Ltd, 2004, doi: 10.1002/0470859334.

[2] V. Sipal, B. Allen, D. Edwards, B. Honary, "Twenty years of ultrawideband: Opportunities and challenges," Communications, IET , vol.6, no.10, pp.1147-1162, July 3 2012, doi: 10.1049/iet-com.2011.0281.

[3] "IEEE Standard for Local and metropolitan area networks–Part 15.4: Low-Rate Wireless Personal Area Networks (LR-WPANs)," in IEEE Std 802.15.4-2011 (Revision of IEEE Std 802.15.4-2006) , vol., no., pp.1-314, 5 Sept. 2011, doi: 10.1109/IEEESTD.2011.6012487.

[4] John, M. and Ammann, M.J. (2005), "Optimization of impedance bandwidth for the printed rectangular monopole antenna," Microw. Opt. Technol. Lett., 47: 153-154. https://doi.org/10.1002/mop.21109

[5] M. John and M. J. Ammann, "Antenna Optimization With a Computationally Efficient Multiobjective Evolutionary Algorithm," in IEEE Transactions on Antennas and Propagation, vol. 57, no. 1, pp. 260-263, Jan. 2009, doi: 10.1109/TAP.2008.2009775.

[6] L. Lizzi, F. Viani, R. Azaro and A. Massa, "Optimization of a Spline-Shaped UWB Antenna by PSO," in IEEE Antennas and Wireless Propagation Letters, vol. 6, pp. 182-185, 2007, doi: 10.1109/LAWP.2007.894157.

[7] A. J. Kerkhoff and H. Ling, "Design of a Band-Notched Planar Monopole Antenna Using Genetic Algorithm Optimization," in IEEE Transactions on Antennas and Propagation, vol. 55, no. 3, pp. 604-610, March 2007, doi: 10.1109/TAP.2007.891563

[8] M. John and M. J. Ammann, "Wideband Printed Monopole Design Using a Genetic Algorithm," in IEEE Antennas and Wireless Propagation Letters, vol. 6, pp. 447-449, 2007, doi: 10.1109/LAWP.2007.891962.

[9] V. Sipal, M. John, D. Neirynck, M. McLaughlin and M. Ammann, "Advent of practical UWB localization: (R)Evolution in UWB antenna research," The 8th European Conference on Antennas and Propagation (EuCAP 2014), The Hague, Netherlands, 2014, pp. 1561-1565, doi: 10.1109/EuCAP.2014.6902082.

[10] M. J. Ammann, A. Dumoulin, M. John and P. McEvoy, "Time-domain performance of printed UWB antennas," 2009 3rd European Conference on Antennas and Propagation, Berlin, Germany, 2009, pp. 3766-3769.

[11] L. Guo, J. Liang, C.C.Chiau, X. Chen, C.G.Parini and J. Yu, " Performance of UWB disc monopoles in time domain", IEE Proceedings on Microwaves, Antennas and Propagation, vol.1, no.4, August 2007, pp. 955-959, doi: 10.1049/iet-map:20050253.

[12] J. Liang, L. Guo, C. C. Chiau and X. Chen, "Time domain characteristics of UWB disc monopole antennas," The European Conference on Wireless Technology, 2005., Paris, France, 2005, pp. 289-292, doi: 10.1109/ECWT.2005.1617714

[13] A. Dumoulin, M. John, M. J. Ammann and P. McEvoy, "Performance evaluation of antennas for UWB radar and positioning systems," IET Irish Signals and Systems Conference (ISSC 2009), Dublin, 2009, pp. 1-6, doi: 10.1049/cp.2009.1729.

[14] "IEEE Standard for Low-Rate Wireless Networks," in IEEE Std 802.15.4-2015 (Revision of IEEE Std 802.15.4-2011) , vol., no., pp.1-709, 22 April 2016, doi: 10.1109/IEEESTD.2016.7460875.

[15] D. Dardari, A. Conti, U. Ferner, A. Giorgetti and M. Z. Win, "Ranging With Ultrawide Bandwidth Signals in Multipath Environments," in Proceedings of the IEEE, vol. 97, no. 2, pp. 404-426, Feb. 2009, doi: 10.1109/JPROC.2008.2008846.

[16] C. E. Shannon, "Communication in the Presence of Noise," in Proceedings of the IRE, vol. 37, no. 1, pp. 10-21, Jan. 1949, doi: 10.1109/JRPROC.1949.232969.

[17] L. Yong, S. Lv, and X. Wang, "Adaptive Sub-Nyquist Spectrum Sensing for Ultra-Wideband Communication Systems" Symmetry 11, no. 3: 342, https://doi.org/10.3390/sym11030342.

[18] S. Cui, "Performance analysis of impulse-radio ultra-wideband techniques for low-rate communications," Doctoral thesis, Nanyang Technological University, Singapore, 2014, https://doi.org/10.32657/10356/61813.

[19] S. -W. M. Chen and R. W. Brodersen, "A Subsampling Radio Architecture for Ultrawideband Communications," in IEEE Transactions on Signal Processing, vol. 55, no. 10, pp. 5018-5031, Oct. 2007, doi: 10.1109/TSP.2007.896056.

[20] C. A. Balanis, "Antenna Theory: Analysis and Design (3rd ed.)", 2005, Chapter 2, page 34.

Chapter 3

Advancements in Industrial RTLSs: A Technical Review of UWB Localization Devices Emphasizing Antennas for Enhanced Positioning

3.1 Introduction

The internet of things paradigm has brought over the past few years, renewed significant interest to indoor positioning, tracking and localization topics, principally as the real-time locating technology allows a reference node to infer the position of tagged target nodes, opening then the leading road to millions of object-to-object awareness applications. This chapter presents a technical review of the available industrial and commercial UWB real-time locating transceivers (RTLS) is realized, with a focus on the frontend antennas integrated in these systems to establish the needed wireless communication for positioning. Then, the different characteristics of these antennas are summarized and discussed along with their impact on the localization performance, notably in terms of the reading range, position information accuracy, object-orientation independent localization and multipath mitigation, and solutions are suggested to bring an antenna-based improvement to the RTLSs' performance.

3.2 UWB Technology in Real-Time Locating Systems

The popularity of positioning and localization field in research has always been soaring since the 1970s, as the US Department of Defense (DoD) decided to design and launch a positioning service with global coverage and continuous-time availability, the Global Positioning System (GPS) [1], at first limited for military use only and then, a decade later, expanded for civil users. This popularity is mostly always related to space-based positioning performed by global navigation satellite systems (GNSSs) such as GPS, Galileo, Glonass and BeiDou, and involving a constellation of satellites fixed on earth-centered orbital planes. However, satellites perform poorly when position-information is sought in harsh propagation environment areas, typically indoor (inside buildings, mines…), where multipath signals reflected from objects and obstacles obscure the localization desired signal. To provide reliable positioning indoors, many terrestrial-based wireless communication systems have been explored and equipped with localization abilities [2], such as localization through WiFi and Bluetooth technologies [3] widely available nowadays in almost any connected mobile device [4, 5], or through radio frequency identification (RFID) [6] by

adjusting subtly its architecture to be able to provide position-information of an object in addition to its identification [7]. However, as these technologies were not initially designed to specifically provide localization services, most of them tend to be limited in important aspects such as accuracy, space coverage and reading range at which objects can still be detected. To tackle these issues, ultrawide bandwidth (UWB) technology was introduced in radio transceivers [8] and evolved with IEEE standards [9, 10], which are then referred to as real-time locating systems (RTLS) and are able to draw consistent centimeter-level accuracy in positioning of objects indoors through their high robustness against parasitic multipath components [11].
The purpose of this work is to study how antennas can improve a RTLS's localization performance through a practical approach. For this reason, the authors propose a technical review of the commercially available industrial UWB radio chips and their evaluation boards, and a highlight summary of the frontend antennas employed or integrated in such systems. Furthermore, we discuss the error sources that can affect the radio propagation of the UWB signal between a reader and a tag in different scenarios, line-of-sight (LOS) and non-line-of-sight (NLOS). These error sources affect the detection of the desired UWB signal from which the distance is supposed to be computed for ranging. The influence of the characteristics of the antennas on the location estimates provided by an RTLS are then discussed and solutions are suggested.
The remainder of this chapter is organized as follows: Section 3 is an overview of the error sources in time-based localization for both LOS and NLOS scenarios, then, Section 4 presents the technical review of today's industrial UWB radio transceivers and RTLSs from different manufacturers, followed by a focus and summary of the antennas employed in each system. Moreover, Section 5 discusses and details the influence of antennas on the UWB localization performance and distance estimates in terms of reading range, accuracy, and tag-orientation dependent detectability and the solutions for improvement. Finally, conclusions are presented in Section 6.

3.3 UWB Localization from an industry point of view

At the earliest stages of real-time locating systems (RTLSs), technologies started from exploiting ultra-sound, sonar (in radar domains), laser from optics (such as telemeters) and vision technologies (such as in the robotics domain) [12, 13]. However, recently the current trend to approach tracking and localization problems is to use standard, low cost and already deployed technologies. Consequently, in the following, we focus only on technologies based on radio signal exchange.
Moreover, the indoor environments are very challenging; thus, multiple technologies have been proposed to cope with their constraints. Indeed, throughout the years, indoor localization has been studied and performed using several technologies, each conforming to different standards and radio frequencies. These technologies are heterogenous and include notably Wi-Fi, Bluetooth, Radio-frequency IDentification (RFID), Near Field Communications (NFC). Although, these wireless communication standards have been designed for other purposes and are not intended for localization and ranging purposes, this did not prevent their exploitation for positioning at the cost of some localization performance limitations such as shorter range, low or average accuracy and, small detectability coverage. However, since the emergence of UWB technology for the specific use in ranging, the industry followed by producing UWB-based radio chips ready for deployment in localization and positioning, that is for the measurements of the reader-to-object distance and

the direction angle of one or several objects. In this section, a review of the existing UWB radio chips and their RTLSs infrastructures (evaluation boards) is realized, and then a comparative focus on the antennas employed in such systems is performed.

3.3.1 Overview of industry available UWB chips and evaluation boards

Table 3.1 presents a summary of the UWB radio chips available in the industrial market and that are aimed at customers that wish to localize objects inside any indoor environment. The UWB spectrum frequencies these chips operate on and the localization techniques they allow are summarized.

Manufacturer	UWB chip	Freq channel	Loclization technique
Qorvo	DW1000 [14]	1, 2, 3, 4, 5	Two-way ranging or TDoA
Qorvo	DW3000 [15]	5, 9	Two-way ranging or TDoA
Apple	U1 [16]	5, 9	Two-way ranging, TDoA or AoA
NXP	SR150 [17] / SR040 [18]	5, 9	Two-way ranging, TDoA or AoA
Sunway	SW UWB chip [19]	5,9	Two-way ranging, TDoA or AoA
STMicroelectronics	MOD1 [20]	1,2,3,4	Two-way ranging or TDoA

TABLE 3.1: Summary of the UWB radio chips available in the industry, their frequencies and localization techniques.

In the following, most of the listed UWB chips and their characteristics are discussed in detail, notably their antenna type and aimed performances.

Qorvo DWM1000 chip

Qorvo's DWM1000 module is based on the DW1000 UWB transceiver IC, which is an IEEE 802.15.4a UWB implementation. It integrates antenna, all RF circuitry, power management and clock circuitry in one module. It can be used in two-way ranging or TDOA location systems to locate assets to a precision of 10 cm and supports data rates of up to 6.8 Mbps.
The antenna used in the module is the Partron dielectric chip antenna (part number ACS5200HFAUWB [21]), which is a Chip Antenna covering UWB bands from 3.2 GHz to 7.2 GHz. The antenna is shown in figure 3.1 and its characteristics are summarized in table 3.2.

FIGURE 3.1: DWM1000 frontend monopole ceramic pcb UWB antenna [21].

Parameter	Value
Type	Non ground mounting type monopole ceramic antenna
Peak gain (azimuth)	4.16 dBi at 6.2 GHz
Average gain (azimuth)	-1.10dBi at 6.2 GHz
Dimensions	8.0 mm x 6.0 mm x 1.2 mm
Polarization	Linear
Matching impedance	50 Ω

TABLE 3.2: Characteristics of the UWB monopole antenna integrated in the Qorvo DWM1000 transceiver [21].

When designing the PCB onto which DWM1000 will be soldered, the proximity of the DWM100 on-board ceramic monopole antenna to metal and other non-RF transparent materials needs to be considered carefully. Two suggested placements schemes are shown in figure 3.2. For the best RF performance, Qorvo advices that the ground copper should be flooded in all areas of the application board, except in the areas marked "Keep-Out Area" in the figure, where there should be no metal either side, above or below, such as batteries.

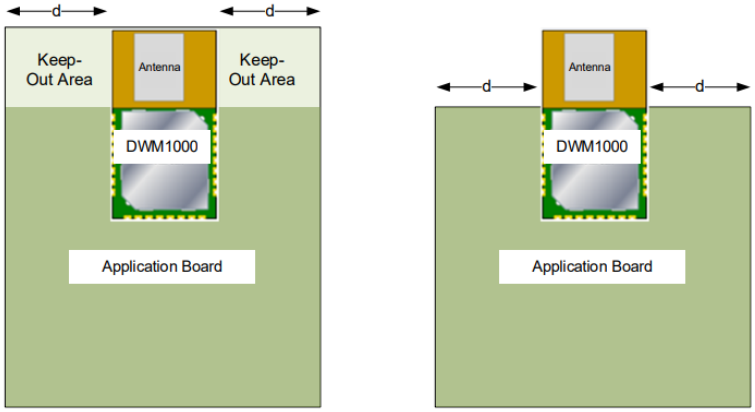

FIGURE 3.2: DWM1000 application board keep-out area for UWB antenna integration [14].

The antenna radiation pattern, was measured in an anechoic chamber for three planes and results were reported by Qorvo [14]. As the antenna is linearly polarised, the vertically polarised field (Theta) is measured in the azimuth plane (figure 3.3) and the horizontally polarised field (Phi) is measured in the elevation planes 1 and 2 (figures 3.4 and 3.5 respectively).

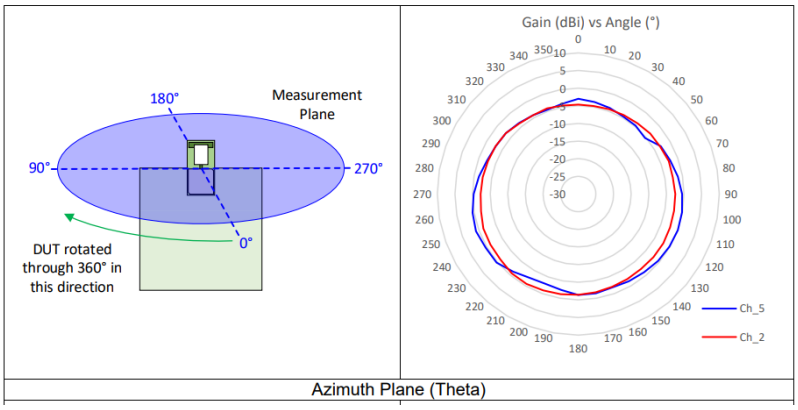

FIGURE 3.3: DWM1000 antenna radiation pattern charateristic on azimuth plane [14].

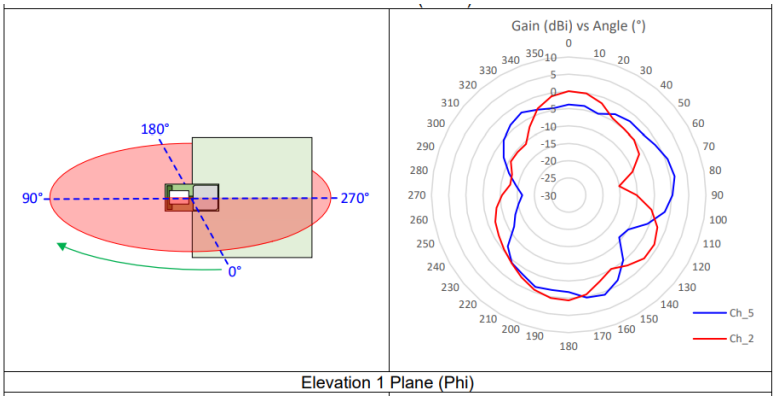

FIGURE 3.4: DWM1000 antenna radiation pattern charateristic on elevation plane (1) [14].

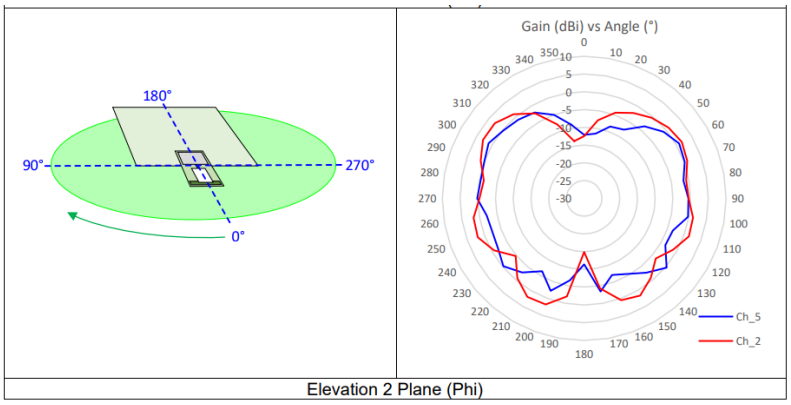

FIGURE 3.5: DWM1000 antenna radiation pattern charateristic on elevation plane (2) [14].

From the figures, the monopole antenna has a dipole-like omnidirectional radiation pattern which is beneficial for large coverage for tag detectability in localization.

- DWM1000 evaluation boards :

DWM1000 can be directly connected to an Arduino board to perform ranging. However, the latest version of the module called DWM3000 [15] is to be used with different evaluation boards, which are the Qorvo's DWM3000EVB [22] (figure 3.6) which

is an Arduino form factor compatible shield designed for the evaluation of this module for use in a scalable real time location system. Another evaluation board is the Makerfab's ESP32 UWB board [23]. In the latter, the module is integrated on the same pcb as the microcontroller. It has two versions the UWB-ESP32 (figure 3.7) and the UWB-ESP32-Pro (figure 3.8) which additionnally includes an OLED display for the location information.

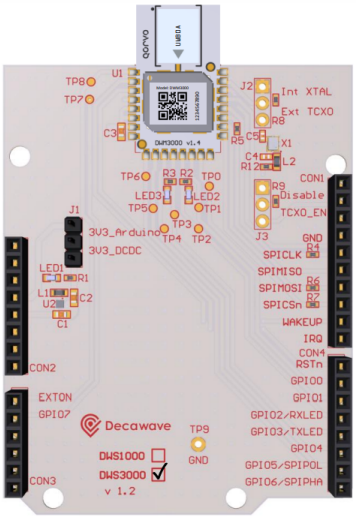

FIGURE 3.6: DWM3000 evaluation board as arduino shield [22].

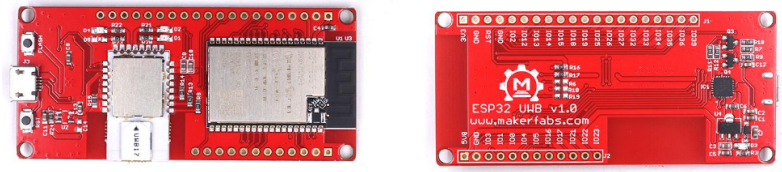

FIGURE 3.7: ESP32 all-in-one evaluation board for UWB tracking [23].

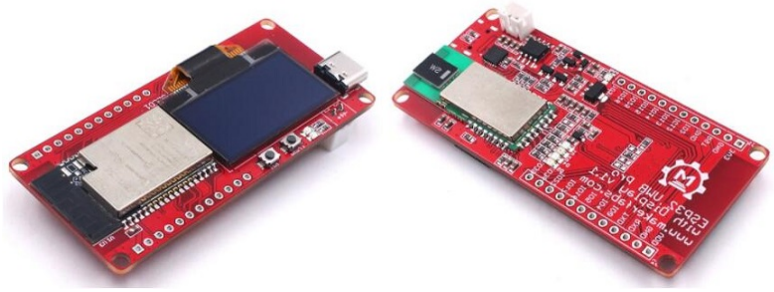

FIGURE 3.8: ESP32-Pro (with display) all-in-one evaluation board for UWB tracking [23].

STMicroelectronics' MOD1 chip

Similarly to the DWM1000 and DWM3000 modules, the MOD1 module (figure 3.9) is a surface mount module for UWB high precision developped by french company previously called BeSpoon, which now is part of STMicroelectronics. It was designed for warehousing and logistics in companies, personal navigation devices, security and building controls, robotics, wearable sensors, healthcare maintenance,

virtual reality (VR) and gaming. It supports Two-Way Ranging and achieves precisions down to 10 cm, it has datarates of up to 2 Mb/s.
The module has its embedded API for firmware operation and updates and master-slave mode selection. The MOD1 module itself does not include an antenna and is only available when integrated in its evaluation kit which is presented in the following.

FIGURE 3.9: STMicroelectronics UWB module MOD1 [20].

- MOD1 evaluation board :

MOD1 chip is integrated in the STMicroelectronics B-UWB-MEK1 evaluation board [24] (figure 3.10) which is equipped with an STM32 microcontroller, it is can be used as a fixed or as a mobile device. The use from four up to sixty boards is possible to prototype a location system.

FIGURE 3.10: B-UWB-MEK1 application board for MOD1 module with external antenna [24].

The MEK1 evaluation kit contains two identical transceivers and two UWB antennas of type 3D monopole, its characteristics are summarized in table 3.3.

Parameter	Value
Frequency	2 - 4.77 GHz
S11	- 8 dB
Gain	2 dBi
Radiation	Omnidirectional
Polarization	Linear (Vertical)
Beamwidth (- 6 dB)	360° (azimuth) / 80° (elevation)
Impedance	50 Ω
Dimensions	44 mm x 67 mm x 62 mm

TABLE 3.3: Characteristics of the UWB 3D monopole antenna of the STMicroelectronics B-UWB-MEK1 evaluation board [24].

Additionnally, the radiation patterns of the monopole antenna are shown in figure 3.11, for both the azimuth and elevation planes, and for all the center frequencies the UWB channels 1, 2 and 3.

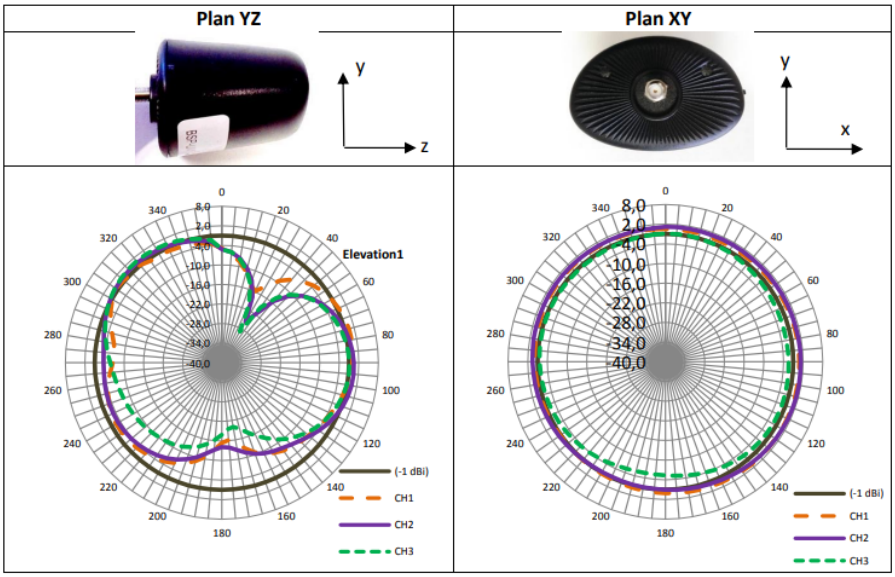

FIGURE 3.11: MEK1 UWB antenna radiation pattern charateristic on azimuth and elevation planes [25].

From the figure, since the commercial antenna is linearly polarized (vertical polarization), it has E-plane (elevation) and H-plane radiations (azimuth). It can be observed that the commercial antenna for channel 2 has omnidirectional radiation along 360◦ with a gain of 2 dBi.

UWB chips interoperable with Apple's U1 chip for interactions

Apple announced the availability of UWB modules and development kits for interaction with its U1 chip. The modules are from either Qorvo or NXP companies. First, the Qorvo DWM3000 previously described is compatible for interaction with the U1 chip. Second, development kits that contain NXP's Trimension chip (SR040 or SR150), they can be used by third party device developers. Since the DWM3000 architecture is similar to the DWM1000 described before, here, we focus on the

NXP based kits. These kits are commercialized by NXP's partners including: Sunway Communications, Murata and Mobile Knowledge. They are approved by Apple® for the purpose of evaluating UWB-enabled accessories that leverage Apple's Nearby Interaction framework in order to interact with Apple products that include the U1 chip. These modules and evaluation boards are listed in the following.

- Sunway Communications's SW-EVK-2 board based on NXP SR150 chip :

Sunway Communications developped a FiRa [26] and IEEE 802.15.4z UWB compliant wireless transceiver module [19] (figure 3.12) based on NXP's SR150 SoC [17]. It allows the location of objects in RTLSs to a secure range precision of 10 cm and an angle precision of 3 degrees. It is characterized by the integration of the SR150 SoC, antenna interface support, power management and clock control which simplifies design integration with minimal RF design required (external antenna).
It supports TWR, TDoA or phase-difference of arrival (PDoA) for AoA scheme in a variety of applications such as industrial, healthcare, smart home, smart retail RTLS, secure hands-free payment and automotive access.
The module supports UWB channels 5, 6, 8, and 9 (frequency range from 6.24 to 8.24 GHz) and allows a support for a 3x1 element antenna array with JSC type antenna connectors.

FIGURE 3.12: Sunway Communications' UWB module SR150 interface for ranging and direction finding [19].

The Sunway UWB Evaluation Kit (Sunway UWB EVK-2) [27] (figure 3.13) is composed of two Sunway's UWB modules in an anchor-tag configuration to allow locating the module operating as a tag and to build and evaluate a RTLS. This board is to be mounted on NXP QN9090 board for operation.

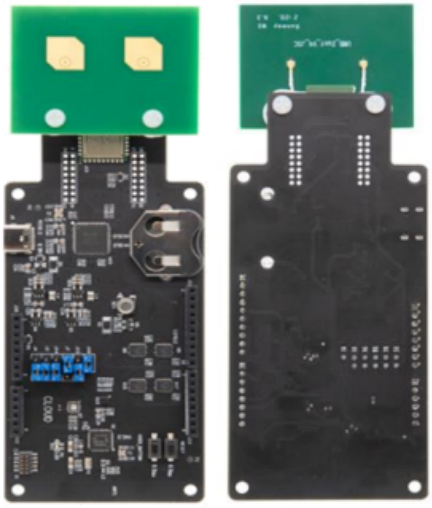

FIGURE 3.13: Sunway UWB module's application board SW-EVK-2 with UWB antennas [27].

The antenna array [28] used in the Sunway evaluation kit is shown in Figure 3.14 and its characteristics are summarized in table 3.4.

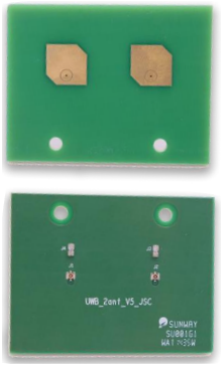

FIGURE 3.14: Sunway Communications' UWB pcb dual patch antenna [28] for SW-EVK-2 evaluation board.

Parameter	Value
Antenna type	2x1 dual pcb patch UWB antenna
Frequency	UWB channel 5 (6.25 GHz - 6.75 GHz)
Reflection coefficient	< - 10 dB
Peak gain	5.92 dBi
Beam width (3 dB)	120°
Impedance	50 Ω
Polarization	Circular (at channel center frequency)
Antenna connectors	2 JSC-male with cables
Dimensions	51 mm x 40 mm x 2.0 mm

TABLE 3.4: Characteristics of the UWB dual patch antenna [28] of the Sunway evaluation board [27].

From the information above, it is important to note that the Sunway module (figure 3.12) [19] accomodates all UWB channels 5, 6, 8 and 9, however, the Sunway

dual antenna (figure 3.14) is only designed to accomodate UWB channel 5, thus if this antenna is used in the evaluation kit, ranging may only be performed on channel 5.
Moreover, at the time of writing of this article, the radiation pattern characteristic plot of the antenna was not published by Sunway.

Murata's Type2BP-EVK board based on NXP SR150 chip

The Type2BP Development Kit by Murata (figure 3.15) [29], based on NXP SR150 enables a wide range of IoT devices to perform localization tasks or create a setup with multiple UWB anchors. The kit is based on Murata's Type2BP [30] ultra-small UWB module (figure 3.16.a), which includes clock, filters and peripheral components, as well as NXP's QN9090 Bluetooth LE solution and a USB-UART conversion IC. The Type-2BP can be controlled through QN9090 with power being supplied via a UWB cable or from the COM port of a PC. The kit integrates an on-board 3 element patch UWB antenna array.

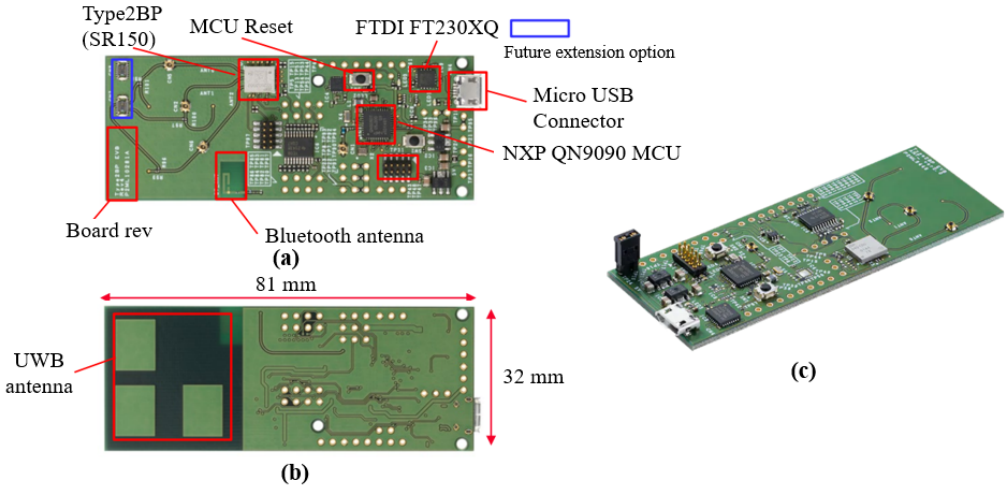

FIGURE 3.15: Murata UWB Trimension™ SR150 based application board Type2BP EVK [29] with UWB antenna : (a) top view, (b) bottom view, (c) perspective view.

In addition to the TYPE2BP module (figure 3.16.a) which is employed in the Murata kit and based on NXP SR150 chip, the company also developped another module called TYPE2DK (figure 3.16.b) which is instead based on the NXP SR040 module. also UWB modules which based on NXP UWB chipset. Both modules integrates NXP UWB chipset, filters, clock, and peripheral components. These modules are ideally suited for general IoT devices, where TYPE2BP [30] is suited for the reader and the TYPE2DK [31] is more suited for the tag role.

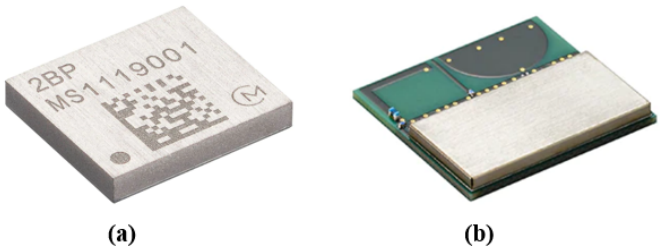

FIGURE 3.16: Murata UWB NXP based modules : (a) Type2BP (built upon the SR150 module), (b) Type2DK (built upon the SR40 module)

For further details, Murata TYPE2BP module is compliant with IEEE802.15.4z HRP PHY, it supports TWR, TDoA and 2D and 3D AoA schemes. It supports UWB channels 5 and 9, and data rates of 6.81Mbps, 7.8Mbps, 27.24Mbps and 31.2Mbps. Its characteristics are summarized in table 3.5.

Parameter	Value
Module type	surface mount
Frequency	UWB channel 5 and 9
Dimensions	6.6 mm x 5.8 mm x 1.2 mm
Antenna integration	no

TABLE 3.5: Characteristics of Murata Type2BP module (based on NXP SR150).

Conversely, the Type2DK module [31] based on NXP's SR40 is an all-in-one UWB + Bluetooth LE combination module which integrates NXP QN9090 Bluetooth® LE + MCU chipset, and on-board antennas for UWB and Bluetooth. This module can be used as a standalone tag which operates as it operates by coin-cell battery. It can also be used with Murata Type2BP evaluation kit described previously to perform ranging tests. Other characteristics are summarized in table 3.6.

Parameter	Value
Module type	surface mount
Frequency	UWB channel 5 and 9
Dimensions	19.6 mm × 18.2 mm × 2.3 mm
Antenna integration	UWB and Bluetooth LE

TABLE 3.6: Characteristics of Murata Type2DK module (based on NXP SR040).

To conclude on Murata modules, the Type2BP module does not contain any antenna. It contains the support (only) of 3 UWB antennas which in the evaluation kit are the elements of a 3 patch type element antenna array UWB. While the Murata Type2DK has on-board integrated antennas, one for Bluetooth LE and the other one for UWB of type printed monopole. Other specifications of the antennas are provided by the manufacturer upon purchase.

3.3.2 Summary of the antennas present in industrial UWB chips and evaluation board

To conclude the technical review of UWB real-time located systems, with a focus on antennas. Tables 3.7 and 3.8 present a summary of the UWB modules, their evaluation boards and antennas. Table 3.7 highlights if the UWB chip itself or its available evaluation boards integrate an antenna or not. Table 3.8 summarizes the characteristics of the UWB antennas integrated to each UWB chip or evaluation board.

Manufacturer	UWB module	Antenna integration	EV boards	EV board antenna
Qorvo / DecaWave	DWM1000 or DWM3000	Integrated ceramic monopole	DWM3000EVB Arduino Shield or Makerfab's ESP32 board	x
STMicroelec.	MOD1	x	MEK1	SMA-connected antenna
NXP	SR150	x	Murata Type2BP-EVK and Sunway SW-EVK-2 (works with separate NXP MCU)	*3 element pcb antenna array *3element pcb antenna array with CP
NXP	SR40	integrated pcb monopole	Murata Type2DK-EVK	no additional

TABLE 3.7: Summary of the industrial UWB chips, their evaluation boards and their antenna integration.

UWB module or Ev. board	Antenna type	Frequency (GHz)	Gain (dBi)	Radiation	Polarization
Qorvo DWM1000	pcb ceramic monopole antenna	3.2 - 7.2	4.16	Omnidir.	Linear
STMicroelec MEK1 ev. board	3D Monopole antenna	2 - 4.77	2	Omnidir.	Linear
Murata Type2BP-EVK (based on NXP SR150 module)	3 patch element pcb antenna array	Ch5 and Ch9	not published	180° dir.	Linear
Sunway EVK-2 ev. board (based on NXP SR150 module)	3 patch element pcb antenna array	6.25 - 6.75 GHz	5.92	180° dir.	Circular
Murata Type2DK module (based on NXP SR40 module)	pcb monopole antenna	Ch5 and Ch9	not published	Omnidir.	Linear

TABLE 3.8: Summary of the UWB antenna characteristics of the industrial UWB chips and / or their evaluation boards.

3.4 Discussion of the antenna influence on the localization performance

An attempt of ranging and localization of objects with electronic devices comprising transmit and receive antennas, especially in time-based schemes which mostly employ UWB technology, is a sensitive process as the final result depends greatly on the nature of the captured signal at the antenna stage. Thus, frontend design must be meticulous to detect the most correct signal, that is the shortest path signal, which leads to the computation of the distance estimate that is closest to the real distance. The shortest path signal can be the direct path or the first arriving reflection in case of complete blockage between the reader and tag). Consequently, the type of antennas used at both the reader and tag matter significantly in a sense that they can either improve or degrade the distance estimation depending on their characteristics, such as: type of antenna, gain, polarization, radiation pattern, etc. In the following, we discuss the influence antenna characteristics can have on the quality of ranging results.

3.4.1 Influence on the localization range

Range of a wireless communication system is directly related to the received power at the receiver side, in this case, at the reader side. This applies in all schemes, not just in received-signal strength (RSS) based localization systems but also in time-based systems such as UWB transceivers. Indeed, as the received power decreases with increased distance between the reader and tag, it determines the limit distance at which the transceiver can no longer detect the signal from the tag and thus can no

longer perform ranging.
Industrial manufacturers of UWB transceivers sometimes publish the measured performance of their UWB chips and evaluation boards, such as Murata for example. The performance in terms of reading range of their NXP SR150 chip based TYPE2BP evaluation kit was measured and reported. Figure 3.17 presents Murata's measurement set up and environment, using two TYPE2BP boards integrating transmit and receive antennas.

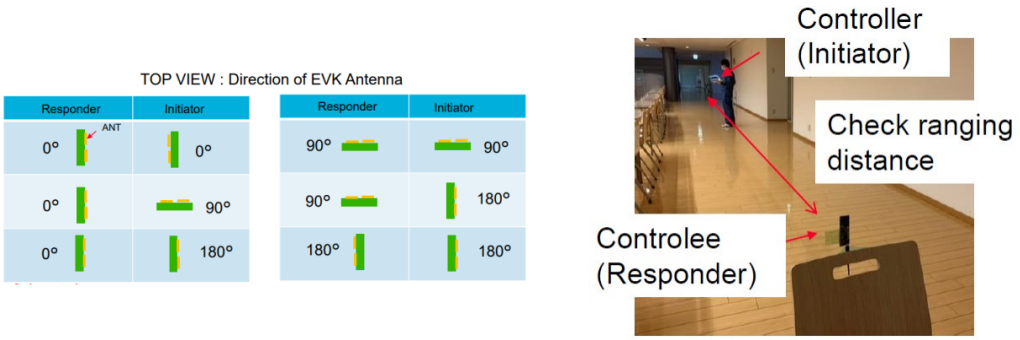

FIGURE 3.17: Range measurement set-up from Murata Type2BP evaluation board [29].

This measurement was aimed to infer the maximum possible reading range at which the tag can be detected. Two Type2BP EVK are connected in a controller (reader) and controlee (tag) configuration to check how long ranging is possible. While doing this, results are reported with several conditions as stated by the manufacturer. These conditions correspond to the different possible antenna orientations of the reader and tag relatively to eachother. The reported ranges are summarized in the table 3.9 below.

EVK (responder)	EVK (initiator)	Max ranging distance
0°	0°	Around 50 m
0°	90°	26 m
0°	180°	25 m
90°	90°	10 m
90°	180°	9 m
180°	180°	4.5 m

TABLE 3.9: Range measurement results from Murata Type2BP evaluation board [29].

The evaluation kit uses patch type antennas with a theoretical 180° directional radiation, and with linear polarization. Consequently, the best case scenario is the condition 0° orientation for the responder and 0° orientation for the initiator, which is reported to achieve a maximum reading range of 50 m. Linear polarization affects the other cases in the received power as cross-polarization (0°-90°, 90°-0°, 0°-180°, 90°-180°) or induces power loss [32, 33]. Moreover, even in the cases where there is no cross-polarization, the radiation pattern also affects the detectability, especially at longer distances, in the cases where the antennas are not facing eachother (such as in 0°-180°, 90°-90° and 180°-180°). For this reason, a solution would be design omnidirectional reader and tag antennas to unsure the transceivers don't miss eatchother in the search phase and discovery process during two-way ranging no matter how

they are placed relatively to eachother. These observations show the significant effect of the transmit and receive antennas on the performance of the RTLS in terms of range. This matter is discussed in further details in Chapters 4 and 5.

3.4.2 Influence on the tag-orientation dependence

From the previous table 3.9, the worst case scenario is the when the responder and initiator antennas are in a 180°-180° orientation configuration relatively to eachother. It can be seen that the maximum distance at which the reponder is detected is 4.5 m, which means further from this distance, not only ranging is impossible but its presence itself cannot be detected. Taking into account the application of UWB transceivers, these are mainly aimed for indoor environments with several mobile objects, unlike for example RFID tracing or Bluetooth tracing, a range of 4.5 m is too low for UWB deployment areas (hospitals, airports, construction mines etc..). Furthermore, in such areas tags and objects are mobile and their orientation cannot manually be adjusted to face the reader's antenna nor to match its vertical or horizontal polarization. For this reason, solutions such as circular polarization of the reader antennas [32, 34] are advised to mitigate cross-polarization induced power loss, even while the tag's polarization may be kept linear for design simplicity. This matter is discussed in further detail in Chapters 4 and 5 of this thesis.

3.4.3 Influence on the accuracy

After the reading range, the performance in terms of accuracy of the ranging estimates of the NXP SR150 chip based TYPE2BP evaluation kit was similarly measured and reported. Figure 3.18 presents Murata's measurement set up and results, using two TYPE2BP boards.

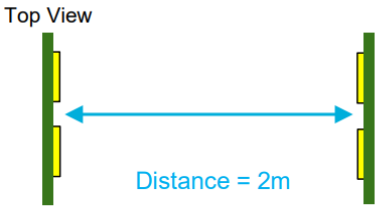

	5ch	9ch
Sample-A	200	202
Sample-B	200	196
Sample-C	199	201
Average	199.6	199.6

Result

FIGURE 3.18: Accuracy measurement from Murata Type2BP evaluation board [29].

For this measurement, their condition on the antennas is that they are placed facing eachother. In most cases, conclusions on accuracy is statistical or based on many measured samples by ranging and comparing to the real distance. The results table shows that three samples A, B and C of ranging were taken at both channel 5 (centered at 6.49 GHz) and channel 9 (centered at 7.9 GHz) and averaged to one value at the end, the values are reported in cm.
Taking into account the real distance of 2 m and the reported average detected distance at both chanels of 1.99 m, an accuracy of 99 % which is most likely due to the fine temporal resolution of UWB signal itself and the placement of antennas in complete line-of-sight without any blockage nor reflecting objects and at a distance of only 2 m. These observations show that, in fact, the theoretical UWB accuracy level

(that is under 10 cm) can be achieved, however only in adjusted conditions as seen in the previous cases. Accuracy depends heavily on the environment, and for practical applications, these environments cannot be prealably decided. This calls for the design of antennas robust to reflections and multipath. For this reason, a solution was proposed in our work [32], and consists in mitigating multipath signals with circular polarization filtering. This method requires both the reader and tag antenna to have circular polarization of the same sense (either right-hand or left-hand), which can filter out reflections on metal as these will switch the CP sense in the middle of the path before arrival. This matter is discussed in further detail in Chapter 5.

3.5 Conclusions

This chapter presented a study of UWB locating systems by, first highlighting the error sources in indoor environments and that can affect time-based localization. Then, a technical review of the currently available industrial UWB chips and real-time locating systems used for object monitoring in indoor scenarios and complex environments was realized. Besides, the antennas employed in the listed systems and their characteristics were highlighted and summarized. Furthermore, a discussion on the influence of frontend antennas of UWB transceivers on the localization quality in terms of reading range, accuracy and object orientation-independent detectability was discussed and solutions were suggested.

Bibliography

[1] G. Bacci, E. Falletti, C. Fernández-Prades, M. Luise, D. Margaria, et F. Zanier, « Chapter 2 - Satellite-Based Navigation Systems », in Satellite and Terrestrial Radio Positioning Techniques, D. Dardari, E. Falletti, et M. Luise, Éd., Oxford: Academic Press, 2012, p. 25-74. doi: 10.1016/B978-0-12-382084-6.00002-7.

[2] M. A. C. Duran et al., « Chapter 3 - Terrestrial Network-Based Positioning and Navigation », in Satellite and Terrestrial Radio Positioning Techniques, D. Dardari, E. Falletti, et M. Luise, Éd., Oxford: Academic Press, 2012, p. 75-153. doi: 10.1016/B978-0-12-382084-6.00003-9.

[3] C. S. Álvarez-Merino, H. Q. Luo-Chen, E. J. Khatib, et R. Barco, « WiFi FTM, UWB and Cellular-Based Radio Fusion for Indoor Positioning », Sensors, vol. 21, no 21, p. 7020, oct. 2021, doi: 10.3390/s21217020.

[4] L. Wang et M. Zawodniok, « RSSI-based localization in cellular networks », in 37th Annual IEEE Conference on Local Computer Networks – Workshops, Clearwater, FL, USA: IEEE, oct. 2012, p. 820-826. doi: 10.1109/LCNW.2012.6424069.

[5] Y. You et C. Wu, « Indoor Positioning System With Cellular Network Assistance Based on Received Signal Strength Indication of Beacon », IEEE Access, vol. 8, p. 6691-6703, 2020, doi: 10.1109/ACCESS.2019.2963099.

[6] T. Sanpechuda and L. Kovavisaruch, "A review of RFID localization: Applications and techniques," in Proc. 5th Int. Conf. Electr. Eng./Electron., Comput., Telecommun. Inf. Technol., May 2008, pp. 769–772.

[7] K. Finkenzeller, RFID Handbook: Fundamentals and Applications in Contactless Smart Cards and Identification, 3rd ed. Hoboken, NJ, USA: Wiley, 2010.

[8] L. Yang, G. B. Giannakis, « Ultra-wide band communications, an idea whose time has come », IEEE Signal Processing Magazine, vol4, p. 1053-5888, November 2004.

[9] IEEE Standard for Low-Rate Wireless Networks, IEEE Standard 802.15.4- 2020 (Revision of IEEE Standard 802.15.4-2015), Jul. 2020.

[10] IEEE Standard for Low-Rate Wireless Networks–Amendment 1: Enhanced Ultra Wideband (UWB) Physical Layers (PHYs) and Associated Ranging Techniques, IEEE Standard 802.15.4z-2020 (Amendment to IEEE Standard 802.15.4-2020), Aug. 2020.

[11] D. Dardari, A. Conti, U. Ferner, A. Giorgetti, et M. Z. Win, « Ranging With Ultrawide Bandwidth Signals in Multipath Environments », Proc. IEEE, vol. 97, no 2, p. 404-426, févr. 2009, doi: 10.1109/JPROC.2008.2008846.

[12] D. Dardari, P. Closas, et P. M. Djuric, « Indoor Tracking: Theory, Methods, and Technologies », IEEE Trans. Veh. Technol., vol. 64, no 4, p. 1263-1278, avr. 2015, doi: 10.1109/TVT.2015.2403868.

[13] N. S. C. J, N. H. A. Wahab, N. Sunar, S. H. S. Ariffin, K. Y. Wong, et Y. Aun, « Indoor Positioning System: A Review », Int. J. Adv. Comput. Sci. Appl., vol. 13, no 6, 2022, doi: 10.14569/IJACSA.2022.0130659.

[14] Qorvo DWM1000 UWB transceiver. Accessed: Dec. 2023. [Online]. Available: https://www.qorvo.com/products/p/DWM1000

[15] Qorvo DWM3000 UWB transceiver. Accessed: Dec. 2023. [Online]. Available: https://www.qorvo.com/products/p/DWM3000

[16] Apple Nearby Interactions, "Locate and interact with nearby devices using identifiers, distance, and direction," Accessed: Dec. 2023. [Online]. Available: https://developer.apple.com/documentation/nearbyinteraction/

[17] NXP Trimension SR150 UWB transceiver. Accessed: Apr. 2023. [Online]. Available: https://www.nxp.com/products/wireless-connectivity/trimension-uwb/trimension-sr150-secure-uwb-solution-for-iot-devices:SR150

[18] NXP Trimension SR040 UWB transceiver. Accessed: Apr. 2023. [Online]. Available: https://www.nxp.com/products/wireless-connectivity/trimension-uwb/trimension-sr040-reliable-uwb-solution-for-iot:SR040

[19] Sunway Communications UWB transceiver for ranging and direction finding. Accessed: Dec. 2023. [Online]. Available: https://en.sz-sunway.com/product/wireless/RF-Connectivity-Module/383.html

[20] STMicroelectronics B-UWB-MOD1 Ultra-wideband module for high-precision indoor location. Accessed: Dec. 2023. [Online]. Available: https://www.st.com/en/wireless-connectivity/b-uwb-mod1.html?rt=db&id=DB4392

[21] Abracon chip antenna integrated in Qorvo DWM1000 module. Accessed: Dec. 2023. [Online]. Available: https://abracon.com/chip-antenna/ACA-107-T.pdf

[22] Qorvo DWM3000EVB for DWM3000 module. Accessed: Dec. 2023. [Online]. Available: https://www.qorvo.com/products/p/DWM3000EVB

[23] Makerfab ESP32 ev.board for DWM3000. Accessed: Dec. 2023. [Online]. Available: https://www.makerfabs.com/esp32-uwb-ultra-wideband.html

[24] STMicroelectronics B-UWB-MEK1 evaluation board for UWB MOD1 module. Accessed: Dec. 2023. [Online]. Available: https://www.st.com/en/wireless-connectivity/b-uwb-mek1.html

[25] STMicroelectronics BeSpoon UWB Omnidirectional Antenna BSP-UWBA-Om4G, Datasheet V.1.0, BeSpoon, France, 2021.

[26] FiRa Consortium for UWB tracking. Accessed: Jan. 2024. [Online]. Available: https://www.firaconsortium.org/

[27] Sunway Communications UWB evaluation board based on NXP SR150. Accessed: Jan. 2024. [Online]. Available: https://en.sz-sunway.com/product/wireless/RF-Connectivity-Module/385.html

[28] Sunway Communications UWB antenna. Accessed: Apr. 2023. [Online]. Available: https://en.sz-sunway.com/product/wireless/RF-Connectivity-Module/411.html

[29] Murata Type2BP UWB development board based on NXP SR150. Accessed: March. 2023. [Online]. Available: https://www.nxp.com/products/wireless-connectivity/trimension-uwb/murata-type2bp-evk-trimension-sr150-uwb-development-kit:UWB-DEV-TYPE2BP-EVK

[30] Murata Type2BP UWB module based on NXP SR150. Accessed: March. 2023. [Online]. Available: https://www.murata.com/en-eu/products/connectivitymodule/ultra-wide-band/nxp/type2bp

[31] Murata Type2DK UWB module based on NXP SR040. Accessed: March. 2023. [Online]. Available: https://www.murata.com/en-eu/products/connectivitymodule/ultra-wide-band/nxp/type2dk

[32] A. Benouakta, F. Ferrero, L. Lizzi and R. Staraj, "Antenna Characteristics Contributions to the Improvement of UWB Real-Time Locating Systems' Reading Range and Multipath Mitigation," in IEEE Access, vol. 11, pp. 71449-71458, 2023, doi: 10.1109/ACCESS.2023.3294622.

[33] A. Benouakta, F. Ferrero, L. Lizzi, L. Brochier and R. Staraj, "Measurements of antenna polarization effects on Ultra-Wideband monitoring and localization," 2021 IEEE Conference on Antenna Measurements and Applications (CAMA), Antibes Juan-les-Pins, France, 2021, pp. 589-590, doi: 10.1109/CAMA49227.2021.9703597.

[34] A. Benouakta, F. Ferrero, L. Lizzi and R. Staraj, "Frequency Reconfigurable and Circularly Polarized Patch Antenna Over Dual Ultra-wideband Channels," 2022 16th European Conference on Antennas and Propagation (EuCAP), Madrid, Spain, 2022, pp. 1-5, doi: 10.23919/EuCAP53622.2022.9769006.

Chapter 4

Localization with UWB antennas: the requirements of RTLSs

4.1 Introduction

As one of the typical and modern applications of UWB technology is the localization and positioning of tags associated to mobile objects, commercial companies and suppliers have and continue to release on the market, many boards, electronic modules, and kits meant for localization. These solutions are pervasive and somehow very profitable as they are popular within the industrials that constantly need to locate assets (from small objects, to smartphones, to cars, etc.. . .).
Accordingly, the growing mobility of these objects in wireless real-life scenarios raises the expectations for the UWB antennas used, more so for the reader (or "anchor") antennas. In fact, to localize an object associated to an UWB transmitting tag-antenna, the UWB receiving anchor-antenna at the other side is expected to possess certain important characteristics.
Hence, this chapter investigates how to improve the quality of the location estimates obtained with UWB localization devices, through choosing suitable antenna specifications. Moreover, it presents and describes the design of a frequency reconfigurable and circularly polarized UWB patch antenna along two UWB channels of 500 MHz meant for UWB anchors.

4.2 Frequency reconfigurable and circularly polarized patch antenna over dual Ultra-wideband channels

This section describes the design and characterization of an UWB patch antenna which is aimed to be an Anchor-antenna in UWB localization systems. It can operate distinctively in two different UWB frequency channels. Both of these channels have 500 MHz bandwidth, the lowband channel is centered at 4 GHz and the highband channel at 6.49 GHz. Reconfigurability to switch from one channel to another is achieved by changing the size of the radiating element. Additionally, this UWB antenna is aimed to be circularly polarized over both channels, which is realized by the means of two branchline couplers placed on a bottom layer. Results of reconfigurability and circular polarization operation are presented by simulation and measurements.

4.2.1 Antenna design specifications

The interest in developping and using UWB antennas has been growing since the FCC of the United States has allocated the 3.1 - 10.6 GHz frequency range to UWB

technology and its applications [1]. UWB communication systems transmit and receive ultra-short electromagnetic pulses over a bandwidth of several GHz [2]. Such systems call for optimized RF front-ends including their UWB antennas.
The most typical application of UWB technology is the localization and positioning of tags associated to mobile objects. Accordingly, the growing mobility of these objects in wireless real life scenarios raises the expectations for the UWB antennas used, more so for the "Anchor" (or reader) antennas. In fact, to localize an object associated to an UWB transmitting tag-antenna, the UWB receiving anchor-antenna at the other side is expected to possess certain important characteristics.
First, increasing the UWB localization system's detection range raises the need for the anchor antenna to have enough gain in order to be able to detect and localize the tag at longer distances.
Second, improving the ability of localization raises the need for an ideally constant received power at the anchor antenna side, no matter the relative orientations of the anchor and tag antennas to each other [3]. This specification calls for circular polarization (CP) at the anchor side in order to avoid the anchor-tag polarization mismatch.
Hence, antennas on the anchor side of UWB localization systems, should not only have an ultra-wide bandwidth, but also a higher gain and ideally, CP to be able to overcome the problem of limited range and polarisation-dependent received power. Moreover, these high gain and CP characteristics could be more easily achieved by UWB antennas if the expectation for them to operate in all the UWB frequency range is removed. In fact, the generally used UWB modules for tracking and localization systems such as the DWM1000 from Decawave [4], operate in channels of 0.5 or 1.3 GHz of bandwidth only instead of all the UWB range.
However, already existing solutions for UWB anchor-antennas mostly represent antennas that cover all the 7.5 GHz of UWB frequency range [5]. Similarly, in terms of frequency reconfigurability, most existing solutions have the characteristic of being "band-notch", as they all mostly tend to cover all the UWB frequency range (3.1-10.6 GHz) as a general case and then obtain the other small configured bands by rejecting the undesired parts of the spectrum. For example, in [6] the authors proposed an 8-states frequency reconfigurable UWB monopole antenna with band rejections at the C band, WLAN, and X band (figure 4.1).

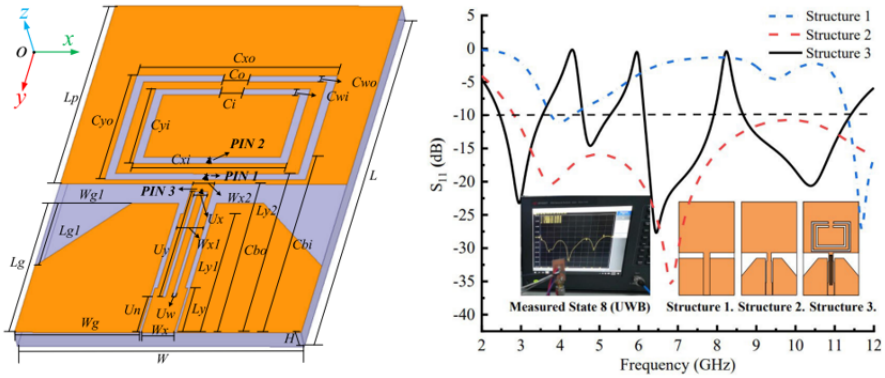

FIGURE 4.1: 8-States frequency reconfigurable UWB monopole antenna [6], with band rejections at the C band, WLAN, and X band by two C-slots and inverted U-slot

Also, in [7], a reconfigurable ground plane with a slot was used in order to obtain switchable bands between, the whole UWB range, a low, middle and upper UWB sub-bands. Also, in [8], all the UWB range and different sub-bands were obtained in a Vivaldi antenna by using switches on its wings (figures 4.2 and 4.3).

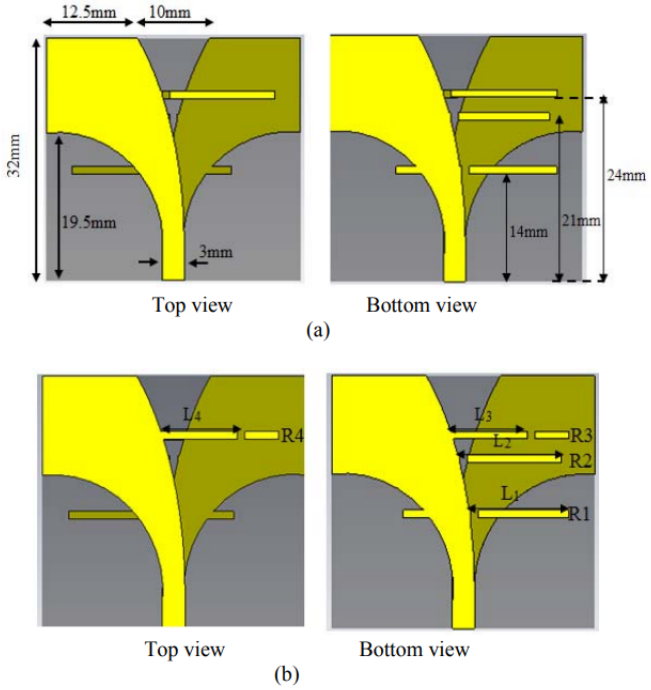

FIGURE 4.2: UWB frequency reconfigurable antipodal Vivaldi antenna [8]: a) operation on UWB mode, b) operation on seven switchable sub-bands.

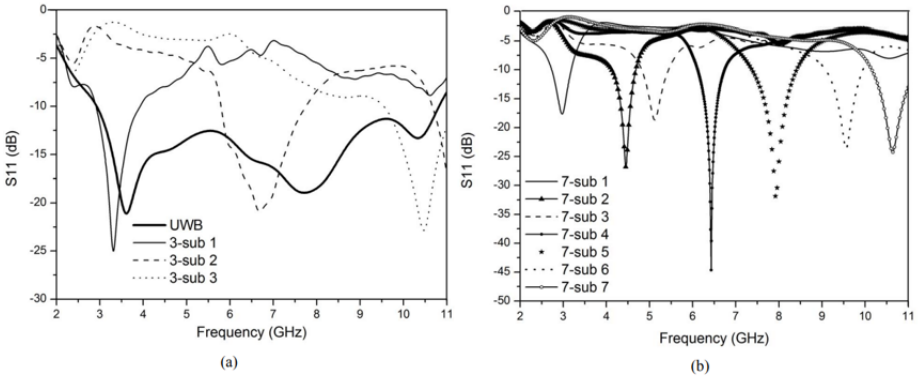

FIGURE 4.3: Reflection coefficient of the UWB frequency reconfigurable antipodal Vivaldi antenna: a) operation on UWB mode and 3 sub-bands, b) operation on 7 switchable sub-bands [8].

Conversely, in this work, the realized anchor antenna combines the high gain of patch antennas with an ultra wide bandwidth while focusing on each 500 MHz UWB channel at a time, by respectively using capacitive feeding of the radiating element and by making the antenna frequency reconfigurable. Its reconfigurability in frequency is based on the modification of the size of the patch and eventually by using three p-i-n diodes. Additionally, this antenna exploits the simple structure and

symmetry of a patch to achieve a CP operation covering all the frequencies in an UWB channel.
First, the design method of the UWB anchor antenna based on capacitive feeding is described, followed by the simulation results in terms of impedance matching bandwidth and CP operation. Then, the fabrication and experimental characterization of the antenna is illustrated and compared to the simulation results. Finally, these results are discussed and followed by a general conclusion.

4.2.2 Anchor antenna design principle

The realized Anchor UWB antenna (figures 4.4, 4.5, and 4.6) is based on the standard microstrip probe-fed patch antenna model. However, to increase the usually narrow band of patch antennas, an air gap is introduced between the substrate and ground plane. Furthermore, to compensate for the inductive effect introduced due to the probe, a capacitive feeding mechanism is applied following the approach used in [4]. This capacitive feed is made of a probe-fed small patch placed on the same substrate layer as the radiating element and at a gap distance from it. The dielectric substrate is suspended in air as illustrated in figure 4.4. The anchor antenna is designed to operate in two UWB frequency channels. From 3.75 to 4.25 GHz and from 6.25 to 6.75 GHz. The first band is called "Channel 2" and the second band "Channel 5", as used in the existing UWB localization system DWM1000 by Decawave [5] for example.

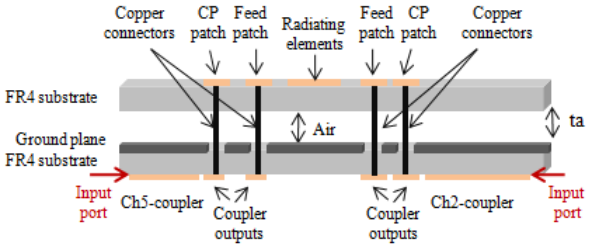

FIGURE 4.4: Side view of the UWB anchor antenna.

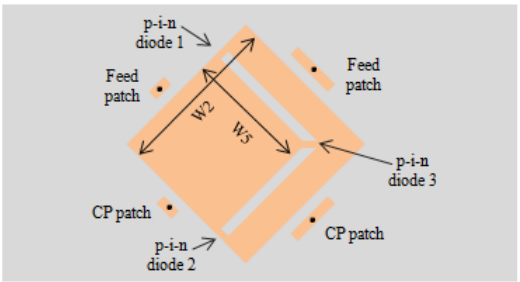

FIGURE 4.5: Top view of the UWB anchor antenna.

The design steps of the UWB Anchor patch antenna are as follows :

- First, two UWB patch antennas operating along the frequency range of channel 2 and channel 5 (each has 500 MHz of bandwidth), are both designed separately.

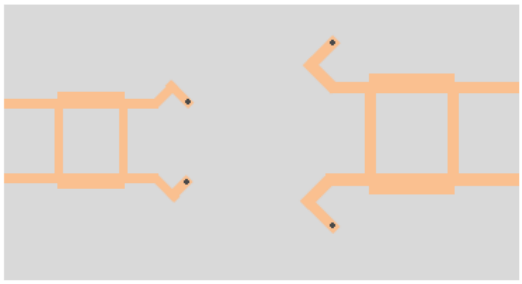

FIGURE 4.6: Bottom view of the UWB anchor antenna.

- Second, as in figure 4.5, both of the realized antennas are "combined" into one reconfigurable patch antenna by modifying the shape of the radiating element using three p-i-n diodes. If the diodes are forward biased, the radiating element operates in the low-band channel, and if the diodes are open, the radiating element operates in the high-band channel.
- Finally, as in figure 4.6, CP is introduced to the frequency reconfigurable UWB antenna, by adding two branchline directional couplers on a second FR4 substrate layer introduced beneath the ground plane. Each coupler operates at the center frequency of one of the channels.

Design of simple UWB patch at Channel 2

In order to achieve a patch antenna resonating along one UWB channel (500 MHz of bandwidth), the approach described in [9] was employed, Figure 4.7 illustrates the simulated structure for the operation in Channel 2 which is centered at 4 GHz.
The substrate used is FR4 with thickness t = 0.8 mm, the dimensions of the radiating

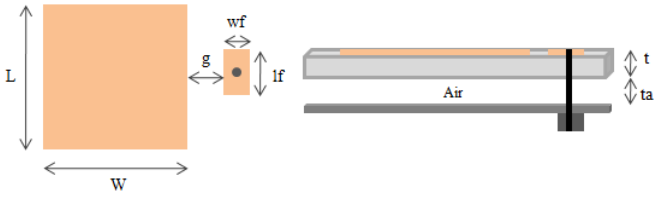

FIGURE 4.7: UWB antenna with capacitive feed and air gap.

element are L = W = 23 mm and were derived from standard patch antenna design. The small feed patch has a width of wf = 1.6 mm and length of lf = 10 mm. It is separated from the radiating patch by a gap distance g = 2 mm. The probe feed center pin has a diameter of 1.3 mm and is placed at the center of the small feed patch.
The effect of the air gap height (between the ground plane and the substrate) on the bandwidth has been studied and illustrated in Fig. 4.8. It can be observed that the bandwidth increases by increasing the air gap height "ta". A height of 8 mm is optimal in this case as the reflection coefficient is under - 10 dB for all the frequency range of Channel 2 (3.75 - 4.25 GHz).

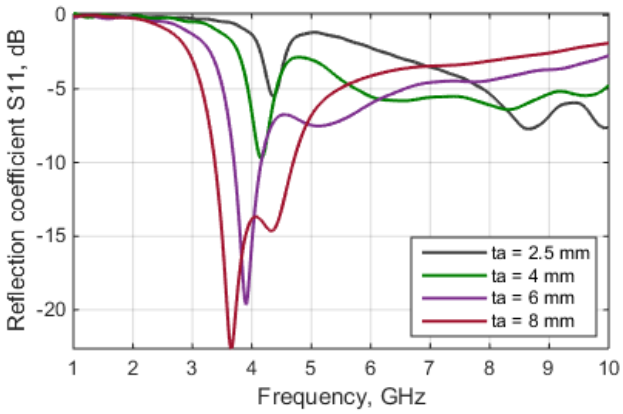

FIGURE 4.8: Air gap height effect on bandwidth of Channel 2

Design of UWB patch at Channel 5

The previous design is used and an L-shaped slot, of 2 mm width, is introduced to the radiating element as illustrated in figure 4.9. The detached patch on the right side of the slot is designed to resonate at the center frequency 6.49 GHz of channel 5 (6.25 - 6.75 GHz). It is a square patch with dimension W5 = 14 mm. A second small patch (of length = 3 mm and width = 1.6 mm) and a probe are also introduced as a feed to the CH5-patch.

FIGURE 4.9: Channel 2 configuration - Channel 5 configuration.

The same study of the bandwidth with varying air gap height was performed and is illustrated in figure 4.10.

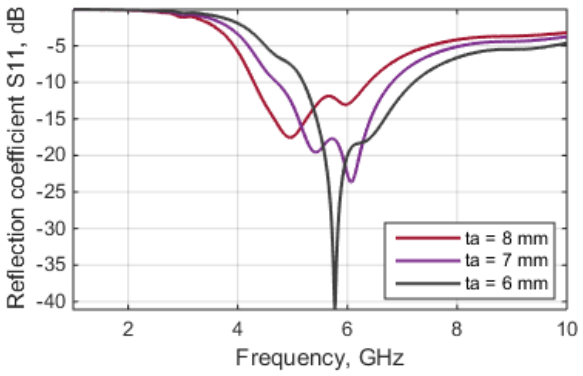

FIGURE 4.10: Air gap height effect on bandwidth of Channel 5.

Intuitively, the initial value was set to be of 8 mm as it was the optimal value found for the CH2-patch previously. However, the resulting bandwidth does not

cover the upper side of the channel 5 bandwidth, which should be until 6.75 GHz. It can conversely be observed, that a lower value of the air gap, 6 mm, results in an ideal bandwidth covering all of the channel 5 range.
These results show that, increasing the air gap height does increase the bandwidth but its increase is limited at some point. This limitation depends on the desired frequency of operation. It seems that the higher the desired frequency is, the lower value of air gap height needed to achieve a certain bandwidth. A more extensive and detailed parameter study of this concept has been described in [10].
Finally, since the CH2-patch and the CH5-patch are both in the same structure, the air gap height needs to be the same for both cases, so a compromise of ta = 7 mm has been chosen for the final reconfigurable structure.
It can also be noted that, other parameters, such as the small feed patch length "lf" and distance between the radiating element and its feed patch "g" do not influence greatly the bandwidth, but instead they have an effect on the impedance matching as studied in [9] and [10]. As an example, the effect of the feed patch length on the reflection coefficient can be observed in figure 4.11. From these results, the length of the second feed patch is taken as lf-ch5 = 3 mm. The effect of the width of the L-slot was also verified in Fig. 4.12, where it can be observed that this parameter does affect the impedance matching, however its effect on the bandwidth is negligible [9].

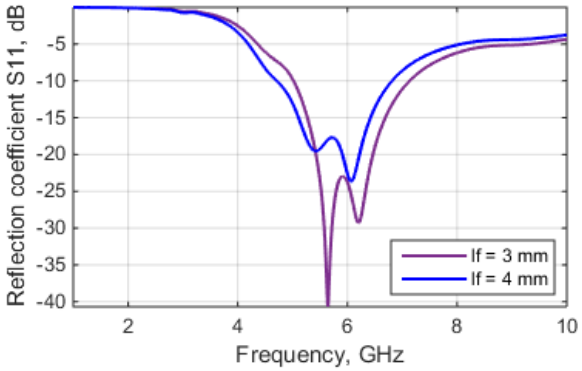

FIGURE 4.11: Feed patch length effect on impedance matching for Channel 5.

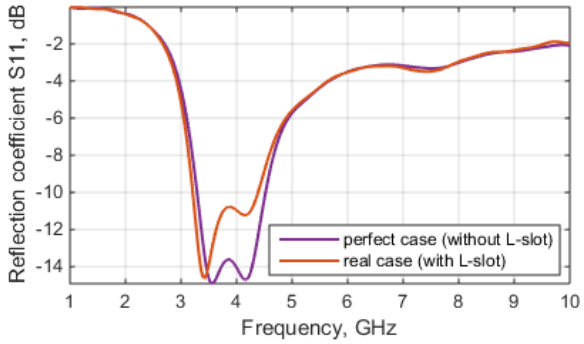

FIGURE 4.12: L-shaped slot width effect on impedance matching for Channel 2.

Circular polarization

CP operation was achieved by :

- Adding two other CP small patches on the top layer, each orthogonal to the feed patch of the radiating element it corresponds to, as illustrated in Fig. 4.5. The result of this, for each radiating element, is a feed patch on either the x-axis (or y-axis) and a similar CP patch orthogonal to it placed on the y-axis (or x-axis respectively). This allows to excite the two orthogonal modes TM01 and TM10 (necessary for CP) in each of the radiating patches.
- Adding two branchline directional couplers, one operating at the 4 GHz frequency and the other at 6.49 GHz, covering each the necessary 500 MHz channel bandwidth. To add both couplers, a second substrate layer was added under the ground plane as illustrated in Fig. 4.4 and Fig. 4.6.
- The two feeding ports are represented by the two inputs of each coupler, as seen in Fig. 4.4. While one output (from each coupler on the bottom layer) was connected using copper pins, to one small feed-patch on the top layer, the other outputs were connected to the small CP patches.

4.2.3 Results

The following are EM simulation results obtained using the final Anchor antenna structure design of figures 4.4, 4.5 and 4.6 in CST Microwave Studio, with the two frequency configurations.

UWB Frequency reconfigurablity

Figure 4.13 illustrates the simulated reflection coefficient of each coupler's input, one which feeds the CH-2 coupler and the other one which feeds the CH-5 coupler. These results were obtained, when the copper connections (which model the p-i-n diodes) were present or absent, for channel 2 and channel 5 respectively. The figure shows good impedance matching for both configurations, as the reflection coefficients are below - 10 dB on all of the channels' bandwidths (3.75 - 4.25 GHz and 6.25 - 6.75 GHz).

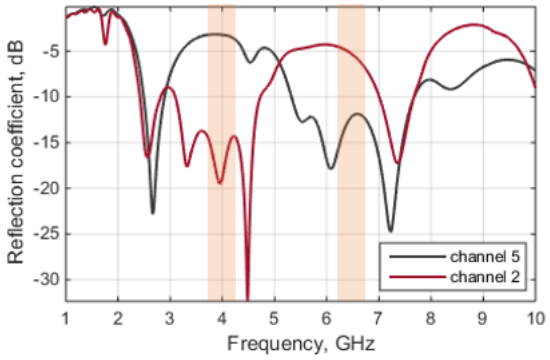

FIGURE 4.13: Reflection coefficients of the reconfigurable antenna.

Circular polarization

CP in simulation was verified by simulation of the axial ratio (AR) value. Fig. 4.14 illustrates the AR on each channel's frequency range for the main direction of radiation. It can be seen that ultra wideband CP of the antenna on both configurations is

verified, as the AR is under 3 dB for all channel 2 frequencies and under 3.37 dB for all channel 5 frequencies.

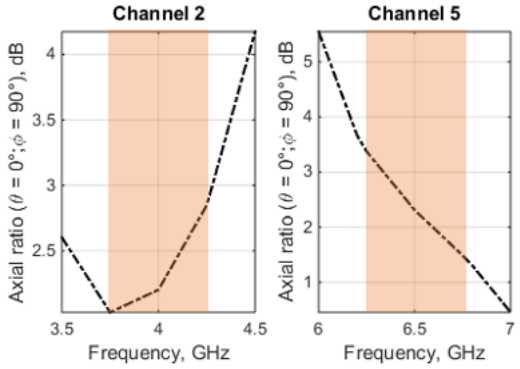

FIGURE 4.14: Simulated axial ratio of the reconfigurable antenna (main radiation direction).

4.2.4 Experimental characterization of the antenna

UWB Anchor antenna prototype

The UWB reconfigurable anchor antenna was fabricated in the lab using a 80.4 mm x 46 mm x 0.8 mm FR4 substrate (for both layers) and 0.035 mm thick copper for conductors and ground plane. The resulting antenna is illustrated in figures 4.15 and 4.16.

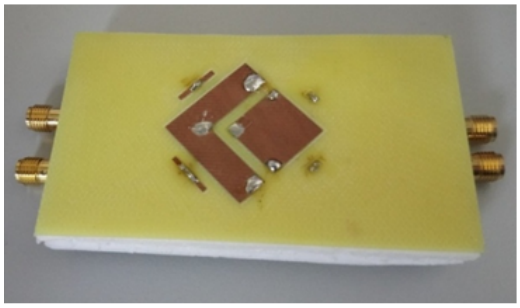

FIGURE 4.15: Top view of the UWB reconfigurable antenna prototype.

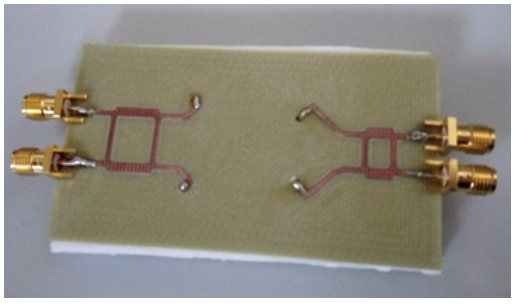

FIGURE 4.16: Bottom view of the UWB reconfigurable antenna prototype.

The final optimized dimensions of the antenna are : W2 = 23 mm, W5 = 14 mm, air gap height ta = 7 mm, L-shaped slot width g = 2 mm, both feed and CP patches' lengths lf2 = 10 mm and lf5 = 3 mm and widths w2 = w5 = 1.6 mm, interlayer pins diameter = 1.3 mm.
In the following, simulation and measurement results will be compared.

Measured frequency reconfigurability

Figure 4.17 illustrates the simulated and measured reflection coefficients along channel 2 and channel 5. Despite a small frequency shift, good agreement between simulation and measurement results is observed, as the measured antenna impedance is matched (S11 is inferior to - 10 dB) on both channels' bandwidths. Thus, UWB frequency reconfigurability of the antenna is verified.

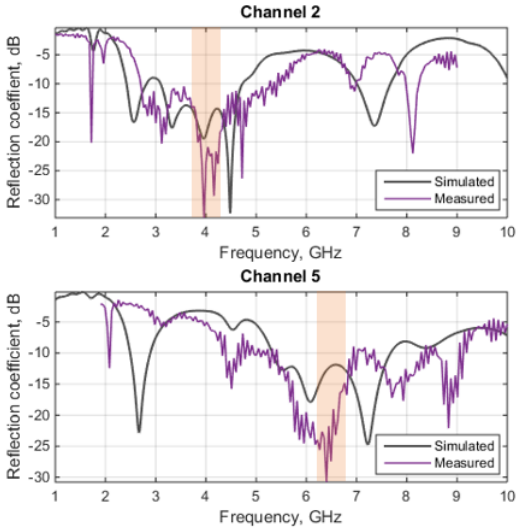

FIGURE 4.17: Reflection coefficient at channel 2 and channel 5.

Measured circular polarization

The measured circular polarization was verified along channel 2 by two means : measurement of the AR and measurements of the realized gain of both right-hand and left-hand circular polarizations (RHCP and LCHP respectively). Figure 4.18 presents the obtained measured AR with respect to frequency. It can be observed that the AR is below 4 dB along all channel 2 frequencies, which verifies the CP operation.

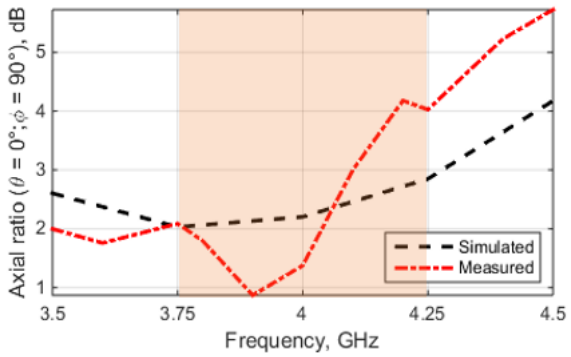

FIGURE 4.18: Measured and simulated axial ratio of channel 2.

Figure 4.19 illustrates the realized gain of RHCP and LHCP. It can be seen that the cross-polarization (here, LHCP) is suppressed at - 18 dBi for $\theta = 0°$ and at - 10 dBi for a 3 dB beamwidth of almost 100°. While, it can be seen that the RHCP polarization gain is of 5 dBi. These results verify the good performance of the UWB CP along channel 2 frequencies and demonstrate that this CP has a right hand sense (RHCP).

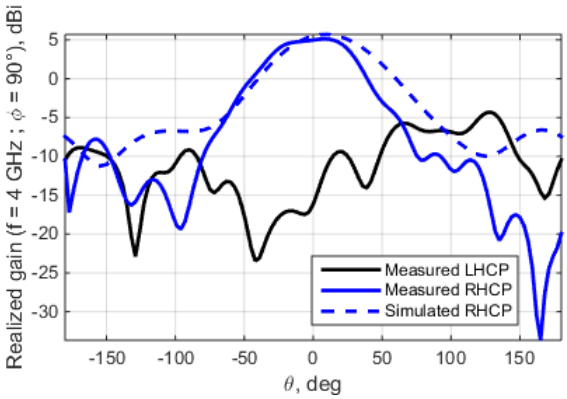

FIGURE 4.19: Measured realized gain of RHCP and LHCP (at 4 GHz and φ 90°)

4.3 Conclusion

This chapter presented a novel frequency reconfigurable UWB patch antenna with circular polarization over two channels, one centered at 4 GHz and the other at 6.49 GHz. The approach of capacitive feeding mechanism and air-suspended substrate were used to obtain a bandwidth of 500 MHz for each frequency configuration. Two branchline couplers on a bottom layer were used to obtain wideband CP operation. The antenna was fabricated and its reconfigurability was verified in terms of good impedance matching on both channels' frequency ranges. Its wideband CP operation along one of the channels (channel 2) was also verified, as it achieved 5 dBi of realized gain for RHCP on the main directions of radiation. These performances make this antenna a very suitable candidate for UWB localization systems' Anchor antennas as it operates in different channels, has a high gain compared to most existing UWB antennas, in addition to its circular polarization which is a very important feature that helps tags and objects' detection for small or large scale ranges.

Bibliography

[1] Federal Communications Commission (FCC), *First Order and Report, Revision of the Commission's Rules Regarding UWB Transmission Systems*, Part. 15, 2002, pp. 02-48.

[2] C.C Cruz, J.R Costa, and C.A Fernandes, "Hybrid UHF/UWB antenna for passive indoor identification and localization systems," IEEE Transl. Antennas and Propagation, vol. 61, no. 1, pp. 354-361, January 2013.

[3] Y. Duroc, A.I. Najam, *UWB antennas: design and modeling*, IntechOpen, 2010.

[4] Decawave, *DW1000 datasheet*, ver. 1.6, 2016.

[5] S.S. Zhong, X.L. Liang,"Progress in ultra-wideband planar antennas," J. of Shanghai University. 11, pp. 95–101, 2007.

[6] J. Nan, J. Zhao, M. Gao, W. Yang, M. Wang and H. Xie, "A Compact 8-States Frequency Reconfigurable UWB Antenna," in IEEE Access, vol. 9, pp. 144257-144263, 2021, doi: 10.1109/ACCESS.2021.3122250.

[7] S. Tripathi, A. Mohan, and S. Yadav, "A compact frequency-reconfigurable fractal UWB antenna using reconfigurable ground plane," Microw Opt Technol Lett. 59, pp. 1800–1808, 2017.

[8] M. Bitchikh, F. Ghanem, and S. Yadav, "A three-resolution UWB frequency reconfigurable antipodal vivaldi antenna for cognitive radios," The 8th European Conference on Antennas and Propagation (EuCAP 2014), pp. 3665-3668, 2014.

[9] G.M. Ridgers, J.W. Odendaal and J. Joubert, "Single-layer capacitive feed for wideband probe-fed microstrip antenna elements," IEEE Transactions on Antennas and Propagation, vol. 51, no. 6, pp. 1405-1407, June 2003.

[10] M. Stanley, Y. Huang, H. Wang, H. Zhou, A. Alieldin and S. Joseph, "A Capacitive coupled patch antenna array with high gain and wide coverage for 5G smartphone applications," IEEE Access, vol. 6, pp. 41942-41954, 2018.

Chapter 5

Antenna Contributions to the Improvement of Localization with UWB Real-Time Locating Systems

5.1 Introduction

Indoor object localization and positioning is part of the space-awareness concept which has seen a rising popularity in recent Internet of Things (IoT) research and applications. This article presents a novel method to improve the localization performance of ultra-wide band (UWB) real-time locating systems (RTLS) by improving the transmitting and receiving reader and tag antennas. Patch directional UWB antennas with relatively higher gain compared to the generally used standard omnidirectional monopole UWB antennas have been exploited to achieve a larger localization range. Furthermore, the patch antennas were designed to have wideband circular polarization to achieve two objectives: a received power independent of the orientation of the tagged objects that need to be detected, and the filtering of unwanted multipath signals. A measurement campaign was conducted using a commercially available RTLS with conventional antennas and then with the newly designed antennas. A comparison between the localization results of the two antenna types demonstrates an improved range with almost 100 m difference, received power independent of tag orientation, and increased multipath mitigation with the directional circularly polarized antennas.

5.2 State of the art

The future of real-time locating systems (RTLS) announces itself to be a prominent topic as its applications find a niche in most domains such as industrial, scientific, economic, and social [1,2].

RTLS technology for high-accuracy localization is based on the impulse-radio ultrawide bandwidth (IR-UWB) standard and was first introduced with the aim of locating objects in indoor environments [3,4] such as inside buildings, mines [5], and anywhere Global Positioning System (GPS) tends to fail owing to harsh propagating conditions. For example, this is the case when the presence of obstacles and reflecting objects leads to multipath components that affect the recognition of the desired signal. Fortunately, the UWB standard is more robust against such propagation hinders thanks to its wide spectrum (3.1 GHz - 10.6 GHz), where one UWB channel has a bandwidth of 0.5 or 1 GHz [6–8].

Current industrial real-time locating architectures target the most accurate indoor localization of objects [9]. Such architectures are primarly composed of one

or several readers and tags. While attempting to locate a tagged object, they receive continuously, real-time ranging signals in both the uplink (target -reader) and downlink (reader -target), or only in the uplink, depending on the ranging method used (two-way ranging (TWR) or time difference of arrival (TDoA), respectively [10]). Although the highest accuracy is targeted during this continuous exchange, as long as the locating system operates in a real imperfect environment, the system will most likely fail to locate the object precisely at least once among its total ranging attempts, especially in the case of changing environment due to the mobility of the tagged object. For this reason, the goodness of an RTLS is not only defined by its accuracy, but also by how consistently this accuracy is achieved. In some applications, such as localization using radio frequency-identification (RFID) technology, meter level accuracy is typically accepted as the objective is only to identify the tag and to know it is present inside a defined area [11]. In contrast, centimeter level accuracy is required in other applications, such as intelligent ressource management, supply and stock tracking in companies and personal medical monitoring in hospitals, which call for the use of UWB technology.

In addition to consistent and high accuracy, research needs to further explore other RTLS design specifications such as reading range, object orientation-independent power, multipath mitigation ability, and detectability without prior knowledge of the target direction.

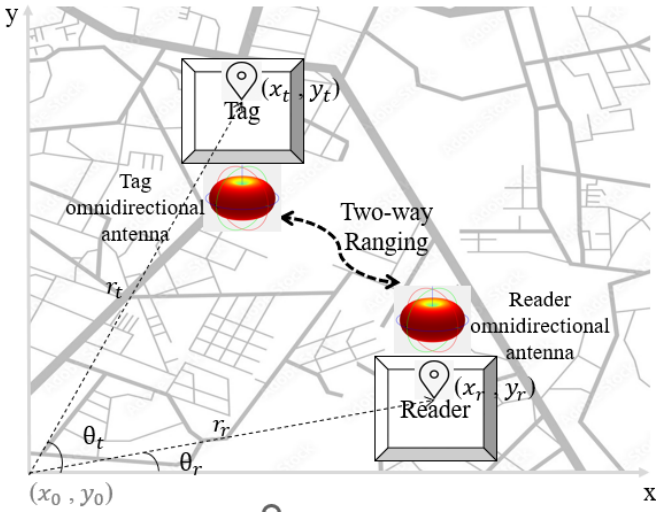

FIGURE 5.1: Conventional real-time locating system configuration.

First, the reading range of the RTLS must be investigated. Because the popularity of RTLS technology is typically for indoor use cases (from small surface retail centers to large warehouses where logistics need to be performed), the need to extend the reading range must be considered when choosing or designing the required RTLS. If this issue is considered from a broad perspective, the range depends first on the technology used for localization. If it is passive or semi-passive, such as RFID systems, then the achieved operating range will be limited to, typically, 10 m [12], as it mostly consists of passive tags, powered through wireless power transfer [13, 14]. However, if the technology is UWB, which mostly consists of battery-powered devices [15], the expected range can exceed 100 m, which is ten times greater than the current passive locating devices' range. If this issue is then considered from a more specific and smaller perspective, that is, with an already chosen technology in mind, the reading range depends deeply and mostly on the transmit power and link

margin of the radio system. In this case, improving the transmit power fed to the front-end antennas would require either increasing the transmitter power itself or choosing an antenna with a higher gain compared to the state-of-the-art dipole-like antennas commonly used in indoor locating systems.

The next step of this study consists of the design of RTLS antennas. Indeed, these front-end components play a significant role in improving localization results, not only in terms of reading range through gain adjustment but also in the ability to enable object-orientation independent power [16] and multipath mitigation [17] through polarization adjustment (from commonly linear to circular polarization). Indeed, in [18], antenna polarization was taken into account to characterize the transfer function of UWB transmitting and receiving antennas. For this reason, their optimization should be considered, particularly when other devices and hardware in the RTLS architecture cannot be optimized nor changed at all. Recently, for this purpose, a novel circularly polarized ultrawide bandwidth high-gain antenna operating over two 500 MHz channels was proposed by the same authors [19]. Moreover, the importance of attenuating multipath components for UWB ranging applications was highlighted in [20–24], thus, solutions such as the help of circular polarization in reducing these components need to be investigated.

Thus, the main contributions of this chapter are :

- To demonstrate, through a real-scenario measurement campaign, the advantages of using the realized directional circularly polarized UWB patch antenna [19] in an available commercial RTLS system [25]. The measurements consist in ranging with an UWB tag and reader in outdoor and indoor environments.
- To highlight the advantages of using a directional circularly polarized antenna by the comparison of the achieved localization quality while employing the directional circularly polarized antenna, with its performance when using commercial omnidirectional linearly polarized dipole-like antennas. This comparison between the two cases, is made in terms of the reading range, object orientation-independent received power, and multipath mitigation.
- To investigate the effect of this antenna's characteristics on the reading range. For this purpose, an outdoor environment was privileged for the ranging measurements, to benefit of unlimited distance for tests. The results showed that the directional circularly polarized antennas achieve about 100 m of increased range compared to the linearly polarized antennas.
- To investigate the effect of the antenna's circular polarization on enabling the independence of the received power from the relative orientations of the reader and tag antennas. For this purpose, ranging was performed for different reader and tag orientations, and an indoor environment was privileged to ensure the validity of the results even in a complex environment, including walls and objects. The received power was found to be independent of the orientations of the reader and tag when using the circularly polarized antennas.
- To demonstrate the effect of the antenna's circular polarization on the attenuation of the multipath signals during ranging measurements. The results showed that, both in indoor and outdoor environments, the multipath is significantly reduced in the case of circularly polarized antennas compared to linearly polarized antennas.

The remainder of this chapter is organized as follows. Section II describes the UWB locating architecture flow. Section III analyzes the employed UWB antenna design characteristics, followed by section IV in which the designed antenna results and a comparison with the commercial antenna are presented. Section V addresses the use case measurement campaign and scenarios, and discusses ranging measurement results in detail through a comparison study. Finally, the conclusions are presented in Section VI.

5.3 Localization with RTLS technology

Real-time locating technology allows the inference of highly accurate position information. It has emerged with the need to localize objects situated in harsh propagation environments, for example, trapped inside buildings or inside mines. Thus, it is employed in indoor scenarios characterized by the presence of multipath signals, reflections, and obstacles. To mitigate these problems and infer centimeter-level accuracy of the localization, RTLS is typically based on UWB signals, as they allow the precise measurement of the time-of-arrival (ToA) [9], from which the distance is then calculated during the received signal post-processing phase.

Fig. 5.1 illustrates the RTLS configuration considered in this study. It is composed of a reader-tag nodes couple that communicates through a two-way ranging (TWR) method, which resorts to ToA measurements to allow the reader to infer the tag's location.

5.3.1 Ranging method

The TWR method allows for ranging, that is, distance estimation between the two nodes. However, to infer tag position estimates of coordinates (x_t, y_t), at least three readers performing ToA measurements are required. In contrast, there is an additional well-known method, that uses only one-way tag-to-reader communication to obtain position information, which is TDoA method. This technique also requires at least three readers and estimates the position of the tag by measuring the difference in the time at which the signal from the tag reaches these readers [9, 10, 26].

In this study, the objective is to highlight the advantage of using more suitable antennas (180° directional radiation antennas with UWB circular polarization) compared to commonly used UWB low-gain omnidirectional antennas with linear polarization, to improve the performance of the general RTLS in terms of reading-range, object orientation independent power and achieved multipath filtering. Consequently, we focus on the TWR method to estimate the distance r_t between the reader and tag, as this objective needs to be initially verified for one reader-tag couple configuration to further seek its implementation in more complex architectures that call for a higher number of fixed readers.

5.3.2 Instrumentation and configuration

In this section, we describe the waterfall of the UWB RTLS system. Table 5.1 below lists the instrumentation components used during the ranging measurements.

Transmitter

In this study, the reader transmits a 500 MHz bandwidth UWB interrogation signal. In the time domain, this signal is a pulse of frequency $f_c = 4\ GHz$ with a pulsewidth

TABLE 5.1: Adopted instrumentation

Reader	UWB transceiver	STMicroelectronics [25]
Tag	UWB transceiver	STMicroelectronics [25]
Antenna 1	Omnidirectional	STMicroelectronics [25]
Antenna 2	180° radiation	this work and [19]

of $T_w = 3\ ns$ generated by the electronics board. The pulse is repeated with a period T_p and applied to an UWB antenna. According to STMicroelectronics documentation [25], the transmitted spectral power density measured at the antenna output has a peak level of $-36\ dBm/MHz$, which complies with the Federal Communications Commission (FCC) mask limits [4, 6, 7]. This limit is imposed on the effective radiated isotropic power (EIRP) and the antenna gain in the maximum direction of the transmitting antenna is considered [4, 10].

Communication link

The tag antenna receives the interrogation signal, which enables the tag to transmit its response signal after a fixed reply delay τ_d of the transceiver module. The TWR method between the reader and tag is illustrated in Fig. 5.2, as explained in [9].

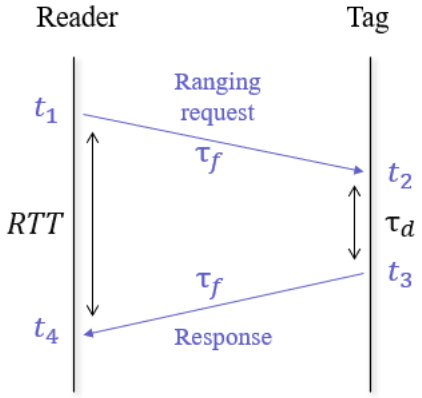

FIGURE 5.2: Two-way ranging principle.

Receiver

Because electromagnetic waves propagate in free space at a speed of light $c = 3 \times 10^8\ m/s$, it is possible to determine the distance between the reader and tag. The reader starts by having the instant t_1 time which is known to the module, sends the request packet to the tag and, then awaits the signal to return after a round trip time (RTT) to obtain the time instant t_4. The response delay, τ_d is primarily known to the device. Therefore, the time of flight between the reader and tag can be obtained from the following equations [9]:

$$\tau_f = \frac{(t_4 - t_1) - \tau_d}{2} \tag{5.1}$$

$$RTT = t_4 - t_1 \tag{5.2}$$

Using the obtained time of flight τ_f, the distance can then be computed, and the ranging is finalized.

5.4 UWB Antenna design

The following section focuses on the antenna component and details the design motivation and steps.

5.4.1 Antenna design motivation

Typically, in the RTLS architecture based on UWB technology, as mentioned previously, both reader and tag antennas exhibit omnidirectional dipole-like radiation behavior. Indeed, this is a key enabler for large coverage because both nodes can detect each other regardless of their relative position. However, for most localization techniques, and their applications inside buildings, retail wear-houses, or industrial infrastructure, readers are mostly fixed on walls or any vertical surface of a device such as a machine or a robot that goes around the facility to track items. This is the case, for example, for RFID and RTLS solutions proposed by "Kathrein" or "Turck Vilant" companies [27, 28].

Fixing a device with an omnidirectional antenna on a vertical surface would not take advantage of this omnidirectionality because half of the radiated wave would be absorbed on the back surface. Another case would be if an omnidirectional antenna is placed on a metallic surface, which would not absorb the wave but would disrupt the antenna performance particularly due to mismatch. Starting from this point, the constraint of omnidirectional radiation could be lightened on antennas for RTLS system readers, as only a 180° coverage would be sufficient to detect tags in the surrounding environment. For this reason, a patch-type antenna, operating along two 500 MHz UWB frequency channels (channel 2 and 5) was proposed in [19].
For details regarding UWB channels allocation in the frequency spectrum, Table 5.2 illustrates the lowband frequency UWB channels' information, among which the channels mentioned in this work are allocated.

TABLE 5.2: European UWB lowband frequency channels

Channel	Center frequency (MHz)	Bandwidth (MHz)
1	3494.4	499.2
2	3993.6	499.2
3	4492.8	499.2
4	3993.6	1331.2
5	6489.6	499.2

As observed, UWB channel 2 is centered at 4 GHz (3.75 GHz to 4.25 GHz), and channel 5 is centered at 6.5 GHz (6.25 GHz to 6.75 GHz). Thus, if desired, the initial antenna in [19] could be frequency reconfigured through p-i-n diodes to choose on which channel to operate, giving it the capability to adapt to different commercial RTLS UWB-based electronics modules provided for localization, which might not be designed to work on the same UWB channel. Furthermore, this antenna has the particularity of being circularly polarized along the UWB bandwidth of each channel enabling object orientation-independent ranging.

To accommodate the commercial RTLS and UWB localization module used for measurements (the B-UWB-MEK1 evaluation module [25] from former BeSpoon company, acquired recently by STMicroelectronics), which operates by default on channel 2, this channel was chosen as the channel along which the new antenna will be designed to operate.

Furthermore, because antenna frequency reconfigurability is not necessarily needed here, a simplified one-channel version of the previous antenna was designed and fabricated to operate along channel 2 and will be used on both reader and tag sides in the measurement campaign demonstrated below in chapter. In the following, we detail design method, characteristics, and results of the channel 2 antenna.

5.4.2 Antenna design

The objective of the design was a high-gain, UWB antenna with circular polarization and 180° radiation coverage. The design steps are summarized as follows:

- To achieve relatively high gain and 180° coverage, a patch-type antenna was chosen.
- Subsequently, a capacitive feed and coupling method was employed to achieve UWB impedance matching over the requested channel.
- Finally, a directional coupler was integrated into the bottom substrate layer to obtain circular polarization along the achieved antenna bandwidth.

The initial frequency reconfigurable antenna [19] profile is illustrated in Fig. 5.3 and the new simplified version (one-channel), designed here, is shown in Fig. 5.4. The adopted capacitive feed technique [29] is aimed at probe-fed patch antennas, and consists of exciting a small element placed on the same substrate layer as the radiating element and at a gap distance from it. The dielectric substrate was suspended in air as shown in Fig 5.3.

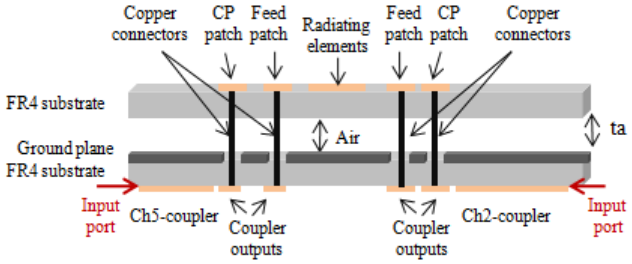

FIGURE 5.3: Side view of the frequency reconfigurable UWB antenna [19].

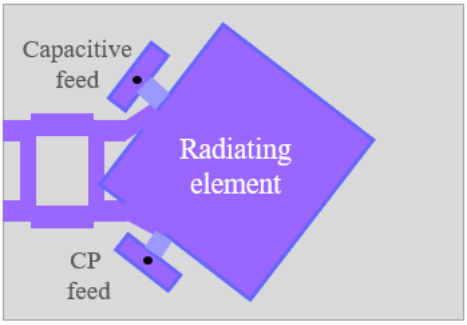

FIGURE 5.4: Simplified circular polarized antenna version, operating on one UWB channel, with radiating element (top layer) and directional coupler (bottom layer).

As illustrated in Fig. 5.4, the new antenna is composed of only one radiating element and one coupler both designed at the center frequency $f = 4\ GHz$. The dimensions of the radiating element are $W = L = 23\ mm$ and were derived from the standard patch antenna design. The two capacitive feed lines ensure two orthogonal feeds and thus circular polarization. They are both of width $wf = 1.6\ mm$ and placed at a gap distance from the radiating element $d = 2\ mm$. These two lines are both fed by vias attached to the coupler outputs which are situated at the bottom substrate. The vias start from this substrate and go through the ground plane, the air gap (ensuring bandwidth), and finally to the upper substrate.

5.5 Antenna simulation and experimental results

This section presents the performance of the antenna achieved by the simulation and measurements in terms of :

- Reflection coefficient (impedance matching) along the frequencies of UWB channel 2.
- Directivity and gain.
- Radiation pattern.
- UWB circular polarization along 180° coverage.

These results will allow the implementation of this antenna in the RTLS architecture for performing ranging measurements.
The circularly polarized UWB antenna operating in channel 2, was fabricated using FR4 substrate of height 0.8 mm for both substrate layers. The antenna prototype is shown in Fig. 5.5. The air gap betweeen the ground plane and the upper substrate was replaced by foam whose dielectric constant is the very close to that of air. The structure has two input ports, which are the inputs of the coupler, one of which is isolated during measurements using a 50 Ω match load.

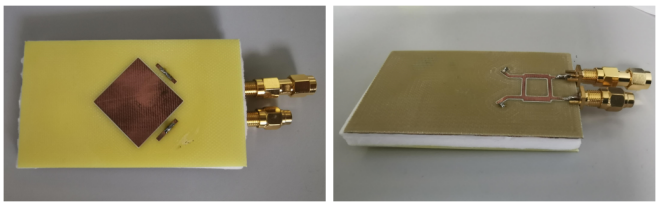

FIGURE 5.5: Prototype of the circularly polarized antenna operating over UWB channel 2.

5.5.1 UWB impedance matching

Fig. 5.6 shows the result of the simulated and measured reflection coefficient of one of the antenna ports ($S11$) with respect to the frequency, with the chosen air gap height $h_{air} = 7\ mm$, considering the symmetry of the structure, the results on port 2 (S22) are the same in both measurement and simulation. With reference to $-10\ dB$, the antenna impedance is matched along a bandwidth covering all UWB channel 2 frequencies. Furthermore, it can be observed that the antenna bandwidth covers more frequencies than the desired channel bandwidth, as it starts around 2.5 GHz

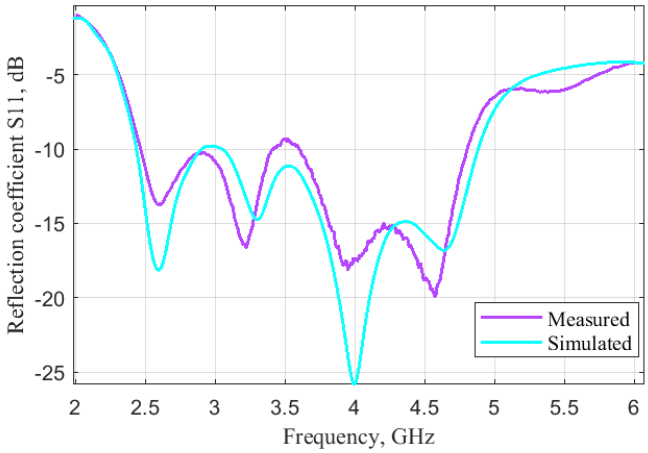

FIGURE 5.6: Antenna reflection coefficient.

and extends until around 4.8 GHz, this is a result of the chosen air gap height of 7 mm as this value is not the minimum limit value to achieve the 500 MHz range. This choice was made to cover the maximum bandwidth possible for other future use of the antenna and was not related to any other restrictions.

5.5.2 Directivity and gain

The antenna was measured in an anechoic chamber and Fig. 5.7 shows the resulting measured antenna directivity and gain with respect to frequency. The observed gain is of approximately 6.5 dBi and is stable along all channel 2 frequencies (3.75 to 4.25 GHz). The directivity follows the same curve but is naturally higher than the gain, maintaining a value of 8 dBi along the channel frequencies.

It must be pointed out that maintaining a stable gain along all the desired chan-

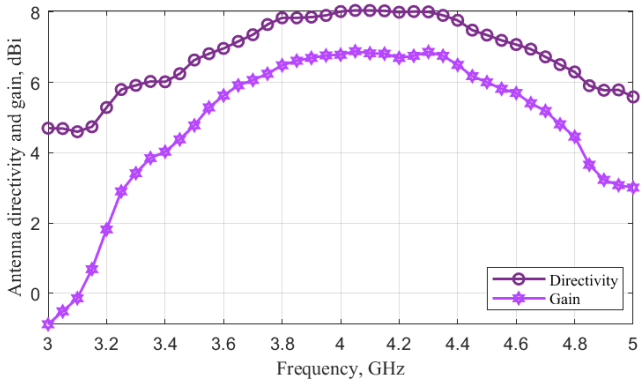

FIGURE 5.7: Measured antenna directivity and gain over the UWB channel 2 frequencies.

nel frequencies is important for UWB antennas to exhibit the same behavior while operating with UWB electronic devices.

5.5.3 Radiation pattern and circular polarization

The measured radiation pattern is presented in terms of polarization gain in the azimuth plane and plotted in Fig 5.8 and Fig 5.9. This radiation is measured at the center frequency $f = 4\ GHz$ varying the azimuth angle, for two elevation angles

0° and 90°. As shown in Fig. 5.8, the circular polarization of the antenna is right-handed (RHCP) because this polarization component has a gain of 6 dBi along the main direction of the radiation (around azimuth 0), which represents a difference of $+$ 16 dB with the contrapolar component in the same direction. Indeed, the cross-polarization, that is, the left-handed (LHCP) polarization, is at least -10 dB lower for any azimuth direction between -50° and 50°.

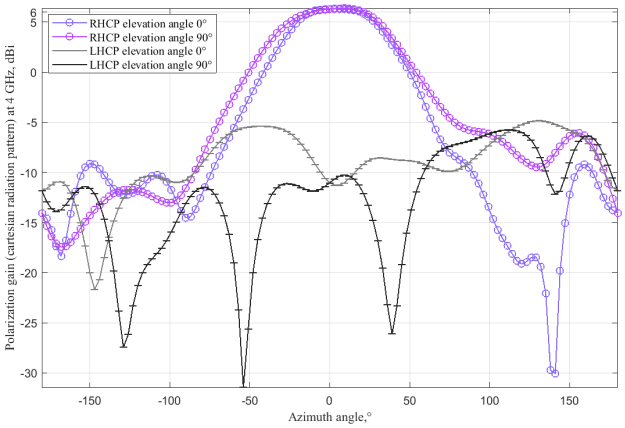

FIGURE 5.8: Measured azimuth antenna radiation pattern (polarisation gain) at center frequency 4 GHz, for elevation angles 0° and 90°.

5.5.4 Comparison with commercial antenna

The purpose of this work is to design a more suitable antenna optimized for real-time localization UWB commercial devices. A comparison with a commercial antenna belonging to the UWB evaluation kit from BeSpoon company (recently STMicroelectronics) [30] is reported in this section.

The radiation patterns of both the designed and commercial antennas are shown in Fig 5.9 and Fig 5.10 respectively. First, we observed the radiation behavior of the designed antenna through the radiation of its dominant RHCP polarization. It can be observed that the antenna radiates directionally with 180° coverage. It specifically maintains a high gain of 6 dBi along 70° azimuth centered at 0° for both elevation planes (0° and 90°, as shown in Fig. 5.9.a and 5.9.b respectively). Back lobes are attenuated on the back surface of the antenna to less than -8 dB.

As shown in Fig. 5.10, as the commercial antenna is linearly polarized (vertical polarization), it has E-plane and H-plane radiations. We intuitively associate its E-plane to the elevation plane and its H-plane to the azimuth plane. As the designed antenna radiation was traced with varying azimuth, we compare Fig. 5.9 RHCP radiation to the commercial antenna H-plane in Fig. 5.10 (varying azimuth, shown on the right figure). It can be observed that the commercial antenna for channel 2 has omnidirectional radiation along 360° with a gain of 2 dBi. Conversely, for the same gain, the designed antenna exhibits directional radiation along 95° azimuth. However, it has a higher gain along 70° in the azimuth plane, which includes the main directions of radiation when the antenna is fixed to a wall or vertical surface. The main differences between the antennas are presented in Table 5.3.

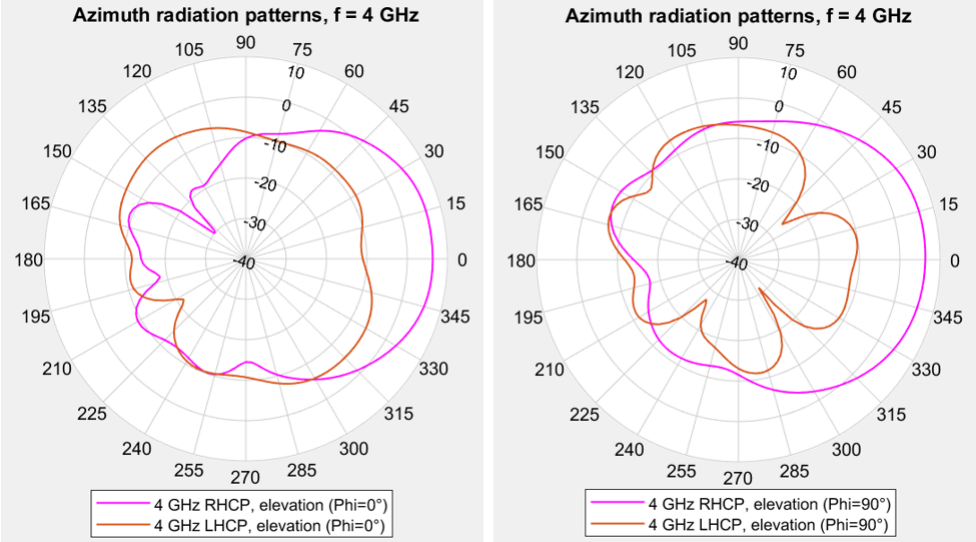

FIGURE 5.9: Designed circularly polarized antenna's measured radiation pattern at frequency 4 GHz in the two polarizations. (a) Elevation 0° (b) Elevation 90°.

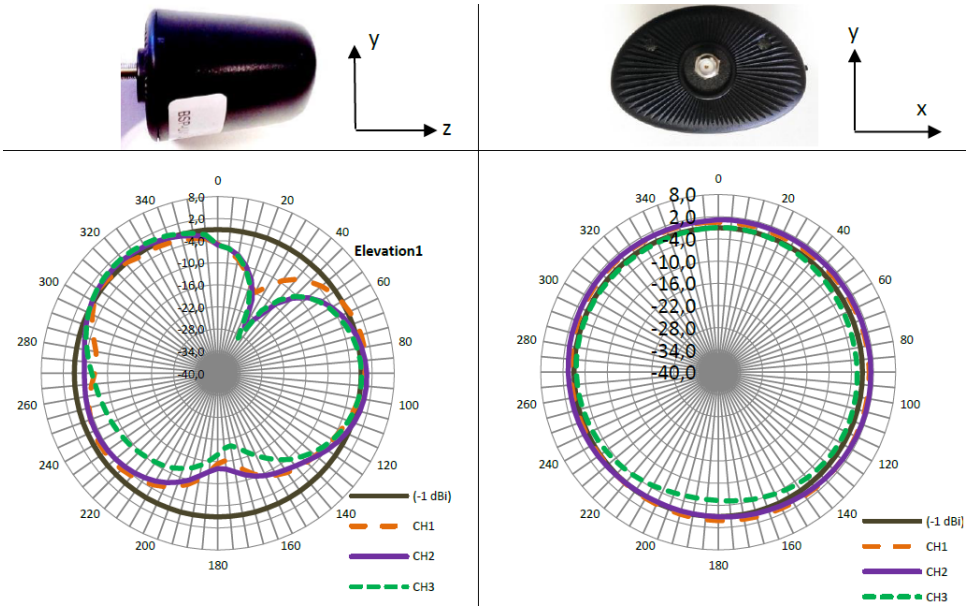

FIGURE 5.10: Commercial linearly polarized antenna's measured radiation pattern at channel 1, 2 and 3 [30].

TABLE 5.3: Antenna radiation comparison

Antenna 1 (commercial)	Antenna 2 (this work)
UWB channel 2	UWB channel 2
Coverage (360° azimuth)	Directional cov. (70° azimuth @ 5 dBi)
Low gain (2 dBi)	High gain (6 dBi @ 60° azimuth)
Linearly polarized	Circularly polarized

TABLE 5.4: Antennae characteristics

Charact. / Antenna	Antenna 1 (commercial [25,30])	Antenna 2 (this work and [19])
Frequency range	$2 - 4.77\ GHz$	$3.75 - 4.25\ GHz$
Reflection coeff.	$< -8\ dB$	$< -10\ dB$
Gain	$2\ dBi$	$6\ dBi$
Radiation	Omnidirectional	180° directional
Polarization type	Linear (vertical)	UWB Circular (Right-hand)

5.6 Measurement campaign and results

The experimental setup and measurements are presented in detail in this section. The objective is to demonstrate the improved efficiency of an RTLS using TWR method, to locate a tagged object by adjusting the antenna specifications to the localization method's needs. A measurement campaign was conducted using the STMicroelectronics UWB transceiver as an anchor and tag, and TWR between the two was performed in two cases:

- First, employing typical commercial UWB omnidirectional monopole antennas with linear polarization.
- Then, employing UWB directional patch antennas with circular polarization.

Measurements were repeated with the two antenna types for two different environments, outdoor and indoor, depending on the studied parameter (reading range, object orientation independence, and multipath mitigation). Finally, both antenna cases are compared and improvements are discussed.

The different characteristics of the antennas employed in these measurements are reported in Table 5.4 and, more specifically, in Table 5.3.

5.6.1 Outdoor scenario for reading-range

Although RTLS localization specializes in locating objects indoors because of its robustness to harsh propagating environments, this part of the measurements was realized in an outdoor environment because of space constraints inside buildings, in order to estimate the maximum reading range of the RTLS at hand, for the two employed antenna types. For this measurement, the transceiver tag was placed in a fixed position, and the transceiver reader was moved. The approach is to start with the reader as close as possible to the tag and then move away until the reader can no longer detect the tag. Thus, it is no longer outputting the ranging results. These ranging results appear on the computer to which the reader is attached as data acquisition is possible through UART on USB, which is also used to power the reader. The tag is powered by a power bank unit. The obtained results of ranging are as follows:

- The time between measurements in milliseconds, knowing that for the TWR mode, the transceiver is able to make a number of measurements up to $204/s$.
- Device ID of the reader board itself.
- Device ID of the tag board.
- The link quality indicator (LQI), which is the ratio of the measured received signal strength to the already known saturation signal strength of the transceiver, it is computed as a percentage.
- The corresponding reader-tag distance in meters.

Figure 5.11 illustrates the measured LQI with respect to the measured distance while moving further away from the tag.

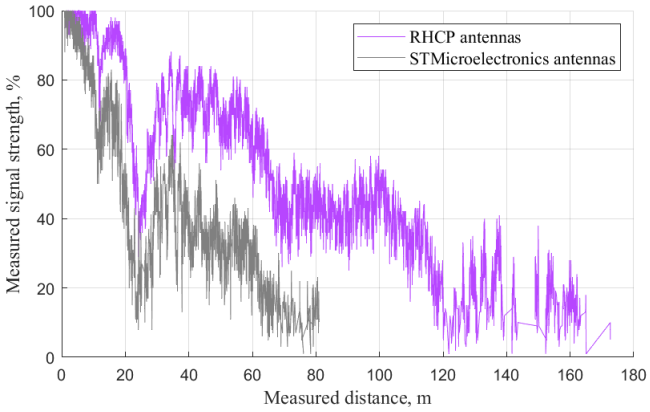

FIGURE 5.11: Comparison of the RTLS reading range when using the commercial antenna and the designed antenna.

Although the objective is to evaluate the performance range-wise, for clarity, the reading range is plotted on the horizontal axis. Indeed, it is easier to observe that the measured maximum reading distance is 82 m when using the commercial linearly polarized (LP) omnidirectional antennas, whereas it is 175 m when using this work's directional CP patch antennas. Thus, an important difference of almost 100 m in the maximum reading range was obtained owing to the antenna gain improvement.
It is important to note that, even in line-of-sight (LOS) conditions, the environment and the initial position of the fixed tag or the position of the mobile reader during the campaign leads to variations in the measurement results, such as the maximum range obtained, due to the random nature of the radio propagation channel. This is to highlight that, for example, the maximum range obtained with the commercial transceiver and antennas here of 82 m is indeed different from the datasheet, which claim a maximum range of 600 m, as typically this value is obtained either theoretically or through LOS measurements within a better propagating environment to obtain the best result possible. In contrast, the measurements in this study were performed in a completely realistic and imperfect outdoor environment. Indeed, other measurement campaigns that we performed with commercial transceivers and antennas were able to exceed 85 m and achieved a maximum range of approximately 120 m in a real environment, which is still significantly lower than the 175 m achieved by the designed antenna. In conclusion, to compare the performance of RTLS parameters such as range, it is essential to ensure that the experimental setup and

environmental characteristics are as closely matched as possible to obtain accurate comparable results.

5.6.2 Indoor scenario for object orientation independence

The objective of the following experiment is to detail and verify the robustness brought to the RTLS by the circular polarization characteristics of the designed antennas. This robustness is mainly against two hindering factors in radio propagation, namely, the multipath signals due to reflections against surfaces or objects, and the received signal attenuation due to polarization mismatch between reader and tag (which depends on tag-reader relative orientation).
The reason why an indoor scenario was preferred for this experiment is that the RTLS has to prove itself robust in a harsh environment (presence of objects and obstacles), as this would mean it will also have good performance in outdoor scenarios that tend to have fewer constraints, such as the absence of walls.
The considered indoor environment was the corridor of the LEAT laboratory that is 50 m long. The tag was mobile and the reader was fixed at one corridor end. Steps of 15 m were set using a laser telemeter to determine the true absolute distances at which the ranging measurements were taken. The reader antenna is kept on a "vertical" configuration and the tag antenna orientation is first set to vertical (0°), and then changed to horizontal (90°) orientation.
Fig. 5.12 and 5.13 illustrate the orientation configurations of the two antennas, the commercial linearly polarized antennas and designed circularly polarized patch antennas, respectively.

FIGURE 5.12: Two-way ranging with the commercial antenna, characterized by 360° omnidirectional radiation and linear polarization.

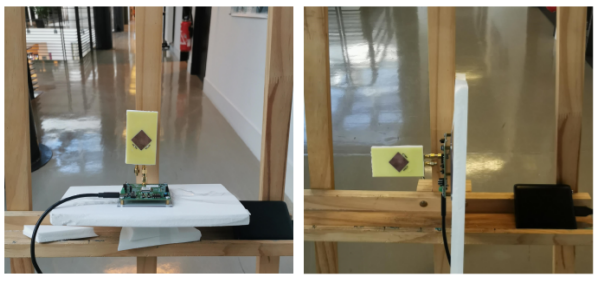

FIGURE 5.13: Two-way ranging with the designed antenna, characterized by 180° directional radiation and circular polarization.

To measure the polarization-mismatch independence of the received power between the reader and tag, a comparison between the LQI results obtained by ranging

(that is, distance measurement) with reader-tag antenna co-orientation and cross-orientation is required. The following steps are followed for each distance point:

- Measurement of the LQI (by ranging) with reader and tag antennas having the same orientation d_{cop} (for example, vertical reader - vertical tag).
- Measurement of the LQI with reader and tag antennas with orthogonal orientations d_{crossp} (for example, vertical reader - horizontal tag).

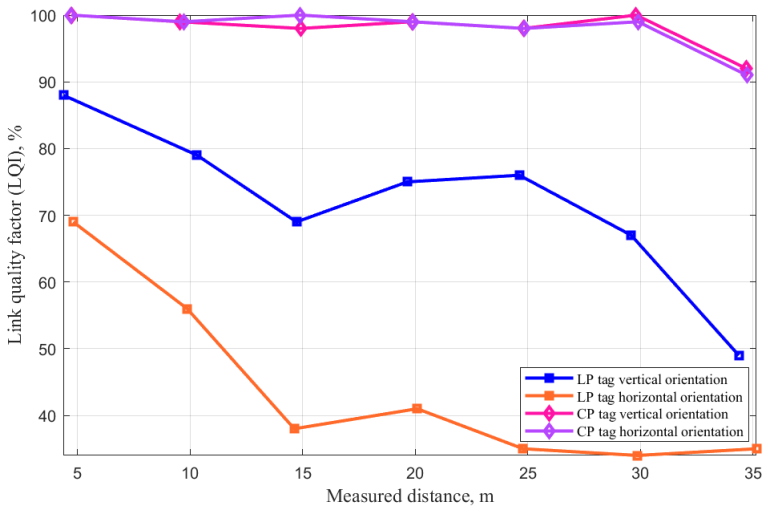

FIGURE 5.14: Object orientation-independence of received power, comparison between linearly and circulary polarized antennas. Reader antenna always in vertical orientation.

Fig. 5.14 illustrates the LQI as a function of the measured distance for the different antenna cases. LQI is proportional to the received power. These results were obtained by ranging indoors to up to 35 m, with the reader antenna always fixed in a vertical orientation.
By comparing the LQI achieved in the figure, it can be observed that, in the case of the circularly polarized reader and tag antennas, the LQI (and thus the received power) is almost identical at all distances, regardless of the orientation of the tag antenna, that is, regardless of wether it's the same as the orientation of the reader antenna.
Differently, in the case of linearly polarized antennas used in both the reader and tag, the received power is very different between co-polarization and cross-polarization cases (blue and orange curves), along all distances. Here, the difference between their LQIs varies between 20 % and 50 %. This is a significant amount of power attenuation caused by polarization-mismatch, which greatly deteriorates the RTLS performance, as some objects may not be detected if their antennas is not oriented in the same orientation as the reader antenna.
It is important to note that polarization-mismatch induced power attenuation (which can occur if the antennas are linearly polarized and have cross-orientations), for longer distances, especially closer to reader sensitivity, can also negatively affect the reading range.
It can also be observed in the same figure that the LQI achieved by the circularly polarized antennas is always $\approx$ 20 % higher than the LQI obtained in the best case

scenario of linearly polarized antennas (ie. both the reader and tag antennas vertical). This difference is mainly owing to the higher gain of the designed directional antennas.

5.6.3 Multipath mitigation with circular polarization

Fig. 5.15 illustrates further indoor and outdoor ranging measurements, where the objective is to investigate wether circular polarization helps mitigate multipath reflection signals, which tend to be more prevalent in indoor environments because of the presence of walls and usually more objects. Behind the reasoning that circular polarization reduces the number of multipaths, is that if the transmitting and receiving antennas both have same-sense circular polarization (here, right-hand sense), the receiver antenna filters out reflected signals from metallic surfaces as they are reflected with circular polarization of opposite-sense [17]. Furthermore, multipath is undesired in localization applications because of the possibility of path-overlap [31], which consists of reflection signals overlapping with the first direct-path signal, from which the time-of-arrival is computed. This path-overlap would then cause non-recognition of the direct path signal which will lead to errors in the time-of-arrival measurement and thus errors in distance estimation.
Thus, we evaluate the LQI curves, obtained through ranging, to determine the multipath effect on the ranging measurement and compare it between the two antenna cases, with linear and circular polarizations.

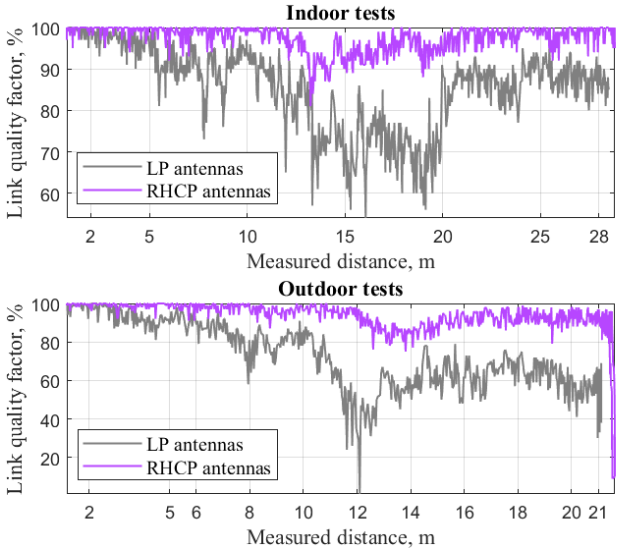

FIGURE 5.15: Multipath and antenna gain effects on received signal strength in ranging.

From the results shown in Fig. 5.15, the curves of the linearly and circularly polarized antennas follow almost the same high-and-low patterns at the same distances, in both indoor and outdoor measurements. This is because the same multipath signal components were present at these distances (that is, identical environment at each distance). Thus, this multipath will affect the propagation in the same manner for both antenna types, indoors and outdoors.
Furthermore, if we compare the linearly polarized antenna curve with the circularly polarized antenna curve (both indoors and outdoors), it can be observed that the LQI and thus received power dips and peaks are less significant and have a low level of variation when using circular polarization compared to linear polarization. This

observation demonstrates that circular polarization with the same direction (here, Right Hand) in both reader and tag antennas helps to filter reflections, precisely those that arrive with opposite circular polarization (here, Left Hand). This can be observed for both the indoor and outdoor cases.

5.7 Conclusion

This chapter investigated the positive effects and advantages of using directional circularly polarized UWB antennas to improve RTLSs in terms of reading range, object-orientation independent received power, and multipath mitigation. Real-environment measurements were conducted in indoor and outdoor scenarios using a commercially available RTLS. The results demonstrate that the reading range was improved in the case of the designed directional antennas compared to conventional omnidirectional UWB antennas by almost 100 m owing to the higher gain, as well as to the suppression of the cross-polarization mismatch effect on the received signal strength by circular polarization. Object-orientation independent received power was also observed in the case of circularly polarized antennas, especially in harsh indoor environment. In contrast, power attenuation caused by polarization mismatch was observed in the case of linearly polarized antennas. Furthermore, circularly polarized antennas were observed to help multipath mitigation in both indoor and outdoor scenarios, as the LQI curves demonstrated less harsh variations compared to linearly polarized antennas.
Thus, we conclude that locating systems can be significantly improved through directionality and circular polarization of antennas compared with the currently widely used omnidirectional linearly polarized UWB monopole antennas. The type of antennas presented in this work can not only improve time-based locating systems, such as the system employed here, but also received signal strength indicator (RSSI) based locating technologies, such as RFID locating, as it would help increase the power and thus help additionally provide precise localization information.

Bibliography

[1] L. Yang and G. B. Giannakis, "Ultra-wideband communications: an idea whose time has come," in IEEE Signal Processing Magazine, vol. 21, no. 6, pp. 26-54, Nov. 2004.

[2] G. R. Aiello and G. D. Rogerson, "Ultra-wideband wireless systems," in IEEE Microwave Magazine, vol. 4, no. 2, pp. 36-47, June 2003.

[3] R. A. Scholtz, "Impulse Radio: How it works," IEEE Communications Letters, Vol. 2, NO. 1, Jan. 1998.

[4] FCC, "Revision of part 15 of the commission's rules regarding Ultra-Wideband transmission systems," Federal Communications Commission, Washington, D.C., Tech. Ref. ET Docket 98-153, Apr. 2002.

[5] Y. Rissa, L. Talbi, and M. Ghaddar, "Experimental characterization of an UWB propagation channel in underground mines," IEEE Trans. Antennas Propag., vol. 60, no. 1, pp. 240–246, Jan. 2012.

[6] "IEEE Standard for Low-Rate Wireless Networks," in IEEE Std 802.15.4-2020 (Revision of IEEE Std 802.15.4-2015) , vol., no., pp.1-800, 23 July 2020.

[7] "IEEE Standard for Low-Rate Wireless Networks–Amendment 1: Enhanced Ultra Wideband (UWB) Physical Layers (PHYs) and Associated Ranging Techniques," in IEEE Std 802.15.4z-2020 (Amendment to IEEE Std 802.15.4-2020), pp.1-174, 25 Aug. 2020.

[8] M. Ghavami, "Ultra Wideband Signals and Systems in Communication Engineering", 1st Edition, Wiley, 2004.

[9] S. Frattasi, F.D. Rosa, and D. Dardari, *Ultra-wideband Positioning and Tracking. In Mobile Positioning and Tracking*, ed. S. Frattasi and F.D. Rosa, 2017.

[10] N. Decarli and D. Dardari, "Time Domain Measurements of Signals Backscattered by Wideband RFID Tags," in IEEE Transactions on Instrumentation and Measurement, vol. 67, no. 11, pp. 2548-2560, Nov. 2018.

[11] T. Sanpechuda and L. Kovavisaruch, "A review of RFID localization: Applications and techniques," 2008 5th International Conference on Electrical Engineering/Electronics, Computer, Telecommunications and Information Technology, pp. 769-772, 2008.

[12] K. Finkenzeller, "RFID Handbook: Fundamentals and Applications in Contactless Smart Cards and Identification," 3rd ed. Wiley, 2010.

[13] D. Dardari et al., "An Ultra-Low Power Ultra-Wide Bandwidth Positioning System," in IEEE Journal of Radio Frequency Identification, vol. 4, no. 4, pp. 353-364, Dec. 2020.

[14] A. Sidibe, M. A. Kassem, A. Takacs, J. Mennekens and J. Dachy, "Autonomous and Battery-Free Wireless Tag combining UWB and BLE Technology," 2022 Wireless Power Week (WPW), Bordeaux, France, 2022, pp. 207-212.

[15] D. Dardari, A. Conti, U. Ferner, A. Giorgetti and M. Z. Win, "Ranging With Ultrawide Bandwidth Signals in Multipath Environments," in *Proceedings of the IEEE*, vol. 97, no. 2, pp. 404-426, Feb. 2009.

[16] C. Su, Y. Liu, L. Liu, M. Yang, H. Zhao, and X. Yin, “Experimental Evaluation of Multipath Mitigation in TDOA-Based Indoor Passive Localization System Using A Beam Steering Broadband Circular Polarization Antenna,” Electronics, vol. 7, no. 12, p. 362, Dec. 2018,

[17] R. Szumny, K. Kurek and J. Modelski, "Attenuation of multipath components using directional antennas and circular polarization for indoor wireless positioning systems," European Radar Conference, 2007, pp. 401-404.

[18] X. Qing, Z. N. Chen, and M. Y. W. Chia, “Characterization of ultrawideband antennas using transfer functions,” Radio Sci., vol. 41, no. 1, pp. 1–10, Feb. 2006.

[19] A. Benouakta, F. Ferrero, L. Lizzi and R. Staraj, “Frequency Reconfigurable and Circularly Polarized Patch Antenna Over Dual Ultra-wideband Channels,” in *16th European Conf. on Antennas and Propagation (EuCAP)*, Madrid, Spain, 2022, pp. 1-5.

[20] A. F. Molisch, D. Cassioli, C.-C. Chong, S. Emami, A. Fort, B. Kannan, J. Karedal, H. G. Schantz, K. Siwiak, and M. Z. Win, “A comprehensive standardized model for ultrawideband propagation channels,” IEEE Trans. Antennas Propag., vol. 54, no. 11, pp. 3151–3166, Nov. 2006.

[21] A. F. Molisch, “Ultra-wide-band propagation channels,” Proc. IEEE, vol. 97, no. 2, pp. 353–371, Feb. 2009.

[22] A. Fathy, A. Yahya, and H. Ragai, “Deterministic UWB channel modeling using ray tracing approach,” in Proc. Int. Conf. Eng. Technol. (ICET), Cairo, Egypt, Apr. 2014, pp. 1–4.

[23] P. Pagani, F. T. Talom, P. Pajusco, and B. Uguen, "Ultra Wide Band Radio Propagation Channels: A Practical Approach,". Hoboken, NJ, USA: Wiley, 2008.

[24] M. Schmieder, F. Undi, M. Peter, E. Koenig, and W. Keusgen, “Directional wideband channel measurements at 28 GHz in an industrial environment,” arXiv preprint arXiv:1907.01346, 2019.

[25] *Evaluation kit for the B-UWB-MOD1 ultra-wideband module*. [Online]. Available : https://www.st.com/en/wireless-connectivity/b-uwb-mek1.html

[26] D. Dardari, N. Decarli, A. Guerra, A. Al-Rimawi, V. M. Puchades, G. Prati, M. De Angelis, F. Fraboni, L. Pietrantoni, "High-Accuracy Tracking Using Ultrawideband Signals for Enhanced Safety of Cyclists," in *Mobile Information Systems*, vol. 2017, Article ID 8149348, 13 pages, 2017.

[27] *Katherein solutions*. [Online]. Available : https://www.kathrein-solutions.com/

[28] *Turck vilant*. [Online]. Available : https://turckvilant.com/

[29] G.M. Ridgers, J.W. Odendaal and J. Joubert, “Single-layer capacitive feed for wideband probe-fed microstrip antenna elements," IEEE Transactions on Antennas and Propagation, vol. 51, no. 6, pp. 1405-1407, June 2003.

[30] *BeSpoon UWB Omnidirectional antenna BSP-UWBA-Om4G, datasheet V.1.0.* [Online].

[31] Y. Shen and M. Z. Win, "Effect of Path-Overlap on Localization Accuracy in Dense Multipath Environments," 2008 IEEE International Conference on Communications, Beijing, China, 2008, pp. 4197-4202.

Chapter 6

Multi-Standard UWB-LoRa High-Accuracy Long-Range Localization

6.1 Introduction

Long-Range Wide-Area Networks (LoRaWAN) allow the transmission of data via radio link from sensors, which are potentially isolated or difficult to access, to gateways and servers that are connected to cellular networks for data processing, exchange, or relay, with low transmission power. This concept employs Long-Range (LoRa) modulation and has led to the emergence of many applications for the monitoring and tracking of objects. However, due to its characteristic of a low data rate for low-power communication, the transmission of information with LoRa tech-nology is not suitable for the fast real-time monitoring of data. Additionally, due to its narrow bandwidth, an attempt to perform localization through the LoRa modulation technique will result in very limited accuracy because of its inability to resolve multipath problems. Thus, in this chapter, we propose a multi-standard Ultra-Wide Bandwidth (UWB) and LoRa end-device that is capable of measuring location with high accuracy using UWB technology and then transmitting the location information through LoRa method to gateways and the Internet of Things Network. The results of measurements in indoor and outdoor scenarios show a UWB localization accuracy that is of sub-meter level, being between 10 and 33 cm, and a UWB range of 124 m in Line-of-Sight (LOS) and 55 m in Non-Line-of-Sight (NLOS) applications, respectively.

The connectivity of objects to gateways using the LoRaWAN protocol has allowed the emergence of many monitoring applications, such as intelligent resource management, predictive maintenance, supply and stock tracking, object and animal tracking and personal medical monitoring [1]. This suggests infinite monitoring possibilities depending on the physical variable detected via the sensor. Besides these monitored variables, it is often necessary for gateways to monitor the location of the sensor itself [2], especially if it is integrated into a mobile object or tag, for example, if this latter feature is moving inside an indoor environment. The task of localizing a mobile sensor could be challenging for the LoRa working scheme, as this type of communication was not orig-inally optimized for such an application [3], especially if the localization is required to be of high accuracy or expected to accommodate both indoor and outdoor scenarios. In contrast, the main advantage of LoRa communication in LoRaWAN networks is that the sensing information can be transmitted along long ranges in the order of kilometers, typically ranging from 5 km in urban areas up to 15 km in remote areas, from the sensor to the gateways [4, 5]. Indeed, the LoRa technique is used to ensure deep-in communi-cation among a large number of devices that have low power requirements and collect and transmit small amounts of data [5,6]. Furthermore, LoRaWAN networks have a high capacity and can handle millions of messages from thousands of gateways. However, despite these advantages, this technology is still not suitable for gateways to locate mobile sensors precisely and as often as is necessary [7]. Indeed, to ensure the low consumption of power, LoRa sensors send data with low packet rate [8, 9], that is, typically one or two packets are sent per day. This is not suitable if the object monitored is mobile in its environment and requires real-time monitoring, or at least partial real-time monitoring, which cannot be achieved with the relatively low data rate of the LoRa technique. Furthermore, if the monitored object needs to be located with high accuracy and/or if it were in an indoor environment, we would require radio communications with wide frequency band-widths to resolve multipath problems [10]; however, this is not the case for narrowband LoRa communications, which have bandwidths of a few MHz.
Conversely, Ultra-Wide Bandwidth (UWB) is the pervasive technology nowadays when it comes to locating objects or tracking assets or any type of targets, especially those in complex indoor environments, such as inside buildings, industrial infrastruc-tures, hospitals, airports, construction sites [11, 12], etc. It is effectively used in time-based ranging and localization techniques such as one-way or two-way ranging with Time-of-Flight (ToF) and Time-Difference of Arrival (TDoA) [13]. It allows high-accuracy distance and position estimates, notably due to the transmission of the ranging infor-mation along a large frequency bandwidth of 500 MHz or more between a reader and a target. Its constraint is that it is considered a short-range communication technology despite having reading ranges of typically 100 to 200 m in Line-of-Sight applications [14], which are mostly enough for indoor use cases but cannot adapt in networks deployed in highly remote outdoor areas, where objects can be spaced with more than those distances, i.e., such as in LoRaWAN networks.

Thus, in this work, we propose combining both LoRa and UWB technologies as complementary Internet of Things (IoT) schemes into one transceiver board to exploit both of their principal features. This combination enables LoRa gateways to locate the sensors that belong to it if they are mobile in their environment, with the high-accuracy and real-time availability of their position information. It also allows for UWB targets to be located at long-range data links such as those of LoRa links.

This solution consists of employing UWB technology in the mobile target LoRa sensor to allow LoRaWAN gateways to track it in real time with high accuracy. The result is a multi-standard UWB-LoRa transceiver, which can work as a sensor-tag or a reader depending on where it is placed in the communication chain. For this reason, we propose equipping the mobile LoRa sensor with UWB technology (LoRa-UWB sensor-tag) and placing the proposed UWB-LoRa reader device as an intermediate node between the target object and the gateway. The reader receives the location information from the sensor-tag in real time through UWB ranging with ToF and sends it to the gateway through LoRa signals.
The remainder of this chapter is organized as follows: Section 2 describes the related work in the context of the localization with LoRa technology Section 3 first describes the overall UWB-LoRa localization system before describing the design and structure of the proposed UWB-LoRa transceiver, and the last subsection focuses on the design of the antenna structure that is included in the transceiver. Section 4 presents the characteri-zation results of both antennas from their reflection coefficient to their radiated patterns, followed by Section 5, in which the achieved localization of the transceiver is discussed and characterized by the UWB localization range and accuracy between the sensor-tag and the reader, as well as the location information transmission from the reader to the network. Finally, Section 6 concludes on the paper contributions and results.

6.2 Related work

Previous research has realized localization attempts via LoRa technology, mostly using the Time Difference of Arrival (TDoA) method [7, 15, 16], which requires at least three gateways to infer the location of the object. For example, in [16], a number of sets of messages sent via the target sensor were used to calculate the TDoAs of these messages and perform location estimation at the gateway level, the authors assessed the efficiency of the performance of the localization and the results indicated that the localization error was greatly affected by the noise of the received timestamps at the base stations. In [17], a similar procedure was followed to implement a LoRaWAN tracking system that was capable of exploiting transmitted packages to calculate the current position, and using LoRa signals and applying a multilateration algorithm on the timestamps received at the gateways, the results demonstrated that it can be feasible to locate a device in a static spot with an accuracy of around 100 m, though this accuracy is not good enough for indoor scenarios.
The reason that the times of arrival were not precise enough is the combination of undesired multipath signals at the receiving gateways, with these signals being due to the environment and unavoidable, especially because LoRa signals' widths in time (142 ns for the 863–870 MHz channel) are not narrow enough for the multipath to be dis-tinguished from the desired path signal. In addition to problems related to low accuracy, the previously cited studies all employed three or more gateways to infer the positions of the sensors via the TDoA method, which represents another constraint, as the already deployed LoRaWAN networks do not always geographically provide this condition.
Other studies employed the ToF method to measure the distance between one gateway and the object [2]; however, the server can only calculate this distance based on the packet metadata provided by the gateway, and these metadata are only sent with low data rates, which make real-time monitoring difficult to achieve. Furthermore, in [18], researchers proposed a ToF-based localization method using a fingerprint

map to handle the accuracy issues and reduce the localization error caused by the noise and multipath; however, the fingerprinting method depends on the environment and needs to be updated for the location estimation to work accordingly, which makes it effort and time consuming.
Other methods include the using Received Signal Strength Indicator (RSSI) to infer the distance. For example, in [19], researchers measured the RSSI in an indoor envi-ronment with a short distance under both LOS and NLOS conditions, and the results showed the occurrence of power loss by the received signal, despite the short distances of measurement, and these losses were more important in the NLOS conditions compared to those observed in the LOS conditions. In [20], the authors investigated the accuracy of LoRa positioning using RSSI measured at the gateways, and, in realistic conditions where the power attenuation caused by the radio link was not known, the work reported ac-curacy errors of up to 588 m. Another recent work [21], proposed an extensive position estimation algorithm to minimize the posteriori RSSI error for multi-anchor cooperative estimation scenarios, and the results showed that the location can be estimated with an accuracy less than 7 m; however, this system was only tested in an outdoor scenario, which tends to be less challenging than indoor scenarios. Indeed, localization via the RSSI method is based on signal power, which makes it very sensitive to multipath, and cannot provide high accuracy information, as the correlation between the received power and the distance is significantly influenced by the environment, which means that it cannot reliably infer the target's location information [22, 23].
In this chapter, the low-accuracy localization problem and the need for multiple gateways or extensive algorithms to improve accuracy are overcome by integrating UWB technology into the LoRa sensor; furthermore, real-time localization is enabled thanks to the UWB's high data rate and ability to detect tags whenever necessary, as judged by the gateways. In this work, we propose a LoRa-UWB transceiver that can be used as both a sensor-tag and an intermediate reader between the sensor-tag and gateway, and this study mainly focuses on the localization rather than the sensing function of the LoRa sensor-tag. The advantage of the proposed solution is that the localization of the mobile sensor-tag is performed before sending anything to the gateways (the distance between the sensor-tag and the UWB-LoRa reader is computed at the reader node). This allows the comparison of the received location information to the previous information, and we only send the data to the gateway if they are different. Location via LoRa would first require directly sending the data packet containing the time of the flight, then calculating the distance. In addition, the possible inconvenience of the proposed solution mainly consists of deter-mining how flexible the application is toward the ability to add the reader node between the sensor-tag and the gateway.

6.3 UWB-LoRa localization method

This section describes, first, the transmission chain of the UWB-LoRa localization scheme and then, the structure of the UWB-LoRa transceiver (reader and sensor-tag) and its contents from modules to the required integrated UWB and LoRa antennas.

6.3.1 LoRa-UWB sensing and ranging approach

Figure 6.1 shows the working transmission chain related to the context in which the LoRa-UWB transceiver is set to operate. As an example, the chain consists of several

LoRa sensors deployed in different locations that communicate with a LoRaWAN gateway, as conventionally performed. In addition to these tags, a UWB- equipped LoRa sensor-tag is placed and can directly communicate with either the gateway to transmit sensing data, or an UWB-LoRa reader device to perform two-way ranging, obtain the Time-of-Flight (ToF) at the reader node and compute the distance between the two measures. The reader then sends the ranging information to the gateway through LoRa signals. Since the gateway is knowledgeable a priori of the reader's location, it can determine the location of the sensor-tag and mon-itor its movement in the environment.

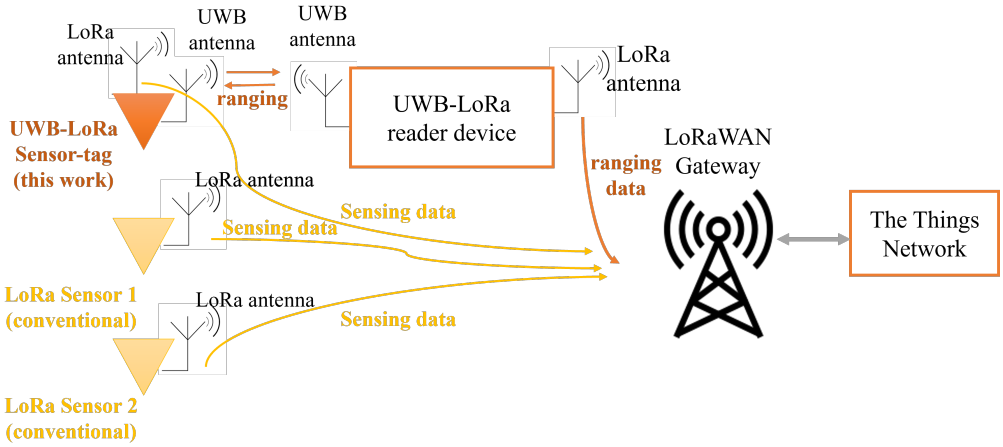

FIGURE 6.1: Communication chain structure from the sensor tags to the network and gateways.

Figure 6.2 presents the working organigram of the system and the roles of each node in more detail. It consists of the LoRa gateway, a sensor-tag and a UWB-LoRa reader that acts as an intermediate node between the two features.

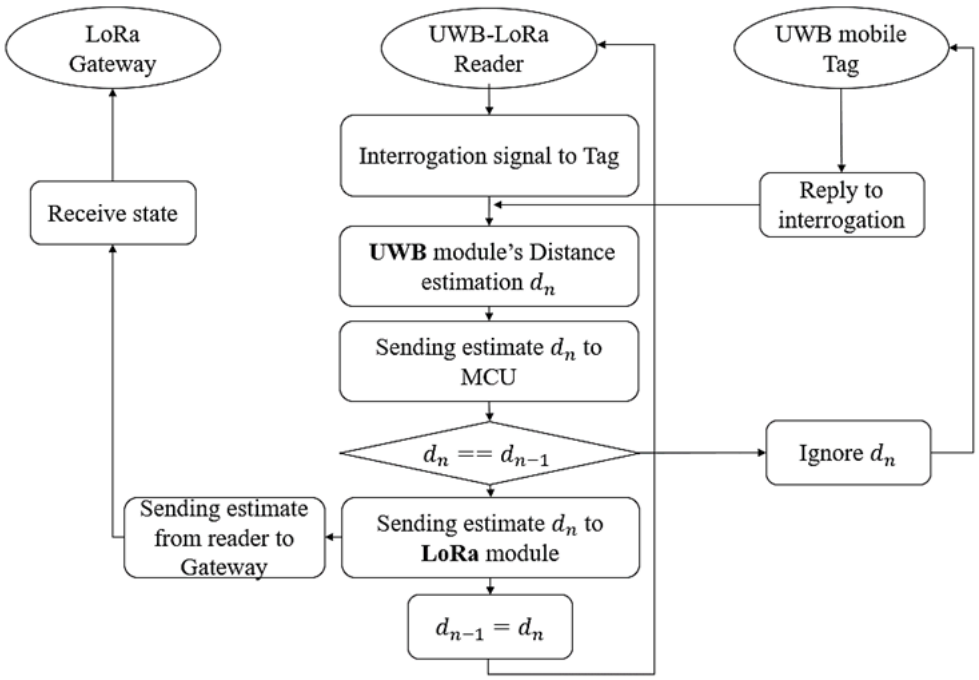

FIGURE 6.2: Organigram of the working localization system highlighting the role of each node.

In this setting, the gateway is required to determine the location of the sensor-tag, especially if this location is moving in its environment. Following the ranging principle using UWB technology, the reader sends an interrogation signal to the sensor-tag, to which the tag replies by an acknowledgment signal. Through the measure of ToF of these signals, the reader obtains a ranging estimate d_n , which is the distance between the sensor-tag and itself. While all these steps have been realized through UWB protocol, the reader, then enters a decision phase: whether to send the obtained location estimate to the LoRa gateway or not. The decision is taken after comparing the actual distance value with the previous one a priori stocked. The reader will only send the location of the sensor to the gateway if this sensor has moved and changed location since the last measure. A microcontroller unit (MCU) assures the communication between the reader's UWB and LoRa modules. If the new distance estimate d_n is not different from $d_{(n-1)}$, then it is ignored, and the interrogation is sent again to the sensor-tag. If it is different, then it means the tag has moved and its location has changed. In this case, the estimate is sent to the LoRa module and automatically from this module to the LoRa gateway through LoRa antennas, and d_n is stocked by replacing $d_{(n-1)}$ for the next loop iterations.
The main advantages of the presented localization technique are:

- The accuracy of the localization is of UWB-level accuracy which is approximately 15 to 20 cm and some cases even less. This accuracy cannot be achieved with standard LoRa localization schemes, as LoRa is a narrow-band communication technology. At the receiving stage of the broadband time domain signal, it is difficult to determine the arrival time precisely compared to UWB narrow time pulses.

- The ability to achieve the real-time property of the localization, thanks to UWB while still consuming as little power as possible. Real-time localiza-tion with LoRa-only systems is not possible, as in this case, the LoRa module needs to send the received packet from the tag to the gateway. This packet contains the time of flight, which makes it necessary to estimate the location at the gateway side each time, without knowing if the tag has moved or not, this continuous packet transmission would consume more power which is against the LoRa principle.

- UWB and LoRa based systems are mostly active (battery powered), in the proposed system, the UWB battery powers both the UWB and LoRa modules. Because LoRa's power consumption is very low, another power unit is not necessary.

6.3.2 Design of the LoRa-UWB transceiver

The designed UWB-LoRa transceiver is a multi-standard device capable of achieving the high-accuracy and long-range UWB localization of objects and sending the lo-cation information to LoRa gateways. Its main purpose is to act either as a sensor-tag or a reader intermediate node between the sensor-tag and the gateway. It performs the localization of the tag and informs the gateway in case this latter has moved in space.
The reader is composed of an UWB module (from STMicroelectronics [24]) and a LoRa module, which communicate through an MCU unit. Hence, the reader has an UWB antenna for RF communication with any UWB module and a LoRa antenna for the RF communication with the LoRa gateways. The UWB module and the antennas of the reader and tag's working frequency channel is the UWB channel 2, which

starts at 3.75 GHz and ends at 4.25 GHz. The LoRa module and antennas work in the 863 to 868 MHz band, which represents the Europe frequency channel for LoRa communications, and it is part of the unlicensed Industrial, Scientific and Medical (ISM) bands.
As illustrated in Figure 6.3, the reader board consists of a upper layer and a bottom layer separated by an air gap. The upper layer consists of the radiating elements of the UWB and LoRa antennas placed on the same FR4 substrate. In contrast, the bottom layer consists of the ground plane and the LoRa module on one side, while on the other side, an FR4 substrate with a branch-line coupler enabling the UWB circular polarization of the UWB antenna is placed, and at a distance from it, the MCU and UWB module are integrated.

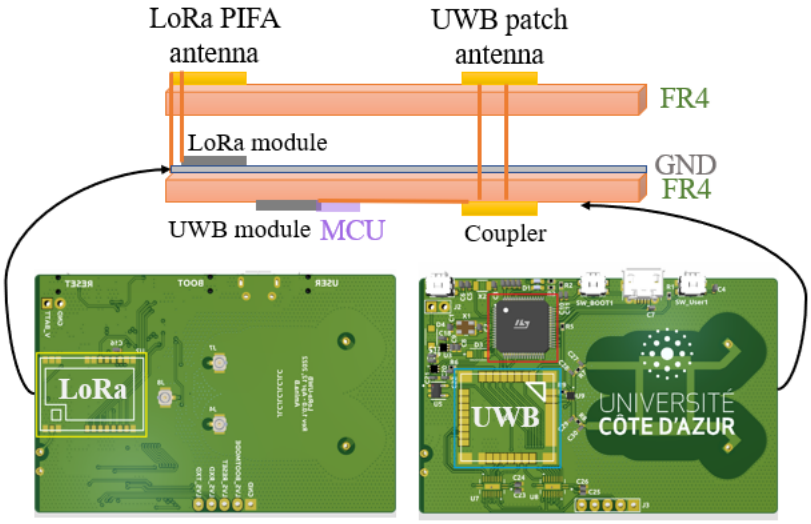

FIGURE 6.3: Structure of the UWB-LoRa transceiver, composed of two layers, an electronics bottom layer and an antenna upper layer, connected through signal vias.

Circular polarization was privileged for the UWB antenna, as it is more advantageous due to it yielding better localization information and ranges compared to linear polarization; its advantages are described in detail in our previous works [14,25]. The common air gap between the two antennas serves as the air gap for standard PIFA (Planar Inverted F-Antenna) design and simultaneously represents the necessary gap between the substrate and ground, which guarantees a 500 MHz bandwidth for the UWB probe-fed patch antenna.
Concerning the electronic part of the transceiver, the system complexity has been kept at a low level during the design process. The main components are the power supply unit, the MCU, the LoRa module and the UWB module. The first three are mandatory and equivalent to any LoRa/LoRaWAN end-devices available on the market, and the circuit connections between them are accordingly made to the conventional systems. In addition, the required connections for the UWB module were realized following the same model and firmware derived from the STMicroelectronics UWB MEK1 localization board [20]. Finally, the UWB module is connected to the MCU, which is also connected to the LoRa module.
Furthermore, the commercial cost of the LoRa module and MCU prevalent is low (within 10 USD), and with the recent announcement of the STM32WL microcontroller from STMicroelectronics, the foreseeable cost will be even lower thanks to the

integra-tion of the LoRa Module into the same die of the microcontroller. In contrast, the costs of the UWB modules currently vary depending on their integration boards. In this work, the module was provided as samples and are only commercialized with the MEK1 board; however, other UWB modules are available at a relatively low price (within 25 USD), such as modules from Decawave. To conclude, the proposed concept of UWB-LoRa lo-calization can be applied and remains feasible, regardless of the types of the LoRa or UWB modules chosen.

6.3.3 Antenna structure design

The structure is composed of two antennas (figures 6.4 and 6.5): a wideband patch antenna operating at the UWB channel from 3.75 to 4.25 GHz and a PIFA antenna operating at the LoRa channel from 863 to 870 MHz. The design and simulation were realized using CST Microwave Studio software, where only the antenna parts of the board were simulated, and the electronics modules positions were considered by leaving the necessary space for their integration, which occurs later in the fabrication process.
As the transceiver has two substrates, the radiating elements of both the UWB and LoRa antennas are placed on the upper layer substrate. The bottom layer contains other antenna elements: the ground plane shared by both antennas; the shorting pin of the LoRa antenna, which extends until the ground plane; the feed vias; and the branch-line coupler of the UWB antenna placed on the back surface of the bottom substrate. Both substrates used are of the FR4 type and have a 0.8 mm thickness.

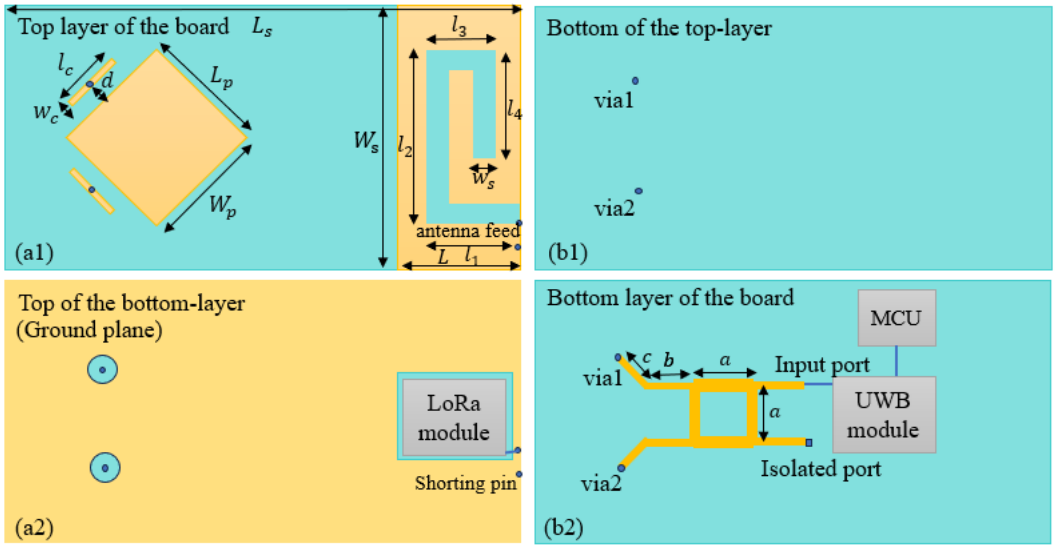

FIGURE 6.4: Antenna structure design consisting of a UWB patch antenna and a LoRa PIFA antenna: (a1) top of the upper layer of the board; (b1) bottom of the upper layer of the board; (a2) top of the bottom layer of the board; (b2) bottom of the bottom layer of the board.

The UWB antenna design and optimization procedure is detailed in [26], it is a probe-fed wideband patch using capacitive feeding from a small conductor printed next to the radiating element. Since it is also designed to have circular polarization, two orthogonal capacitive elements are designed. These two small rectangular elements are fed with vias originating from the coupler outputs placed at the bottom layer. The dimensions of the UWB antenna (figure 6.4) are as follows: Substrate

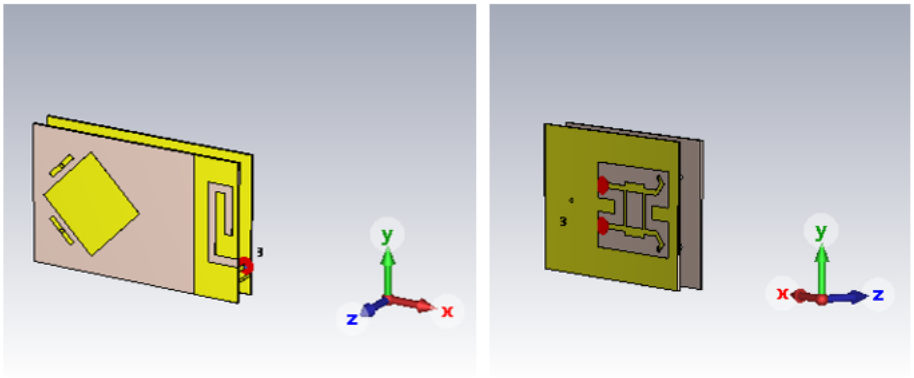

FIGURE 6.5: Antenna structure design, consisting of a UWB patch antenna and a LoRa PIFA antenna.

length and width are respectively $L_s = 69\ mm$ and $W_s = 43\ mm$. The patch dimensions are $L_p = W_p = 23\ mm$, designed with standard method to work at the center frequency of 4 GHz. Each capacitive element's length and width are $l_c = 10\ mm$, $w_c = 1.5\ mm$, and the distance separating it from the radiating element is d=2 mm. Finally, the classical branchline coupler is designed to operate at the same center frequency of 4 GHz, from which its dimensions are derived.
The LoRa antenna is a slotted PIFA antenna. The slot starts from the feed point and extends to help decrease the resonating frequency to the desired LoRa channel frequencies. The external dimensions of the antenna (figure 6.4) are $L = 14.5mm$, and its width is the same as the substrate width $(W_s = 43mm)$. The slot width is 2.5 mm and its length dimensions are: $L_1 = 10\ mm$, $L_2 = 24.5\ mm$, $L_3 = 8\ mm$, and $L_4 = 15\ mm$. The feed and short points are separated by a distance of 2.5 mm.
All antenna dimensions are summarized in Table 6.1.

UWB antenna	Dimensions	LoRa antenna	Dimensions
Substrate length L_s	69 mm	Conductor length L	14.5 mm
Substrate width W_s	43 mm	Conductor width W_s	43 mm
Patch length and width L_p,W_p	23 mm	Slot length l_1	10 mm
Capacitive element length l_c	10 mm	Slot length l_2	24.5 mm
Capacitive element width w_c	1.5 mm	Slot length l_3	8 mm
Capacitive element separation from the patch d	2 mm	Slot length l_4	15 mm
Coupler dimension a	10 mm	Slot width w_s	2.5 mm
Coupler dimension b	5.7 mm	Separation between feed and shorting pin	2.4 mm
Coupler dimension c	2.87 mm	Air gap (distance from ground plane)	7 mm

TABLE 6.1: Summary of the physical dimensions of the antennas.

As both antennas share the same ground plane, the air gap between this factor

and the upper layer substrate is an optimized distance of 7 mm. The optimization of this distance to accommodate both antennas is highly important as it significantly affects the patch bandwidth and the PIFA antenna's resonance performance.

6.4 Results and characterization

A prototype of the UWB-LoRa transceiver was realized and is presented in figure 6.6. The upper and bottom layers were realized separately and then were assembled by soldering the feed connections from the coupler outputs to the capacitive small patches next to the radiating element for the UWB antenna, and the feed and shorting connec-tions from the ground plane to the upper layer PIFA element. The transceiver board is powered by a small external battery and both antennas' inputs (LoRa and UWB) are powered by a signal via coming from their respective modules (as shown in figure 6.3).

(a) (b)

FIGURE 6.6: Prototype of the UWB-LoRa transceiver board: (a) the upper layer of the board containing the ra-diating elements; (b) bottom layer of the board containing the MCU, the modules and the branch-line coupler.

6.4.1 Antenna measurements

Impedance matching

To measure the impedance matching of the antennas before testing the board, UFL-type connections were designed a priori at both inputs of the branch-line coupler (which represent the two input ports of the UWB antenna), and UFL-to-SMA cables were used for measurements using a VNA (Vector Network Analyzer), as illustrated in figure 6.7.

The SMA side of the cable connected to one of the coupler's inputs is then loaded by a 50 Ω match. In the case of the LoRa antenna, it can be seen that its feed was connected directly to an SMA connector for the measurements (figure 6.7). Foam with the same dielectric constant as air was also used between the two layers of the board to facilitate the assembly of the board.
Figure 6.8 presents the simulated and measured reflection coefficient of the PIFA antenna. Our results show a shift in frequency between the simulation and measurement. This shift is due to the slot of length l_4, which was removed by covering it with copper tape in the fabricated prototype, as shown in figures 6.6.a and 6.7.b.
In fact, the simulated result with the slot l_4 shows that the antenna resonated at the

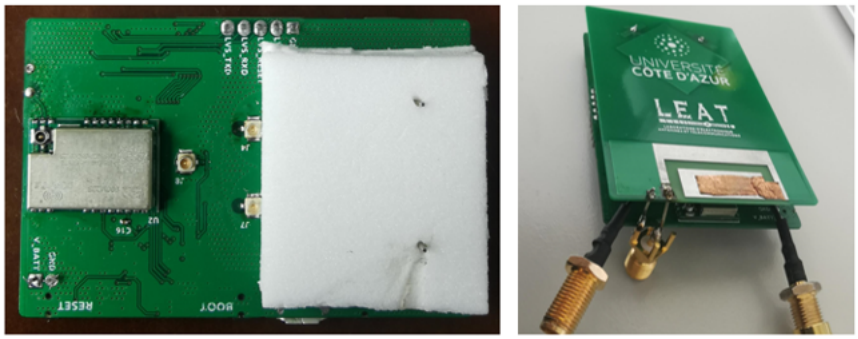

FIGURE 6.7: Board assembly and measurements: (a) prototyping using foam to separate the layers and UFL connectors at the coupler inputs; (b) stand-alone antenna matching measurement set up, using a SMA connector for the LoRa antenna and UFL-to-SMA cables from the coupler inputs for UWB antenna characterization.

desired frequencies; however, after the prototyping, it was observed that l_4 lowered the resonance frequency below 850 MHz, which is why it was covered. A slight difference in bandwidth is also observed, which is due to the reflection coefficient being higher after adjusting the frequency, which led to the dampening of the bandwidth. Finally, the measured result shows that the antenna's impedance is matched at - 10 dB from around 845 to 875 MHz, which includes the desired LoRa channel (863 to 868 MHz) for LoRaWAN communication with the sensors and gateways.

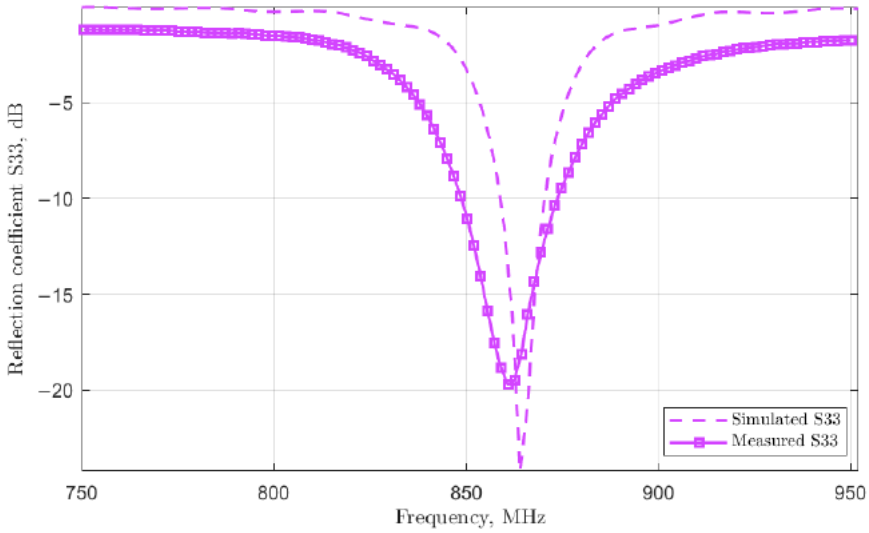

FIGURE 6.8: Reflection coefficient of the LoRa PIFA antenna.

The measured and measured reflection coefficient of the UWB antenna is illustrated in figure 6.9. This coefficient was measured separately, via two measurements, for both ports corresponding to the two inputs of the branch-line coupler by alternating the isolation load between the two inputs. In both cases, one of the ports must be isolated with a 50 Ω load. The advantage of choosing which port is the input to the antenna is that the sense of the circular polarization can be chosen, that is, left or right circular polarization can be obtained. The ability to choose the polarization sense implies that the antenna can be integrated into different systems regardless of polarization specifications, such as in cases where, for example, the

reader and tag antennas are required to have a specific polarization sense or the polarization of a reader (or tag) antenna is required to match the polarization of a tag (or reader) antenna. A comparison between the simulation and measurement shows

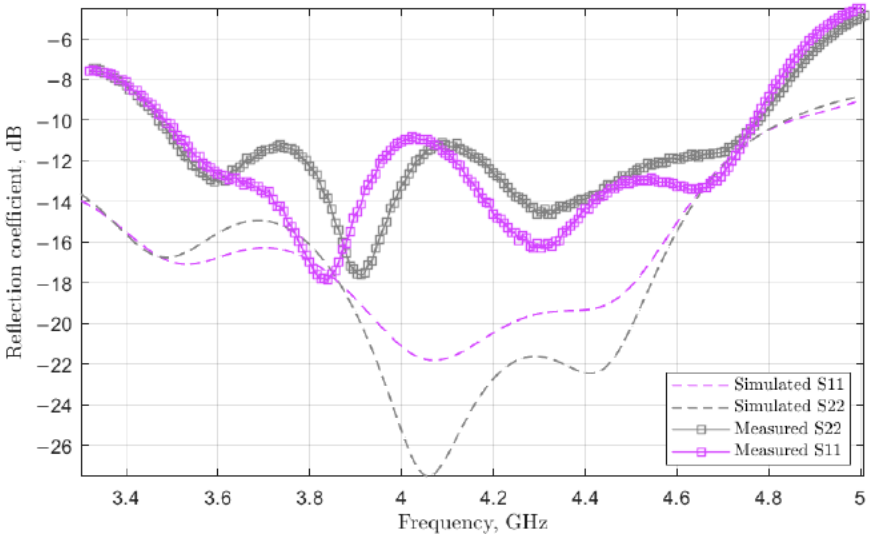

FIGURE 6.9: Reflection coefficient of the UWB patch antenna for both ports of the coupler (S11 and S22).

that the impedance matching of the antenna via simulation presents better results, as it ranges between - 20 and - 28 dB, compared to - 12 and - 18 dB in the measurement. This difference is due to factors such as the possible difference in air gap during the assembly process, which can have a significant effect on the bandwidth and impedance matching; another factor is the electronics modules and circuits, which were not simulated with the antenna design. Finally, regardless of the port chosen, our results show that the antenna's measured reflection coefficient is matched at - 10 dB (from 3.55 GHz to 4.74 GHz), which includes the desired UWB channel (3.75 GHz to 4.25 GHz) in both cases. A slight difference between the two curves is observed, which is due to the presence of the PIFA antenna, which is not completely symmetrical with respect to the antenna axis.

Efficiency and gain

Further antenna measurements were realized in anechoic chamber to assess the gain and radiation efficiencies of the antennas. Figures 6.10 and 6.11 show the simulated and measured characteristics, respectively, for the LoRa and UWB antennas.

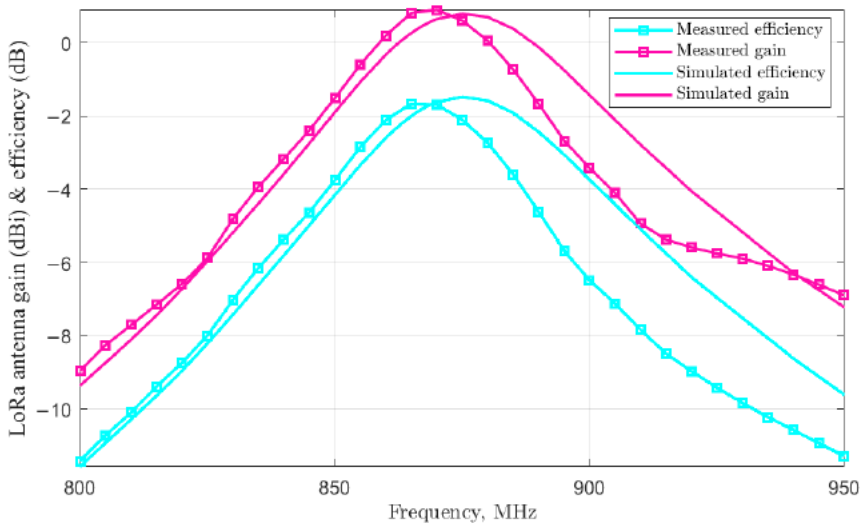

FIGURE 6.10: LoRa antenna's gain and efficiency characteristics.

The result of the measurement of the LoRa antenna shows a maximum efficiency and gain at the operation frequency channel (863–870 MHz). The gain ranges between 0.82 and 0.91 dBi, while the efficiency is between - 1.65 and - 1.69 dB (corresponding to 68 % of the radiation). A shift in frequency is observed between the measured and simulated curves for both the efficiency and gain, which is due to the simulated design including the slot l_4, in contrast to the prototype, in which it was removed to adjust the resonant frequency.

Furthermore, the UWB antenna's simulated and measured efficiency and gain are illustrated in figure 6.11. The results show stable gain and efficiency along the desired frequency channel (3.75–4.25 GHz) in terms of both simulation and measurement. Furthermore, the measured gain ranges between 5.1 dBi and 6 dBi on these frequencies, where this variation of less than 1 dB is small enough to ensure that the antenna behavior is considered identical at all the frequencies of the channel. Similarly, the radiation efficiency varies between - 1.26 and - 1.4 dB, which corresponds to radiation of between 72 and 75 %.

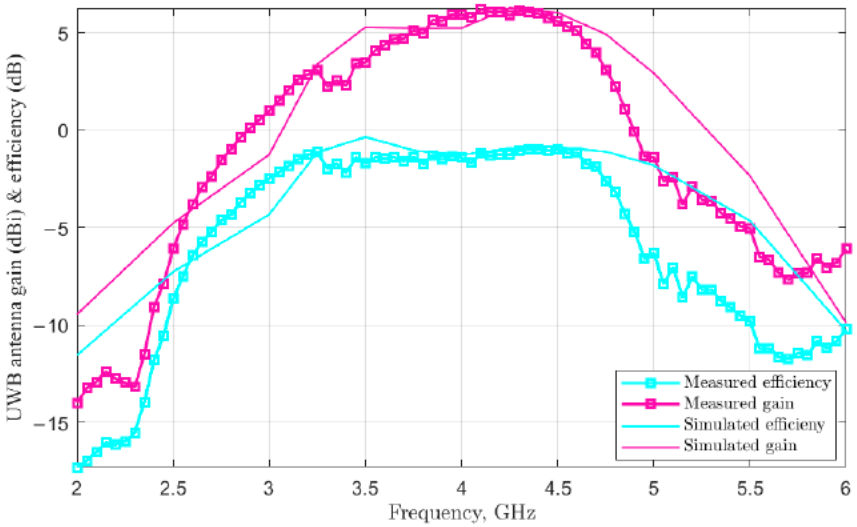

FIGURE 6.11: UWB antenna's gain and efficiency characteristics.

Radiation pattern

Figure 6.12 illustrates the measured radiation pattern of the UWB antenna, through the realized gain of the co-polarization and cross-polarizations (here, the measurements correspond to one arbitrary chosen port). The pattern is measured for the UWB channel's center and edge frequencies (3.75 GHz, 4 GHz, and 4.25 GHz) to ensure the stability of its wideband operation.

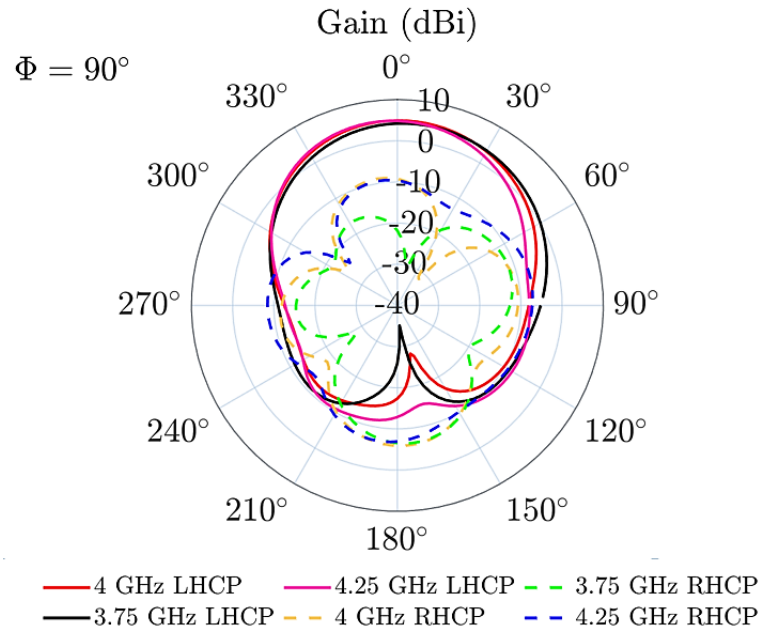

FIGURE 6.12: Radiation pattern (azimuth) of the UWB antenna at the channel's center and edge frequencies, through polarization realized gain.

As shown in the results, the antenna exhibits a 180° directional azimuth pattern at all frequencies, and the circular polarization sense achieved is left hand (for the measured port), with stable peak gains of 6 dBi.

Figures 6.13 and 6.15 illustrates the simulated polar and 3-dimensional radiation patterns (realized gain) of the LoRa PIFA antenna around the transceiver board, at a frequency of 868 MHz. As shown in these results, the antenna exhibits an omni-directional radiation pattern and showcases two radiation dips along the PCB axis. The antenna achieves measured peak gains between 0 and 1 dBi.

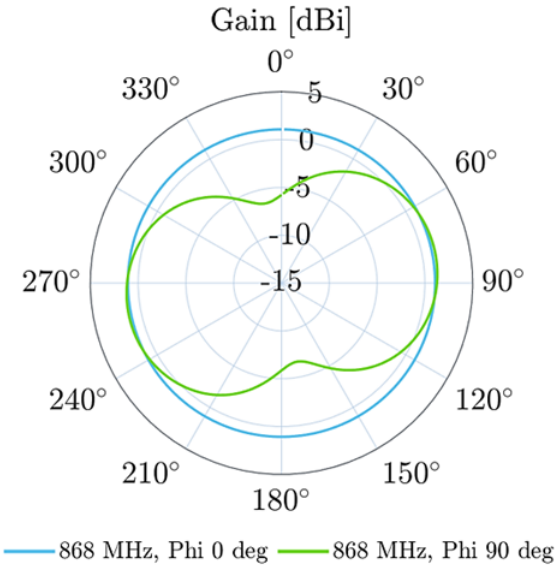

FIGURE 6.13: Polar radiation pattern of the LoRa antenna at a frequency of 868 MHz.

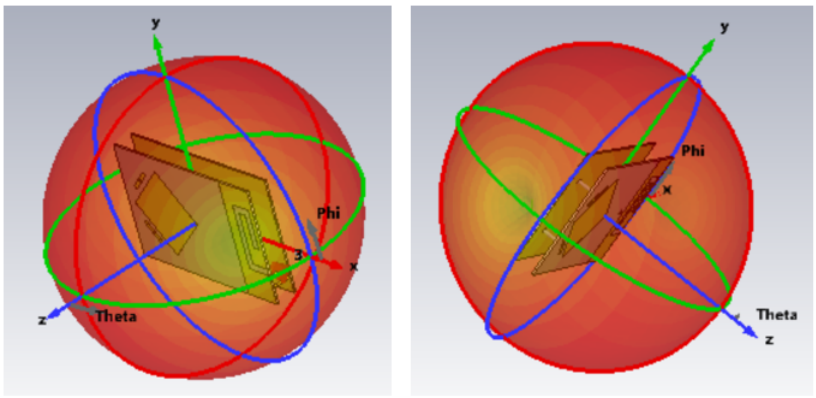

FIGURE 6.14: Three-Dimensional radiation pattern of the LoRa antenna at 868 MHz frequency, with a view on both left and right sides of the antenna structure.

6.5 Discussion and experimental characterization of the board

To assess the localization performance, two steps are investigated. The first one is the UWB two-way ranging realized between the sensor-tag and the reader, and the second one is the transmission of the location information to the LoRa gateway and network. These steps are detailed in the following section.

6.5.1 From the Sensor-Tag to the Reader

Ranging measurements were performed using two prototypes of the UWB-LoRa transceiver, with one used as a sensor-tag and another one used as a reader. It is important to note that experimental tests with UWB signals are not prone to interference with other devices operating in the same environment [27, 28] because they are spread over a wide band and transmitted at power spectral density levels close

to the noise floor of conventional radio receivers, such as WiFi, Bluetooth, etc.
Figure 6.15 shows the set-up and environment of the measurements. An outdoor scenario was privileged, as it enables more available space compared to buildings, allowing us to measure the performance at LOS and analyze the maximum range of detection that is achieved through UWB localization. This range does not de-scribe the whole system's UWB-LoRa range but only that of the UWB part of the system. This maximum distance gives an idea of where the intermediate reader node needs to be placed in such system, that is, how far from the sensor-tag it can be placed and still be able to detect it.

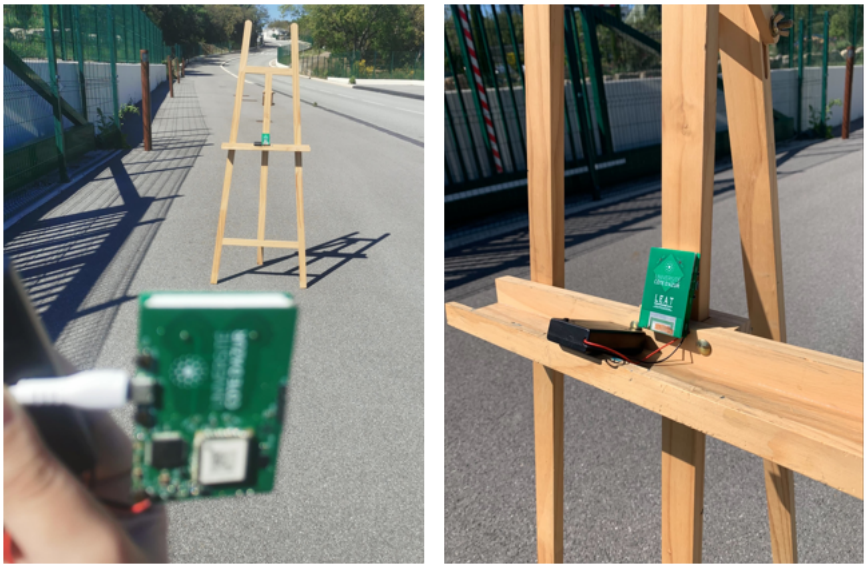

FIGURE 6.15: Ranging with two LoRa-UWB transceivers, the first being a sensor-tag and the second being a reader.

Figure 6.16 illustrates the result of the ranging, through the Link Quality Indicator (LQI) with respect to the distance measured via the reader (using its UWB feature). The LQI is the ratio of the measured received signal strength to the already-known saturation signal strength of the transceiver. It is a metric used by STMicroelectronics for localization using their UWB module, which was integrated into the designed transceiver.

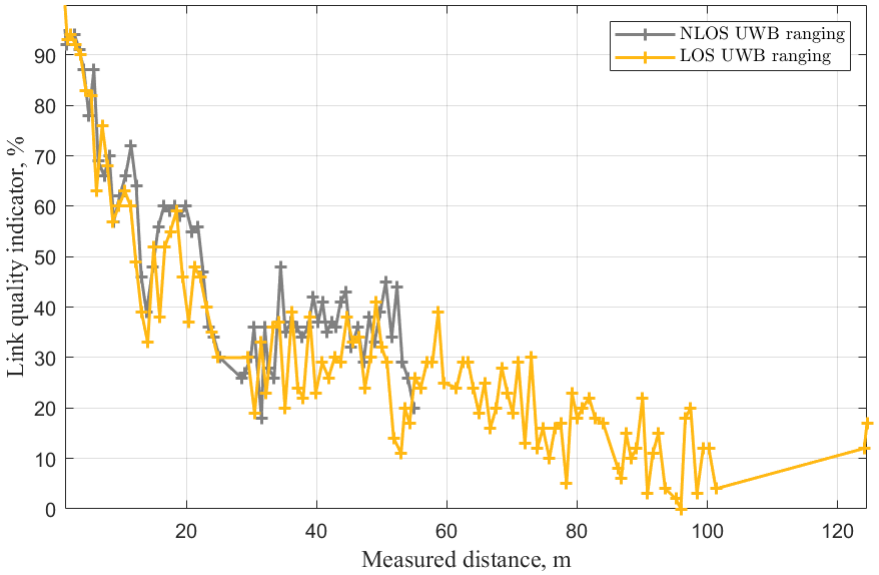

FIGURE 6.16: Ranging measurements of the UWB localization between the sensor-tag and the reader, in LOS and NLOS scenarios (outdoor).

Firstly, the results show that the LQI and, thus, the received power decreases with respect to the distance, which is due to signal path loss. Indeed, having higher levels of power is beneficial for obtaining longer ranges of detectability. For this reason, solutions to overcome path loss exist in the literature and include the modeling of the UWB propagation channel [29,30], the estimation of the channel path loss [31] and the compensation for it at the signal processing level; however, the objective in this work leans more toward demonstrating the feasibility of the UWB-LoRa localization concept by comparing it to conventional UWB and LoRa localization systems, the performances of which are known in terms typical range and accuracy.
Thus, the second observation from these results is that the reader can detect the mobile sensor-tag up to distances of 120 m and 55 m in the LOS and NLOS scenarios. The LQI naturally decreases with the increase in distance and presents small fluctuations between close-distance measurements, as it depends on the environment around the mobile tag at that time instant. The ranges achieved conform with typical maximum UWB ranges present in systems used in industry and the literature (approximately 100–200 m for LOS).
It is necessary to mention that the LoRa feature of the sensor-tag in this work does not have a role in the UWB localization process, which involves ToF measurements. Indeed, its role is like that of any LoRa sensor, i.e., to allow the direct transmission of sensing information to the gateway, which does not require sending it to the intermediate reader. Indeed, the intermediate reader and UWB communication part of the sensor-tag only intervene if the sensor-tag has to be located via the gateway.

6.5.2 From the Reader to the Gateway and Network

After the ranging is performed, the reader node sends the location information of the sensor-tag to the LoRa gateways, albeit only in case the latter has moved since the last measurement. The reader transceiver compares the current obtained distance separating it from the sensor-tag and the previously computed distance. If it is different, the reader sends the information through LoRa to the gateway. Figure 6.17 shows the information packet received by the network, and it displays the

reader and the sensor-tag's Identification Numbers (ID), the distance measured and the LQI.

FIGURE 6.17: Ranging information of the sensor as displayed after its reception via the LoRa network.

The results demonstrate that as long as the UWB-LoRa reader node is placed at an appropriate distance from a LoRa-UWB (or UWB-only) sensor-tag, it is able to localize through UWB high-accuracy ranging. The LoRa gateways placed at distances of kilometers from a sensor will be able to monitor this latter feature and stay informed of its precise location whenever it changes in real time.

6.5.3 Localization accuracy

Localization using UWB is known to ensure the accuracy of the location information that is of a sub-meter level. To observe this process, ranging measurements were realized with the designed transceivers in an indoor scenario, where multipath effects were often present, along a limited corridor of 35 m inside the LEAT laboratory. The reader transceiver was placed at a fixed position, and the tag was moved, starting from 10 to 35 m away from the reader. The measurements of the distance between the reader and tag were performed for each step of 5 m. This operation was repeated three times, and the measured distances were compared to the true distance between the reader and tag. Figure 6.18 illustrates this comparison for all three measures.

The results show that for all three measures, the distance measured via the UWB reader follows the reference curve (true distance) very closely. Measure 2 seems to show the furthest measure from the reference curve. However, its accuracy remains at the sub-meter level. Indeed, an example is shown at the 20 m distance, where the UWB reader's distance estimation is 19.67 m, which corresponds to an estimate error of only 33 cm. All the other estimates (measure 1 and 3) achieve lower estimate errors of between 10 and 30 cm. This result allows us to confirm the achieved sub-meter accuracy due to UWB signals' fine temporal characteristics (pulse width of 2 ns). The achieved centimeter-level accuracy with UWB greatly benefits the LoRa infrastructure; indeed, the conventional localization attempts using only the LoRa technique to allow a gateway to locate a sensor, as shown in the literature, are typically characterized by accuracy levels that exceed 10 m using Time-of-Flight

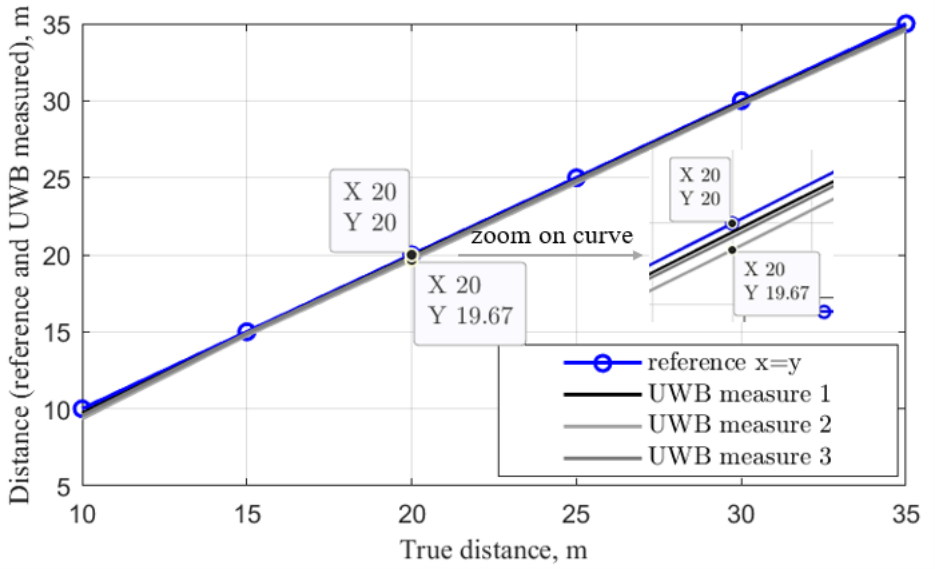

FIGURE 6.18: Comparison of UWB-measured distances with the true distance between a reader and a tag in an indoor environment.

measurements, which may be low enough for outdoor approximate localization; however, this accuracy level cannot accommodate indoor environments.

6.6 Conclusion

This chapter investigated the possibility of achieving high-accuracy, long-range localization through UWB and LoRa technologies. A multi-standard transceiver board was proposed as a solution. It consists of a UWB module, a LoRa module and an MCU, ensuring the communication between them. The transceiver can either be a sensor-tag deployed in the LoRa infrastructure, a reader device, or both. It allows the localization of a sensor-tag with UWB-level accuracy (a few centimeters) and the transmission of the location information to LoRa gateways kilometers away from the sensor-tag to the network. The UWB-LoRa transceiver was fabricated, and two prototypes were used for ranging measurements in both outdoor and indoor scenarios. The results demonstrated conformal UWB localization ranges and accuracy, as well as their successful transmission to the LoRa gateway for the real-time monitoring of the sensor, all while maintaining the low power requirements of the LoRa communications. In future work, the improvement in the proposed localization transceiver could focus on the miniaturization aspect of the antennas, especially for the sensor-tag, to help its integration into different objects that need to be tracked. The miniaturization can be achieved by choosing a higher frequency channel and optimizing the antennas accordingly. Another improvement aspect would be the integration of direction detectability in addition to ranging, and this can be achieved via the design of an antenna array for the reader side, which can intercept the ranging signals using the array elements and determine the angles of arrival related to the direction component.

Bibliography

[1] Khutsoane, O.; Isong, B.; Abu-Mahfouz, A.M. IoT devices and applications based on LoRa/LoRaWAN. In Proceedings of the IECON 2017—43rd Annual Conference of the IEEE Industrial Electronics Society, Beijing, China, 29 October–1 November 2017; pp. 6107–6112. https://doi.org/10.1109/IECON.2017.8217061.

[2] Merhej, D.; Ahriz, I.; Garcia, S.; Terré, M. LoRa Based Indoor Localization. In Proceedings of the 2022 IEEE 95th Vehicular Technology Conference: (VTC2022-Spring), Helsinki, Finland, 19–22 June 2022; pp. 1–5. https://doi.org/10.1109/VTC2022-Spring54318.2022.9860962.

[3] Marquez, L.E.; Calle, M. Understanding LoRa-Based Localization: Foundations and Challenges. IEEE Internet Things J. 2023, 10, 11185–11198. https://doi.org/10.1109/JIOT.2023.3248860.

[4] Mekki, K.; Bajic, E.; Chaxel, F.; Meyer, F. A comparative study of LPWAN technologies for large-scale IoT deployment. ICT Express 2019, 5, 1–7. https://doi.org/10.1016/j.icte.2017.12.005.

[5] Augustin, A.; Yi, J.; Clausen, T.; Townsley, W.M. A Study of LoRa: Long Range and Low Power Networks for the Internet of Things. Sensors 2016, 16, 1466. https://doi.org/10.3390/s16091466.

[6] Devalal, S.; Karthikeyan, A. LoRa Technology—An Overview. In Proceedings of the 2018 Second International Conference on Electronics, Communication and Aerospace Technology (ICECA), Coimbatore, India, 29–31 March 2018; pp. 284–290. https://doi.org/10.1109/ICECA.2018.8474715.

[7] Muppala, R.; Navnit, A.; Devendra, D.; Matera, E.R.; Accettura, N.; Hussain, A.M. Feasibility of Standalone TDoA-based Localization Using LoRaWAN. In Proceedings of the 2021 International Conference on Localization and GNSS (ICL-GNSS), Tampere, Finland, 1–3 June 2021 ; pp. 1–7. https://doi.org/10.1109/ICL-GNSS51451.2021.9452311.

[8] Kombo, O.H.; Kumaran, S.; Bovim, A. Design and Application of a Low-Cost, Low- Power, LoRa-GSM, IoT Enabled System for Monitoring of Groundwater Resources With Energy Harvesting Integration. IEEE Access 2021, 9, 128417–128433. https://doi.org/10.1109/ACCESS.2021.3112519.

[9] Ferrero, F.; Truong, H.-N.-S.; Le-Quoc, H. Multi-harvesting solution for autonomous sensing node based on LoRa technology. In Proceedings of the 2017 International Conference on Advanced Technologies for Communications (ATC), Quy Nhon, Vi-etnam, 18–20 October 2017; pp. 250–253. https://doi.org/10.1109/ATC.2017.8167627.

[10] Dardari, D.; Closas, P.; Djuric, P.M. Indoor Tracking: Theory, Methods, and Technologies. IEEE Trans. Veh. Technol. 2015, 64, 1263–1278. https://doi.org/10.1109/TVT.2015.2403868.

[11] Dardari, D.; Conti, A.; Ferner, U.; Giorgetti, A.; Win, M.Z. Ranging with Ultrawide Bandwidth Signals in Multipath Envi-ronments. Proc. IEEE 2009, 97, 404–426. https://doi.org/10.1109/JPROC.2008.2008846.

[12] IEEE Std 802.15.4z-2020; IEEE Standard for Low-Rate Wireless Networks–Amendment 1: En-hanced Ultra Wideband (UWB) Physical Layers (PHYs) and Associated Ranging Techniques. IEEE: New York City, NY, USA, 2020. pp. 1–174.

[13] Coppens, D.; Shahid, A.; Lemey, S.; Marshall, B.V.H.C.; De Poorter, E. An Overview of Ultra-WideBand (UWB) Standards and Organizations (IEEE 802.15.4, FiRa, Apple): Interoperability Aspects and Future Research Directions. IEEE Access 2022, 10, 70219–70241. https://doi.org/10.1109/ACCESS.2022.3187410.

[14] 14. Benouakta, A.; Ferrero, F.; Lizzi, L.; Staraj, R. Antenna Characteristics Contributions to the Improvement of UWB Real-Time Locating Systems' Reading Range and Multipath Mitigation. IEEE Access 2023, 11, 71449–71458. https://doi.org/10.1109/ACCESS.2023.3294622.

[15] Pospisil, J.; Fujdiak, R.; Mikhaylov, K. Investigation of the Performance of TDoA-Based Localization Over LoRaWAN in Theory and Practice. Sensors 2020, 20, 5464. https://doi.org/10.3390/s20195464.

[16] Daramouskas, I.; Mitroulias, D.; Perikos, I.; Paraskevas, D.; Kapoulas, V. Localization in LoRa Networks Based on Time Difference of Arrival; Springer: Cham, Switzerland, 2022; pp. 130–143. https://doi.org/10.1007/978-3-030-90528-6-12.

[17] Fargas, B.C.; Petersen, M.N. GPS-free geolocation using LoRa in low-power WANs. In Proceedings of the 2017 Global Internet of Things Summit (GIoTS), Geneva, Switzerland, 6–9 June 2017; pp. 1–6. https://doi.org/10.1109/GIOTS.2017.8016251

[18] Ha, G.Y.; Seo, S.B.; Oh, H.S.; Jeon, W.S. LoRa ToA-Based Localization Using Fingerprint Method. In Proceedings of the In-ternational Conference on Information and Communication Technology Convergence (ICTC), Jeju, Republic of Korea, 16–18 October 2019; pp. 349–353. https://doi.org/10.1109/ICTC46691.2019.8939702.

[19] Aarif, L.; Tabaa, M.; Hachimi, H. Experimental test and performance of RSSI-based indoor localization in LoRa Networks. Procedia Comput. Sci. 2022, 203, 420–425. https://doi.org/10.1016/j.procs.2022.07.055.

[20] Strzoda, A.; Marjasz, R.; Grochla, K. How Accurate is LoRa Positioning in Realistic Conditions? In Proceedings of the Pro-ceedings of the 12th ACM International Symposium on Design and Analysis of Intelligent Vehicular Networks and Applica-tions, Montreal, QC, Canada, 24–28 October 2022; Association for Computing Machinery: New York, NY, USA, 2022; pp. 31–35. https://doi.org/10.1145/3551662.3561260.

[21] Li, B.; Xu, Y.; Liu, Y.; Shi, Z. LoRaWAPS: A Wide-Area Positioning System Based on LoRa Mesh. Appl. Sci. 2023, 13, 9501. https://doi.org/10.3390/app13179501.

[22] Kwasme, H.; Ekin, S. RSSI-Based Localization Using LoRaWAN Technology. IEEE Access 2019, 7, 99856–99866. https://doi.org/10.1109/ACCESS.2019.2929212.

[23] Lam, K.-H.; Cheung, C.-C.; Lee, W.-C. RSSI-Based LoRa Localization Systems for Large-Scale Indoor and Outdoor Environ-ments. IEEE Trans. Veh. Technol. 2019, 68, 11778–11791. https://doi.org/10.1109/TVT.2019.2940272.

[24] B-UWB-MEK1—Evaluation kit for the B-UWB-MOD1 ultra-wideband module—STMicroelectronics Available online: https://www.st.com/en/wireless-connectivity/b-uwb-mek1.html (accessed on 3 February 2023).

[25] Benouakta, A.; Ferrero, F.; Lizzi, L.; Brochier, L.; Staraj, R. Measurements of antenna polarization effects on Ultra-Wideband monitoring and localization. In Proceedings of the 2021 IEEE Conference on Antenna Measurements and Applications (CAMA); Antibes Juan-les-Pins, France, 15–17 November 2021; pp. 589–590. https://doi.org/10.1109/CAMA49227.2021.9703597.

[26] Benouakta, A.; Ferrero, F.; Lizzi, L.; Staraj, R. Frequency Reconfigurable and Circularly Polarized Patch Antenna Over Dual Ultra-wideband Channels. In Proceedings of the 2022 16th European Conference on Antennas and Propagation (EuCAP); Madrid, Spain, 27 March–1 April 2022; pp. 1–5. https://doi.org/10.23919/EuCAP53622.2022.9769006.

[27] Ghavami, M.; Michael, L.B.; Kohno, R. Ultra Wideband Signals and Systems in Communication Engineering; 1st ed.; Wiley: Ho-boken, NJ, USA, 2007. https://doi.org/10.1002/9780470060490.

[28] Duran, M.A.C.; D'Amico, A.A.; Dardari, D.; Rydström, M.; Sottile, F.; Ström, E.G.; Taponecco, L. Chapter 3—Terrestrial Network-Based Positioning and Navigation. In Satellite and Terrestrial Radio Positioning Techniques; Dardari, D., Falletti, E., Luise, M., Eds.; Academic Press: Oxford, UK, 2012; pp. 75–153. https://doi.org/10.1016/B978-0-12-382084-6.00003-9.

[29] Ghassemzadeh, S.; Greenstein, L.; Kavcic, A.; Sveinsson, T.; Tarokh, V. An Empirical Indoor Path Loss Model for Ul-tra-Wideband Channels. J. Commun. Netw.—JCN 2003, 5, 303–308. https://doi.org/10.1109/JCN.2003.6596612.

[30] Frattasi, S.; Rosa, F.D.; Dardari, D. Ultra-wideband Positioning and Tracking. In Mobile Positioning and Tracking; Frattasi, S., Rosa, F.D. Eds.; Wiley: Hoboken, NJ, USA, 2017. https://doi.org/10.1002/9781119068846.ch9.

[31] Rubio, L.; Reig, J.; Fernández, H.; Rodrigo-Peñarrocha, V.M. Experimental UWB Propagation Channel Path Loss and Time-Dispersion Characterization in a Laboratory Environment. Int. J. Antennas Propag. 2013, 2013, e350167. https://doi.org/10.1155/2013/350167.

General conclusion

The work realized in this thesis consisted in bringing enhancements to time-based indoor localization, which is performed by real-time locating systems (RTLSs), which employ Ultra-Wide Bandwidth (UWB) technology. The localization results obtained with these systems call for improvements because they are mostly employed in complex environments involving many mobile objects which makes precise localization challenging. The principal enhancements and contributions realized in this work focused on the conception of UWB antennas that are more optimized to the needs of such RTLSs compared to the conventional antennas already integrated in most commercial solutions.

The first chapter, presented an introduction to indoor localization, its techniques, the error sources that can be encountered in different scenarios (line-of-sight and non-line-of-sight). The technologies on which indoor localization is based were explained, with a focus on UWB technology by listing its advantages, applications, regulations, standards, and consortiums. Then, a state of the art of the conventional broadband and UWB antennas was realized. Finally, the old and recent requirements of UWB antennas were summarized and the recent expectations from UWB antennas were highlighted.

In the second chapter, conforming to the recent IEEE standards specifying the emitted UWB signal and its characteristics such as pulse width and pulse shape, a time-domain study was realized through simulations by applying this signal to an UWB transmitting antenna. The signal was generated by frequency upconversion to the center frequency of the worldwide UWB channel centered at 7.9 GHz. The far-electric-field received by field probes was analyzed in terms of pulse distortion, magnitude, and time delay (or arrival). By extracting the time of arrival and comparing it for different azimuth and elevation angles, it was confirmed that this time corresponds in fact to the radial distance by considering the transmitting antenna as a point source far from the receiver. It was also found that, while this time varies with the distance, it does not vary with azimuth and elevation angles. This analysis helps to conclude that the radiation pattern of an antenna does not affect the localization results in time-based techniques such as UWB.

In the third chapter, a technical review of the UWB radio chips and evaluation boards available in the industry was realized. The main UWB radio chips are from the manufacturers : Qorvo, NXP, Apple and STMicroelectronics. Their characteristics and the localization techniques they allow were summarized, some of these radio chips allow not only ranging but also direction finding through the angle-of-arrival (AoA) technique. Then, a focus on the antennas employed in these commercial systems highlighted that most of the antennas are conventional UWB antennas, such as: linearly polarized monopole antenna, linearly polarized patch antenna or patch antennas circularly polarized, however only at the center frequency of the UWB channel. The chapter highlighted the influence of the chosen antennas on the localization results and that manufacturers always present the range and accuracy allowed by their radio chips with conditions on the orientations of the reader and tag antennas. In fact, the best localization result is always only achieved in a certain orientation of the antennas. This discussion helps to conclude that by making the antennas more efficient with higher gain and circular polarization, the localization will be improved and most importantly will be robust to antenna orientations ensuring constant confidence in the localization quality.

In the fourth chapter, the conception of a frequency reconfigurable and circularly polarized UWB antenna was realized. The antenna type was chosen to be patch for higher gain compared to standard monopole UWB antenna. The bandwidth of the patch was enhanced up to 500 MHz by suspending the substrate on air, and a capacitive feed mechanism was employed to compensate for the inductive effect brought by the feeding probe. The frequency reconfigurability on two UWB channels (Channels centered at 4 GHz and 6.5 GHz) was achieved by modifiying the dimensions of the radiating element by the means of copper connections which can eventually be replaced by p-i-n diodes. The circular polarization was realized by the means of two branchline couplers on a bottom substrate, each working at the center frequency of one channel. The antenna was experimentally characterized and showed good bandwidth and axial ratio performance.
In the fifth chapter, the previously designed antenna, working on the UWB channel centered at 4 GHz, was tested in a commercial RTLS evaluation board from STMicroelectronics and localization results achieved were compared to the results achieved when using the commercial UWB antenna from the same manufacturer. Experimental results obtained by ranging with a reader and tag allowed to demonstrate the advantages brought by the designed antenna to the localization performance, in terms of the improvement of : the reading range, the received power remaining stable no matter the relative orientation of the reader and tag antennas, and in terms of attenuation of the multi-path reflections which influence the received UWB signal and thus the localization quality.
Finally, in the sixth chapter, a new concept was introduced to achieve both high-precision and long-range localization by combining the two technologies : UWB technology and Long-Range (LoRa) technology. Therefore, a multi-standard RTLS transceiver board was designed and fabricated. The transceiver is composed of a UWB module, a LoRa module, a microcontroller and of an antenna structure composed of the previously designed UWB patch antenna and a planar inverted-F antenna (PIFA) for LoRa operation at the 863 - 870 MHz channel. This transceiver was placed as an intermediate node between a LoRa gateway and as a sensor which is needs to be located. Experimental ranging was performed to assess the communication between the sensor, the reader (both represented by the same transceiver) and the location information was sent to and received at the LoRa gateway and network.

Perspectives

Building upon the work conducted in this thesis and its continuation, several further developments and ways for improvement have been identified.

Concerning the time-domain analysis performed (chapter 2), while the time of arrival was studied in function of the radiation pattern angles of the antenna, a system-oriented study could be performed where the user could estimate the parameters of the localization system such as its reading range, or its accuracy in the case of the presence of obstacles such as metal for example in the environment of the antenna.

Concerning the frequency reconfigurable UWB antenna designed (chapter 4), and which is meant for anchor systems, although its higher gain enables a longer reading range, it was designed with the hypothesis that most anchor RTLSs are usually fixed on walls or ceilings, or placed on surfaces in indoor environments. Thus, if the anchor were to be placed in a different location, it would be difficult to detect tags if they are placed outside of its radiation pattern coverage. For this reason, complementary additions could be made by designing an anchor antenna with many facets to allow for an omnidirectional radiation while still benefiting of the high gain of the antenna.

Another possible development axis could be the study of direction-finding RTLSs in addition to the range and localization RTLSs studied in this work. In fact, the measurement of the direction of the tagged object is performed through the angle-of-arrival (AoA) scheme, which requires the reader antenna to possess two or three elements, that is, for this antenna to be an array antenna. In this case, the difference between the times at which the signal from the tag arrives at these antenna elements can be calculated and thus direction can be found.

Finally, to conclude, with the evolving potential of UWB technology and its presence being more and more pervasive in the most recent smartphones, cars and wearables, it could be said that this technology has a promising future in scientific research which could help its further development into a more standard communication scheme.

List of Publications

- International journals :

1. A. Benouakta, F. Ferrero, L. Lizzi and R. Staraj, "Advancements in Industrial RTLSs: A Technical Review of UWB Localization Devices Emphasizing Antennas for Enhanced Accuracy and Range," MDPI Electronics 2024, 13, 751, doi: 10.3390/electronics13040751

2. A. Benouakta, T. M. Nguyen, F. Ferrero, L. Lizzi and R. Staraj, "Design of a Multi-Standard UWB-LoRa Antenna Structure and Transceiver Board for High-Accuracy and Long-Range Localization Applications," MDPI Electronics 2023, 12, 4487, doi: 10.3390/electronics12214487

3. A. Benouakta, F. Ferrero, L. Lizzi and R. Staraj, "Antenna Characteristics Contributions to the Improvement of UWB Real-Time Locating Systems' Reading Range and Multipath Mitigation," in IEEE Access, vol. 11, pp. 71449-71458, 2023, doi: 10.1109/ACCESS.2023.3294622.

- International Conferences :

1. A. Benouakta, F. Ferrero, L. Lizzi and R. Staraj, "Frequency Reconfigurable and Circularly Polarized Patch Antenna Over Dual Ultra-wideband Channels," 2022 16th European Conference on Antennas and Propagation (EuCAP), Madrid, Spain, 2022, pp. 1-5, doi: 10.23919/EuCAP53622.2022.9769006.

2. A. Benouakta, F. Ferrero, L. Lizzi, L. Brochier and R. Staraj, "Measurements of antenna polarization effects on Ultra-Wideband monitoring and localization," 2021 IEEE Conference on Antenna Measurements Applications (CAMA), Antibes Juan-les-Pins, France, 2021, pp. 589-590, doi: 10.1109/CAMA49227.2021.9703597.

- National Conferences :

1. A. Benouakta, F. Ferrero, L. Lizzi, R. Staraj, "Antenne Ancre Ultra-Large Bande Reconfigurable en Fréquence pour applications de localisation et de positionnement d'objets," Journées Nationale Microondes (JNM), Limoges, France, June 2022.

2. A. Benouakta, F. Ferrero, L. Lizzi, R. Staraj, "Antenne Ancre Ultra-Large Bande Reconfigurable en Fréquence pour applications de localisation et de positionnement d'objets," Conférence Plénière du GDR-Ondes, Lille, France, December 2021.

3. A. Benouakta, F. Ferrero, L. Lizzi, R. Staraj, "Conception d'une Structure Antennaire Multi-Standards ULB-LoRa Pour Applications de Localisation à Haute Précision et de Longue Portée," Journées Nationale Microondes (JNM), Antibes Juan-Les-Pins, France, June 4 - 7th 2024.